

University of Alabama in Huntsville

LOUIS

Theses

UAH Electronic Theses and Dissertations

2012

Preliminary trajectory analysis of a nuclear fusion propulsion fly-by mission to Saturn and beyond

Brian Riehm

Follow this and additional works at: <https://louis.uah.edu/uah-theses>

Recommended Citation

Riehm, Brian, "Preliminary trajectory analysis of a nuclear fusion propulsion fly-by mission to Saturn and beyond" (2012). *Theses*. 418.

<https://louis.uah.edu/uah-theses/418>

This Thesis is brought to you for free and open access by the UAH Electronic Theses and Dissertations at LOUIS. It has been accepted for inclusion in Theses by an authorized administrator of LOUIS.

PRELIMINARY TRAJECTORY ANALYSIS OF A
NUCLEAR FUSION PROPULSION FLY-BY MISSION
TO SATURN AND BEYOND

by

BRIAN RIEHM

A THESIS

Submitted in partial fulfillment of the requirements
for the degree of Master of Science in Engineering
in
The Department of Mechanical and Aerospace Engineering
to
The School of Graduate Studies
of
The University of Alabama in Huntsville

HUNTSVILLE, ALABAMA

2012

In presenting this thesis in partial fulfillment of the requirements for a master's degree from The University of Alabama in Huntsville, I agree that the Library of this University shall make it freely available for inspection. I further agree that permission for extensive copying for scholarly purposes may be granted by my advisor or, in his/her absence, by the Chair of the Department or the Dean of the School of Graduate Studies. It is also understood that due recognition shall be given to me and to The University of Alabama in Huntsville in any scholarly use which may be made of any material in this thesis.

Brian M. Riehm

Brian M. Riehm

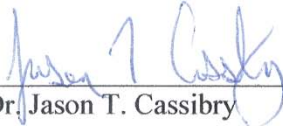
6/29/2012


(Date)

THESIS APPROVAL FORM

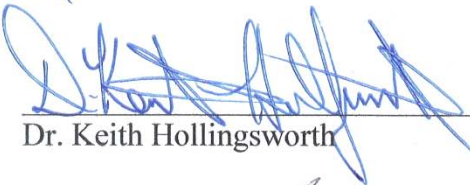
Submitted by Brian Riehm in partial fulfillment of the requirements for the degree of Master of Science in Engineering and accepted on behalf of the Faculty of the School of Graduate Studies by the thesis committee.

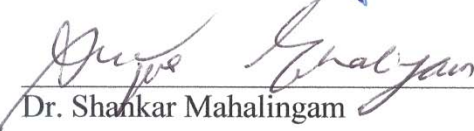
We, the undersigned members of the Graduate Faculty of The University of Alabama in Huntsville, certify that we have advised and/or supervised the candidate on the work described in this thesis. We further certify that we have reviewed the thesis manuscript and approve it in partial fulfillment of the requirements for the degree of Master of Science in Engineering.

 6/25/12 Committee Chair
Dr. Jason T. Cassibry (Date)

 7/9/12
Dr. Robert A. Frederick Jr.

 06/28/2012
Dr. Matthew W. Turner

 Department Chair
Dr. Keith Hollingsworth

 06/28/12 College Dean
Dr. Shankar Mahalingam

 7/10/12 Graduate Dean
Dr. Rhonda K. Gaede

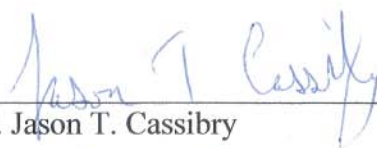
ABSTRACT

The School of Graduate Studies
The University of Alabama in Huntsville

Degree Master of Science College/Dept. Engineering/Mechanical and
Aerospace Engineering.
Name of Candidate Brian Riehm.
Title Preliminary Trajectory Analysis of a Nuclear Fusion Propulsion Fly-by Mission
to Saturn and Beyond.

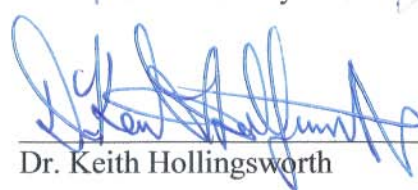
Thermonuclear fusion propulsion provides high specific impulse and moderately high thrust enabling interplanetary trip times that are roughly one third of missions utilizing chemical propulsion. A detailed trajectory analysis is performed using the General Mission Analysis Tool (GMAT) on a spacecraft utilizing a fusion propulsion system. The spacecraft initially departs from the Earth-Moon L1, swinging by the Moon and then the Earth before entering the heliocentric leg of its trajectory. The spacecraft begins in a near elliptical orbit around the Sun until it gradually accelerates to a hyperbolic trajectory on its way to Saturn and subsequently into deep space. Comparisons are made between this trajectory, which includes asymmetric gravitational models and N-body effects, against patched conic and gravity free models. Trip times are compared against existing robotic missions showing that fusion systems can potentially enable trip times of $\sim 1/3$ of conventional chemical systems and permit science research farther into space.

Abstract Approval: Committee Chair



Dr. Jason T. Cassibry

Department Chair



Dr. Keith Hollingsworth

Graduate Dean

 7/5/12

Dr. Rhonda K. Gaedel

ACKNOWLEDGMENTS

I would like to thank my advisor and committee chair, Dr. Jason Cassibry, for his guidance and patience these last few years. I would also like to thank the other members of my thesis committee, Dr. Frederick and Dr. Turner, for deciding to participate on such short notice.

I would also like to include the members from NASA and any other organization that helped with the development of the software program GMAT and allowing the program to be open source and available to the public for free.

Finally, I would like to thank my family for their support through all levels of my education. Without their support I would not have been able to advance academically and professionally.

TABLE OF CONTENTS

	Page
LIST OF FIGURES	xii
LIST OF TABLES	xiv
LIST OF ABBREVIATIONS AND ACRONYMS	xvi
LIST OF SYMBOLS	xx
Chapter	
I. INTRODUCTION	1
II. BACKGROUND OF NUCLEAR FUSION PROPULSION	4
2.1 Fusion Propulsion Classifications.....	6
2.1.1 Magnetic Confinement	7
2.1.1.1 Gasdynamic Mirror.....	8
2.1.2 Inertial Confinement	9
2.1.2.1 Fusion-Fission Hybrid	10
2.1.3 Inertial Electrostatic Confinement.....	10
2.1.4 Magneto-Inertial Fusion	11
2.2 Fusion Fuels.....	12
2.3 Fusion Propulsion Trajectory Analysis.....	13
2.3.1 Trajectory Analysis from NASA TP-2003–212691	14
2.3.1.1 VARITOP Setup.....	15
2.3.1.2 Comparison of the MTF propulsion system missions	16

2.4	Continued Development	18
III.	GENERAL MISSION ANALYSIS TOOL (GMAT) SOFTWARE	19
3.1	Background History.....	19
3.2	GMAT Architecture.....	20
3.2.1	Program Interface	21
3.2.1.1	User Interfaces	21
3.2.1.2	Interpreters	23
3.2.1.3	External Interfaces	23
3.2.1.4	Subscribers.....	23
3.2.2	Engine	23
3.2.2.1	Executive.....	23
3.2.2.2	Configuration	24
3.2.2.3	Factory	24
3.2.3	Model.....	24
3.2.3.1	Environment.....	25
3.2.3.2	Resources	25
3.2.3.3	Commands	29
3.2.3.4	Parameters.....	30
3.2.4	Utilities.....	30
3.2.4.1	Date/Time	30
3.2.4.2	Matrix Algebra.....	31
3.3	GMAT Script Setup.....	31
3.3.1	Setup of Resources.....	33

3.3.1.1	Spacecraft Properties	33
3.3.1.2	Propagators	36
3.3.1.3	Coordinate Systems	38
3.3.1.4	Variables/Arrays/Strings.....	38
3.3.1.5	Output	39
3.3.2	Setup of Mission Sequence.....	42
IV.	MODELS	47
4.1	Spacecraft Design	47
4.2	Saturn Fly-by	53
4.3	Beyond Saturn.....	63
4.4	Gravity Free and Central-Body only Models	67
V.	COMPARISON TO OTHER TYPES OF PROPULSION MISSIONS	71
5.1	Chemical Propulsion.....	71
5.1.1	Chemical Propulsion Background	71
5.1.1.1	Liquid Propellants	72
5.1.1.2	Solid Propellants	72
5.1.1.3	Hybrid Rockets	73
5.1.2	Cassini-Huygens	74
5.1.2.1	Cassini-Huygens Trajectory and Mission.....	75
5.1.2.2	Comparison to Cassini-Huygens Mission.....	79
5.1.3	New Horizons	80
5.1.3.1	New Horizons Trajectory and Mission.....	81
5.1.3.2	Comparison to New Horizons.....	84

5.2	Electrical Propulsion.....	85
5.2.1	Electrical Propulsion Background	85
5.2.1.1	Electrothermal.....	86
5.2.1.2	Electrostatic.....	86
5.2.1.3	Electromagnetic	87
5.2.2	Dawn.....	88
5.2.2.1	Dawn Trajectory and Mission.....	89
5.2.2.2	Comparison to Dawn	93
5.3	Conclusion	95
VI.	CONCLUDING REMARKS.....	99
6.1	Additional Fly-by Missions	99
6.2	Rendezvous and Return Missions.....	100
6.3	Precision of Trajectory Analysis.....	101
6.4	Remarks on Future Work.....	102
APPENDIX A	SPICE.....	104
A.1	History	104
A.2	Concept	105
A.3	Summary of Kernels	106
APPENDIX B	GMAT SCRIPT	108
B.1	Commands to Propagate Spacecraft to 1000 AU	121
APPENDIX C	GMAT EQUATIONS.....	122
C.1	Solar Radiation Pressure.....	122
C.2	Thrust and Specific Impulse Equations	123

C.3	Runge-Kutta 89 Table of Coefficients.....	124
APPENDIX D	SPHERE OF INFLUENCE CALCULATIONS.....	126
D.1	Earth’s radius of sphere of influence:	126
D.2	Saturn’s radius of sphere of influence:	127
D.3	Moon’s radius of sphere of influence:	127
APPENDIX E	CALCULATIONS OF SPACECRAFT DESIGN MODEL	128
E.1	Approximation of trip time:.....	128
E.2	Specific Impulse:	128
E.3	Exhaust Velocity.....	129
E.4	Mass Flow Rate	129
E.5	Thrust and Recalculated Mass flow Rate	129
E.6	Propellant Mass.....	129
E.7	Empty Mass of Spacecraft	129
E.8	Conformity Check.....	129
APPENDIX F	MATLAB® SCRIPT FOR TIME STEP SIZE.....	130
References	132

LIST OF FIGURES

Figure	Page
2-1: Comparison of Propulsion System Capabilities.....	6
2-2: Gasdynamic Mirror	7
2-3:Schematic of a Spherical Tokamak Reactor System.....	8
2-4: Schematic of ICF Ignition Point Design Target.....	9
2-5: Inertial Electrostatic Confinement Engine System.....	11
2-6: ΔV Penalty for Tangentially Directed Thrust.....	16
2-7: 2D Trajectory of MTF D-D for Earth to Callisto Round Trip Mission.....	18
3-1: GMAT Architecture Flow Chart	21
3-2: Screenshot of GMAT GUI at Startup.....	22
3-3: Propagator Window with Default Settings.....	29
3-4: Screen shots of Resource and Mission Tabs	32
4-1: 3D Trajectory of Spacecraft from Epoch to Earth Orbit	55
4-2: 2D Trajectory of Spacecraft from Epoch to Earth Orbit	55
4-3: 3D Trajectory of Spacecraft from Epoch to the Earth SOI.....	56
4-4: 2D Trajectory of Spacecraft from Epoch to the Earth SOI.	57
4-5: 3D Trajectory of Spacecraft during Accelerating Phase	58
4-6: 2D Trajectory of Spacecraft during Accelerating Phase	59
4-7: 3D Trajectory of Spacecraft from Epoch to Closest Approach of Saturn.....	60

4-8: 2D Trajectory of Spacecraft from Epoch to Closest Approach of Saturn.....	60
4-9: 3D Trajectory of Spacecraft Fly-by of Saturn.....	62
4-10: 2D Trajectory of Spacecraft Fly-by of Saturn.....	62
4-11: Spacecraft B-plane Closest Approach at Saturn (T Vector along Equator)	62
4-12: 3D Trajectory of Spacecraft from Epoch to Edge of Kuiper Belt.....	64
4-13: 2D Trajectory of Spacecraft from Epoch to Edge of Kuiper Belt.....	64
4-14: Plot of Spacecraft Distance verses Time from epoch to 100 years	65
4-15: Plot of Spacecraft Velocity Time from Epoch to 100 years.....	66
4-16: Plot of Spacecraft Velocity verses Time from Epoch to 10 years.....	66
4-17: Comparison of Trajectory Methods.....	70
4-18: Comparison of GMAT scripts with respect to Saturn	70
5-1: 3D Trajectory of Cassini-Huygens from Launch to Saturn.....	78
5-2: 2D Trajectory of Cassini-Huygens from Launch to Saturn.....	79
5-3: 3D Trajectory of New Horizons from Launch to Pluto.....	83
5-4: 2D Trajectory of New Horizons from Launch to Pluto.....	84
5-5: 3D Trajectory of Dawn in Heliocentric J2000.0 Coordinates from Earth to Ceres	92
5-6: 2D Trajectory of Dawn showing acceleration and coasting phases	93
5-7: Plot of Spacecraft's Magnitude Distance from the Sun versus Trip Time.....	97
5-8: Plot of Spacecraft's Magnitude Distance from the Sun versus Year	98

LIST OF TABLES

Table	Page
2-1: Fusion Fuel Reactions	12
2-2: Catalyzed-Deuterium-Deuterium with 100% burnup of Tritium and Helium-3.....	13
2-3: MTF Configuration Values	17
3-1 Description of Equation of Motion Terms	26
3-2: Initial Spacecraft Orbital Elements Input	34
3-3: Spacecraft Ballistic/Mass Inputs	34
3-4: Fuel Tank Inputs.....	35
3-5: Thruster Inputs.....	36
3-6: List of Runge-Kutta89 Integrator Default Settings	36
3-7: Force Model Propagator Settings	38
3-8: Orbit View Major Settings	40
3-9: Report File Settings	42
3-10: Calculated Radius of Sphere of Influence Values.....	42
3-11: Parameter List of First Report Command	44
4-1: Spacecraft Design Parameters	53
4-2: Force Model Propagator Point Mass Setting.....	69
5-1: Date when Fusion Propulsion Spacecraft will reach Escaping Spacecraft	98

C-1: Thrust and Specific Impulse Coefficient Units.....	123
D-1: Characteristics of Planets, Sun and Moon	126

LIST OF ABBREVIATIONS AND ACRONYMS

AU	Astronomical unit
CA	closest approach
cm	centimeter(s)
D-D	Deuterium-Deuterium
DOE	Department of Energy
EDT	Eastern Daylight Time
EP	Electrical Propulsion
FFHS	fusion-fission hybrid system
FP	Fusion Propulsion
FPS	Fusion Propulsion System
GDM	Gas Dynamic Mirror
GEM	graphite epoxy motor
GMAT	General Mission Analysis Tool
GRC	Glenn Research Center
GSFC	Goddard Space Flight Center
GUI	Graphical User Interface
HAMO	high altitude mapping
He	helium
HOPE	Human Outer Planet Exploration
HTPB	hydroxyl-terminated polybutadiene

ICF	Inertial Confinement Fusion
IEC	Inertial Electrostatic Confinement
in.	inch(s)
IPS	ion propulsion system
JD	Julian Date
JPL	Jet Propulsion Laboratory
KBO	Kuiper Belt Object
kg	kilogram(s)
km	kilometer(s)
kW	kilowatt(s)
L1	Lagrange Point 1
LAMO	low altitude mapping
LOX	liquid oxygen
LTTT	Low Thrust Trajectory Tool(s)
m	meter(s)
MALTO	Mission Analysis Low-Thrust Optimization
MCF	Magnetic Confinement Fusion
MICE	SPICE for MATLAB
MIF	Magneto-Inertial Fusion
MJD	Modified Julian Date
mm	millimeter(s)
MMH	mono-methyl hydrazine
mN	millinewton(s)
MPD	magnetoplasmadynamic
mT	metric ton (tonne)

MTF	Magnetized Target Fusion
N	newton(s)
NAIF	Navigation and Ancillary Information Facility
NASA	National Aeronautics and Space Administration
NH	New Horizons
NSTAR	NASA Solar Technology Application Readiness
NTO	nitrogen tetroxide
ODE	ordinary differential equation
P10	Pioneer 10
P11	Pioneer 11
Pa	pascal
PI	principle investigator
PPT	pulsed-plasma thruster
PRM	probe release maneuver
RCS	Reaction Control System
RSS	root sum square
RTG	radioisotope thermal generator
s	seconds
SOI	sphere of influence
SPICE	Spacecraft Planet Instrument C-Matrix
SRM	solid rocket motor
SRP	solar radiation pressure
TCM	trajectory correction maneuver
TP	Technical Paper
UTC	Coordinated Universal Time

V1	Voyager 1
V2	Voyager 2
VISTA	vehicle for interplanetary space transport application
W	watt(s)
XIPS	xenon ion propulsion system
ΔV	Delta V (change in velocity)

LIST OF SYMBOLS

a	semimajor axis of ellipse
A	area
A_{\odot}	area exposed to the Sun
C_R	coefficient of reflectivity
d	derivative
e	exponent symbol, times ten raised to the power
F_T	thrust
G	universal gravitational constant
g_0	standard gravity
I_{sp}	specific impulse
m	mass
\dot{m}	mass flow rate
P	pressure
P_{SR}	solar radiation pressure
R, r	magnitude distance
\mathbf{R}, \mathbf{r}	vector distance
t	time
T	temperature
V, v	velocity

x, y, z axis directional distance

Greek Letters

α specific power

β plasma pressure over magnetic pressure

λ payload mass fraction

μ gravitational parameter

ρ air density

Subscripts

b burn

e empty, escape, exhaust

f final

i initial

k, j index

p propellant

pl payload

ps propulsion system

s structural, spacecraft

ref reference

x, y, z axis direction

\odot Astronomical symbol for the Sun

CHAPTER I

INTRODUCTION

For thousands of years people have been looking up in the night sky to observe, study, and theorize the motion of celestial bodies. Well before the first satellite was ever launched, the basic mathematics and physics for motion in the vacuum of space were already known. After the launch of Sputnik 1 on 04 October 1957, the study of orbital mechanics (astrodynamics) transformed from a natural science into a discipline of engineering. Since Sputnik 1, hundreds of spacecrafts have been launched into the vacuum of space with several traveling to other planets, some landing on the surface of celestial bodies, and others traveling to the outer limits of the solar system and beyond. Unfortunately, the time required for current robotic spacecrafts to reach these extremely distant destinations can be measured in years, and if the destination is an outer planet, the time required to reach the planet could be nearly a decade. The required time to travel to another planet must be shortened significantly in order to reduce the cost of each robotic mission and eventually have crewed missions to other celestial bodies.

For current chemical propulsion systems along with newly operational electrical propulsion systems, the size of the propulsion system needed to significantly shorten travel (trip) times would be so massive that the launch costs for orbit assembly are prohibitively expensive. More advanced spacecraft propulsion systems beyond the technologies currently

available are essential for further understanding of the universe achievable to a person well within his or her lifetime. Nuclear fusion propulsion is a candidate that can potentially provide the solution for decreased travel times to other celestial bodies [1]. As part of the development of fusion reactors for propulsion, orbit analysis studies must be conducted in order to identify the benefits to continue motivating the field while pinpointing potential problems with performance in the models utilized. Numerous mission studies have been conducted but most often rely on the ‘gravity free’ assumption vehicle trajectories. Utilizing just a few predetermined performance and design parameters for a spacecraft propelled by a fusion propulsion system, a realistic trajectory analysis can be conducted to identify departures from these assumptions, while elucidating the opportunities that are made available for additional science.

This document describes, in detail, a trajectory analysis conducted on a fusion propulsion propelled spacecraft simply denoted ‘Fusion Propulsion’ throughout. The primary mission of the Fusion Propulsion spacecraft involves a fly-by past Saturn with an extremely short trip time of just over one year. Secondary missions include studying one or more Kuiper belt objects while the spacecraft travels through the belt and investigating the structure of the outer heliosphere before eventually exiting the solar system. The trajectory of the Fusion Propulsion spacecraft consists of just two phases. The first phase is the acceleration phase and involves the spacecraft accelerating due to the thrust provided by the propulsion system. The second phase is the coasting phase and does not require the use of the propulsion system. During this phase of the trajectory, the spacecraft’s velocity will continuously decrease because of the gravitational acceleration from the Sun. Fortunately, gravitational acceleration for an object is proportional to the distance between the object and

the Sun (or some other primary body). As a spacecraft (or an object in the solar system) travels farther and farther away from the Sun, the gravitational acceleration from the Sun on the spacecraft decreases. As the gravitational acceleration from the Sun decreases, the rate of change of the spacecraft's velocity during the coasting phase of its trajectory also decreases, and eventually the rate of change of the spacecraft's velocity will be nearly negligible. Although, this will not occur until at least a decade after the spacecraft is initially launched. The acceleration phase is designed to be approximately half of the trip time to Saturn. A gravity-free space equation initially developed by W. E. Moeckel is used to approximate the trip time to Saturn [2]. All trajectory analysis conducted for the Fusion Propulsion spacecraft is created with NASA's General Mission Analysis Tool (GMAT) [3].

The remainder of the thesis is organized as follows. First, in Chapter 2 a short description is provided on the types of fusion propulsion systems, fusion fuels, and previously conducted trajectory analyses. This chapter is followed by a detailed description of GMAT and the GMAT setup for the Fusion Propulsion spacecraft in Chapter 3. Chapter 4 includes the design of the Fusion Propulsion and trajectory analysis; while Chapter 5 compares the Fusion Propulsion spacecraft's trajectory to a few existing spacecraft trajectories (two chemically propelled spacecrafts and one electrically propelled spacecraft) and then to the trajectories of the current spacecrafts that will eventually leave the solar system (all of which are chemically propelled). Finally in Chapter 6, recommendations are given to conduct trajectory analysis on additional mission to one or more of the gas giant planets utilizing the Fusion Propulsion spacecraft or a slight variant of the design as well as methods to increase precision for trajectory analysis on fusion propelled spacecrafts.

CHAPTER II

BACKGROUND OF NUCLEAR FUSION PROPULSION

Nuclear fusion is the process of two or more light nuclei elements merging or “fusing” together to form a heavier atomic element. For some of the reactions, this results in an energy release over 10^6 times greater per unit mass than any chemical reaction. This process usually results in a sizable amount of released energy. With the abundance of deuterium, lithium, hydrogen, and boron on Earth, the energy requirements for society could be met for millennia with fusion-fueled terrestrial power stations. Terrestrial electric power stations will produce electricity through a thermodynamic process in which water is vaporized in order to propel a turbine generator; while spacecraft propulsion systems will use the released energy kinetically instead of thermodynamically. The released energy will propel the exhaust gas (plasma) at very high speeds resulting in specific impulse values much higher than chemical and comparable to electrical rockets. The relationship between specific impulse and spacecraft velocity is determined through the ideal rocket equation [4].

$$\Delta V = g_0 I_{sp} \ln \left(\frac{m_i}{m_f} \right) \quad (2-1)$$

where

- ΔV = change in velocity, m/s
- g_0 = standard gravity, 9.81 m/s
- I_{sp} = Specific Impulse, seconds
- m_i = initial mass
- m_f = final mass

Figure 2-1 illustrates the different types of propulsion system at different values of specific impulse, thrust-to-weight ratio, and specific power values. The main purpose of this chart is to illustrate the role that fusion propulsion can play in in-space propulsion. For completeness, we discuss the other propulsion system niches as well. Electric propulsion (EP) systems are characterized into electrothermal, electrostatic, and electromagnetic thruster categories and require a separate electrical power source that is power limited. Higher specific impulse at a fixed power results in decreased thrust, acceleration, and trip time. While fusion has similar limitations, the ability to mix the very high temperature exhaust stream with a colder, higher molecular weight propellant enables simultaneously moderate thrust (1 to 100 kN) and high specific impulse through thrust augmentation giving these systems higher thrust to weight ratios *at* higher specific impulse values. An increase in the thrust-to-weight ratio results in the spacecraft being able to travel the same distance in a shorter time due to the larger vehicle acceleration value from the increased thrust-to-weight ratio. Even though fusion propulsion systems have greater thrust-to-weight ratios than electrical propulsion systems, the best fusion propulsion system barely has the same thrust-to-weight ratio as some of the lowest performing chemical systems. Even with the substantial specific impulse value, the thrust-to-weight ratio for the best fusion propulsion system is still not enough to overcome the Earth's gravitational influence on the surface. Thus, in order to launch spacecrafts into space complex chemical rockets are the only resource currently available. Chapter 5 discusses more on chemical and electrical propulsion systems.

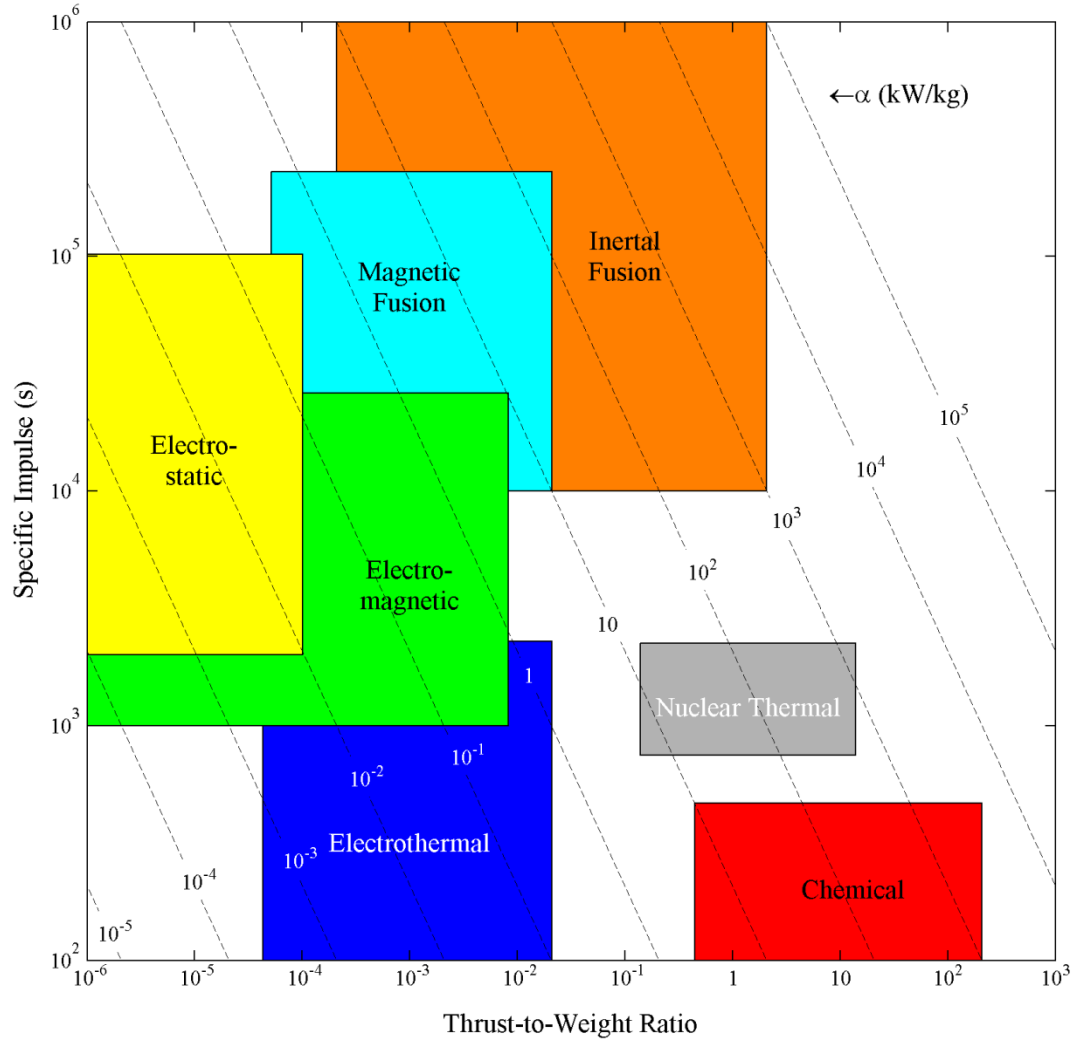


Figure 2-1: Comparison of Propulsion System Capabilities. Thrust-to-Weight Ratio referenced to Earth's surface gravity.

2.1 Fusion Propulsion Classifications

Fusion propulsion systems are typically classified by the type of confinement used to create the fusion reaction. The two most dominate types of fusion confinement are magnetic and inertial [5]. Other types of confinement include inertial electrostatic [6] and a hybrid system of magnetic confinement and inertial confinement known as magneto-inertial fusion [7].

2.1.1 Magnetic Confinement

Magnetic Confinement Fusion (MCF) utilizes superconducting coils to generate a strong magnetic field. The field generates a magnetic pressure sufficient to confine the internal high temperature plasma. MCF requires a plasma β value (plasma pressure over magnetic pressure) to be less than 1 for confinement. Unfortunately, existing magnetic technology would require the use of massive magnets in order to generate a magnetic pressure value larger than the plasma pressure value resulting in an inefficient propulsion system. MCF design concepts include the spherical tokamak (a.k.a. spherical torus) shown in Figure 2-3, the spheromak (a compact torus design) and the gasdynamic mirror (GDM) shown in Figure 2-2. The spherical tokamak and spheromak are currently being researched by the Department of Energy (DOE) and other international energy departments for use in terrestrial power stations. The GDM design is more compatible for spacecraft propulsion than both the spherical tokamak and spheromak. Further development in magnetic technologies is needed in order to increase the magnetic field while simultaneously decreasing the mass of the magnet.

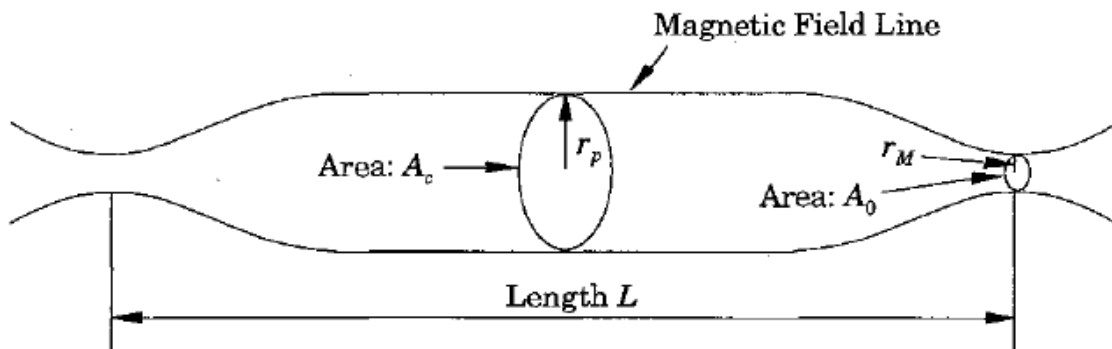


Figure 2-2: Gasdynamic Mirror[8]

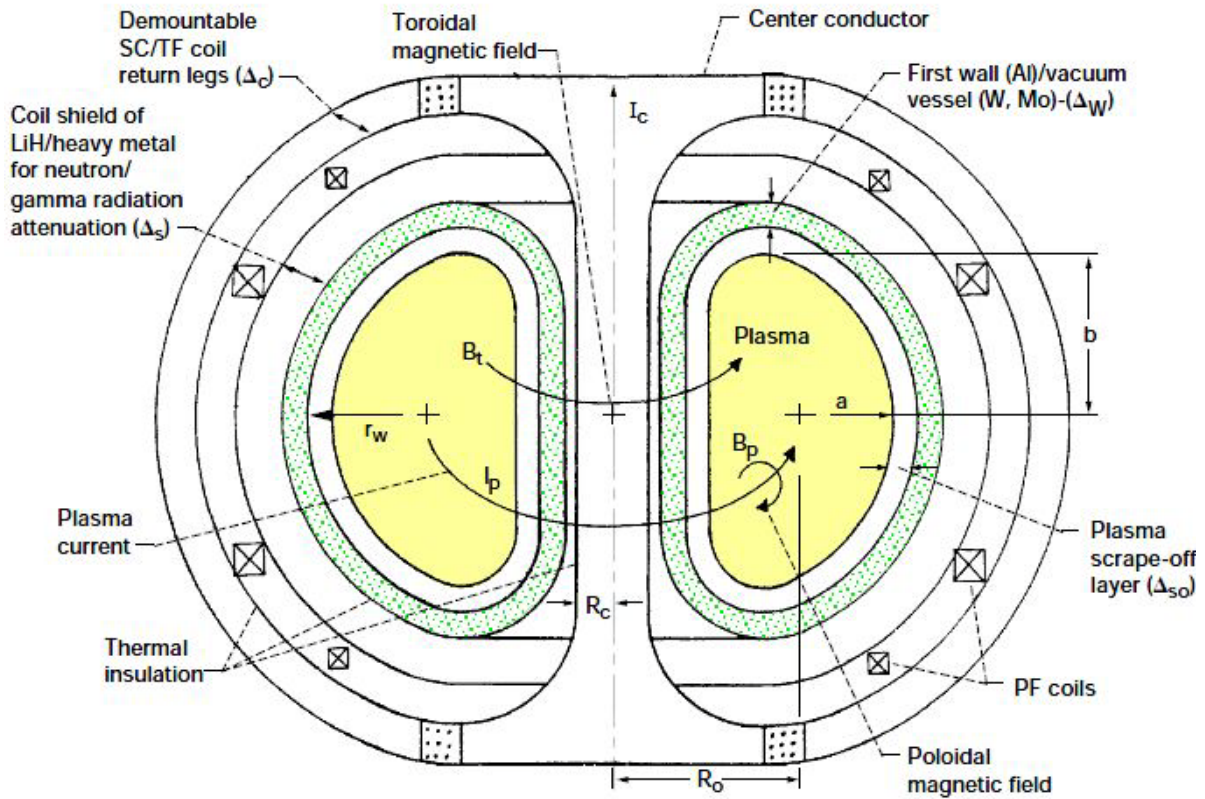


Figure 2-3: Schematic of a Spherical Tokamak Reactor System [9]

2.1.1.1 Gasdynamic Mirror

In a GDM a high density plasma is confined in an open-ended fusion system and heated to thermonuclear temperatures [8]. When the collision free path is much smaller than the length of the reactor, the sufficiently dense plasma behaves much like a fluid and can be ejected from the fusion reactor similarly to a hot gas exiting a conventional rocket nozzle. The gaseous fusion reactions are increasing in velocity in the radial direction by a strong axial magnetic field with the ends held slightly open by the much stronger magnetic fields of the magnetic mirrors. The high speed gaseous fusion reactions escaping from the exit mirror result in very high values of specific impulse.

2.1.2 Inertial Confinement

Inertial Confinement Fusion (ICF) utilizes large powerful lasers or heavy ion beams to heat and compress a pellet or hohlraum to thermonuclear ignition, and research on ICF continues at facilities for the DOE such as the Lawrence Livermore National Laboratory. Research on a vehicle for interplanetary space transport application (VISTA) powered by ICF has been ongoing for over two decades. Initial calculations utilizing VISTA indicate a round trip time of less than 145 days to Mars with 100 mT of payload [10]. Unfortunately, the laser systems needed for ICF tend to be massive and complicated, leading to a not so practical method for spacecraft propulsion system but still a good candidate for terrestrial power stations, but another method for ICF to be used for spacecraft propulsion replaces the lasers with a fission reactor in order to thermally ignite the pellets [11]. This method would not be a feasible design for terrestrial power stations because the required energy to create a fission reaction would be greater than the released energy from the fusion reaction, but if the fission reactor was relatively light weight then a fusion-fission hybrid could be used as a spacecraft propulsion system. A Schematic of an ICF system is shown in Figure 2-4.

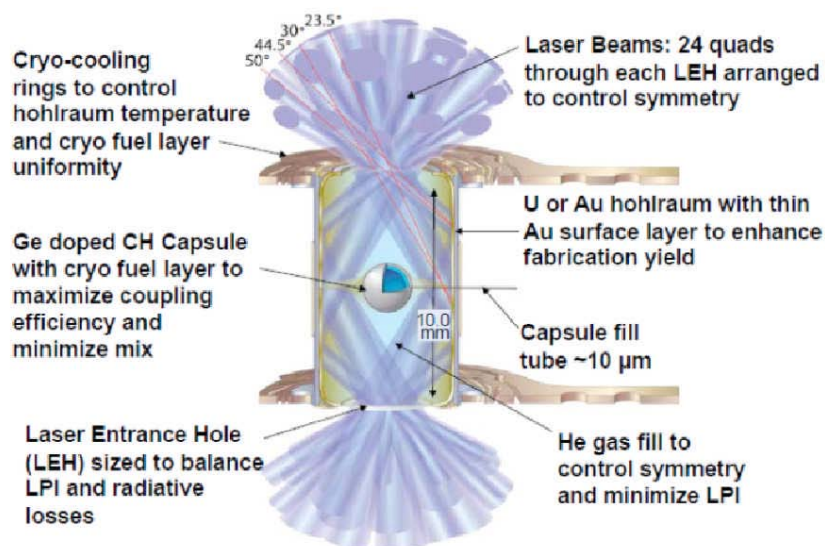


Figure 2-4: Schematic of ICF Ignition Point Design Target [12]

2.1.2.1 Fusion-Fission Hybrid

Also known as a fission-driven-fusion system, the fusion-fission hybrid system (FFHS) produces thrust at very high specific impulses by utilizing the energy produced from a fission reaction to power a fusion reaction. The fission reaction produces energy in the form of heat, and the heat is then used to raise the temperature of the plasma inside the fusion reactor in order to cause a fusion reaction. An additional advantage to a FFHS is utilizing some of the fission power to create thrust. The thrust created from a fusion reaction is relatively low; whereas the thrust created from a fission reaction can be much higher but with a lower specific impulse. Combining the thrust produced from a fusion reactor with some of the heavy particles from a fission reaction can produce a high specific impulse with a moderate thrust-to-weight ratio. This combined thrust method is referred to as a fission-augmented-fusion propulsion system [11].

2.1.3 Inertial Electrostatic Confinement

Inertial electrostatic confinement (IEC) operates by generating energetic ions from a plasma discharge and injecting the ions into a spherical vacuum vessel, where they are accelerated radially inward by a negatively biased grid-type spherical electrode. A dense central core region is formed from the energetic ions and causes fusion. This results in an extremely high power density. Unfortunately, continuous (steady-state) use of an IEC power source requires many drawbacks including grid heating and erosion. To compensate for grid heating and erosion, one solution could be to increase the grid radius and distance to the fusion core. This solution is limited by the ion-beam focusing core and the desire to minimize the structural weight of the grid [13]. Pulsed operation is another solution that also results in an increase of the fusion gain (fusion power out/electrical power in). One

suggested use of IEC is to power an ion thruster in order to produce a very high specific impulse value [6]. Figure 2-5 shows an illustration of an IEC engine system.

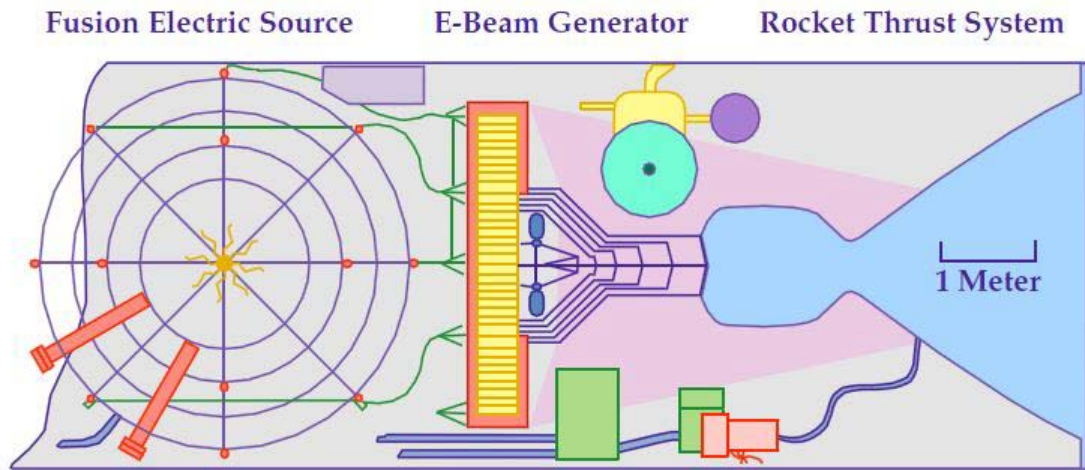


Figure 2-5: Inertial Electrostatic Confinement Engine System [6]

2.1.4 Magneto-Inertial Fusion

Magneto-Inertial Fusion (MIF) is a variant on ICF. The target consists of a magnetized plasma of fusion fuel which is compressed to thermonuclear conditions by an imploding plasma liner. Confinement is provided by the inertia of the surrounding liner, while the presence of the magnetic field traps the electrons, suppressing thermal conduction losses [7]. This latter feature lowers the power required by the drivers for the liner implosion. MIF operates in a physics regime in between the low density (10^{20} m^{-3}) MCF and high density (10^{32} m^{-3}) ICF concepts [14]. The relatively high density (comparable to densities between air and water) results in reacting volumes that are much smaller than MCF. These attributes avoid the use of massive reacting volumes and superconducting coils compared to ICF and similarly sized high power lasers in ICF, thus reducing the mass of the system significantly. Variants are commonly classified according to the driver for the imploding liner. Solid liner magnetized target fusion (MTF) utilizes a metal liner in which an axial current and self-induced magnetic field implode and compress a field reversed

configuration plasma [15]. MTF has been suggested as a simpler, cheaper, and less massive alternative fusion propulsion system [16]. Plasma liner MIF replaces the solid liner with an imploding plasma liner. Other types include z-pinch and θ -pinch. In most cases, MIF drivers involve electromagnetic acceleration driven by pulsed power. Other types of MIF propulsion systems include pinches such as the z-pinch and θ -pinch.

2.2 Fusion Fuels

Since fusion involves nuclei of lighter elements to fuse together to create nuclei of heavier elements, the initial fuels used for fusion would be located at the top of the periodic table. A rigorous analysis of the fusion fuels is beyond the scope of this thesis. However, for completeness, we provide a brief summary of some of the more important reactions. Table 2-1 lists the amount of released energy for each of the mainstream fusion reactions being considered for fusion propulsion. Table 2-2 describes how the secondary reactions from a fusion reaction involving deuterium can have a dramatic impact on the total energy released for a fusion propulsion system.

Table 2-1: Fusion Fuel Reactions [17]

Fusion Fuel	Chemical Equation	Energy Released (MeV)
Deuterium-Deuterium	${}^2_1\text{D} + {}^2_1\text{D} \rightarrow {}^3_1\text{T} + \text{p}^+$	4.03
(50%-50% Probability)	${}^2_1\text{D} + {}^2_1\text{D} \rightarrow {}^3_2\text{He} + \text{n}^0$	3.27
Deuterium-Tritium	${}^2_1\text{D} + {}^3_1\text{T} \rightarrow {}^4_2\text{He} + \text{n}^0$	17.6
Tritium-Tritium	${}^3_1\text{T} + {}^3_1\text{T} \rightarrow {}^4_2\text{He} + 2\text{n}^0$	11.33
Deuterium-Helium-3	${}^2_1\text{D} + {}^3_2\text{He} \rightarrow {}^4_1\text{He} + \text{p}^+$	18.3
Helium-3-Helium-3	${}^3_2\text{He} + {}^3_2\text{He} \rightarrow {}^4_2\text{He} + 2\text{p}^+$	12.9
Proton-Lithium-6	$\text{p}^+ + {}^6_3\text{Li} \rightarrow {}^4_2\text{He} + {}^3_2\text{He}$	4.02
Proton-Boron-11	$\text{p}^+ + {}^{11}_5\text{B} \rightarrow 3{}^4_2\text{He}$	8.7

Table 2-2: Catalyzed-Deuterium-Deuterium with 100% burnup of Tritium and Helium-3 [17]

	Chemical Equation	Energy Released (MeV)	
Primary Reactions	${}^2_1\text{D} + {}^2_1\text{D} \xrightarrow{50\%} {}^3_1\text{T} + \text{p}^+$	4.03	proton branch
	${}^2_1\text{D} + {}^2_1\text{D} \xrightarrow{50\%} {}^3_2\text{He} + \text{n}^-$	3.27	neutron branch
Secondary Reactions	${}^2_1\text{D} + {}^3_1\text{T} \rightarrow {}^4_2\text{He} + \text{n}^-$	17.6	Tritium Reaction
	${}^2_1\text{D} + {}^3_2\text{He} \rightarrow {}^4_2\text{He} + \text{p}^+$	18.3	Helium-3 Reaction
Result	$6{}^2_1\text{D} \rightarrow 2{}^4_2\text{He} + 2\text{p}^+ + 2\text{n}^+$	43.2	

2.3 Fusion Propulsion Trajectory Analysis

Trajectory analysis of rendezvous and round trip probe missions to other planets such as Mars were first conducted shortly after satellites were capable of being sent into space [18]. These early trajectory analyses utilized the patched conics approximation in which the trajectory is divided into parts in order to solve the parts with two-body equations. They also required calculating ΔV values with impulsive trajectory maneuvers rather than finite maneuvers. This was expectable at the time because chemical propulsion typically involves “burn” times that are much shorter than trip times. The results from these early trajectory analyses indicated that extremely high ΔV (change in velocity) values were needed for very short trip times to other planets. A chemical propulsion system that is able to satisfy the extremely high ΔV requirement for a very short trip time is nearly impossible prohibitively large. This realization invoked the need for trajectory analysis on more advanced propulsion systems than chemical systems. Unfortunately, these advanced propulsion systems (i.e. electrical, nuclear) have much lower thrust-to-weight ratios causing “burn” times to be much longer than chemical propulsion systems. New trajectory analysis calculations needed to be created in order to include the extremely long “burn” times from the more advanced propulsion systems; and because of the availability of computers at the time, the equations also needed to be simple enough to be calculated by hand. This resulted in equations free

from gravitational influences referred as equations in gravity-free space [2]. Estimating the spacecraft propulsion system performance values in gravity-free space is still used today for determining initial propulsion characteristics and is utilized in Chapter 4 of this document in order to calculate the trip time of the Fusion Propulsion spacecraft from Earth to Saturn. Optimization software packages for extremely long “burn” times were then developed as the availability of computers became more accessible. These packages become known as Low Thrust Trajectory Tools (LTTT) because the thrust values involved with extremely long “burn” times are typically much less than traditional chemical propulsion systems (when dealing with the thrust-to-weight ratio). NASA currently utilizes several different types of LTTT with many available for academic and commercial use. Descriptions of each of the LTTT currently utilized by NASA are available on the Glenn Research Center’s Space Flight Systems website (<http://spaceflight systems.grc.nasa.gov/SSPO/ISPTProg/LTTT/>). One of the first LTTT first used by the Jet Propulsion Laboratory (JPL) was the program VARITOP developed by Carl Sauer. It is also the trajectory program used for all the round trip missions to Jupiter’s moon Callisto described in Ref. [19]. The trajectory analysis conducted in this Technical Publication (TP) is one of the most detailed to date for fusion propulsion systems and further discussion is included in 2.3.1 of this document.

2.3.1 Trajectory Analysis from NASA TP-2003–212691

The NASA Technical Publication 2003-212691 entitled “Conceptual Design of In-Space Vehicles for Human Exploration of the Outer Planets” depicted an Earth-to-Callisto mission for several different propulsion systems as well as different amounts of stay time at Callisto for the same propulsion system [19]. Trajectory analyses were also conducted on the MTF propulsion system utilizing both deuterium-deuterium and deuterium-helium-3

propellants. The maximum mission time of 650 days (not including Earth escape and capture) was chosen for the MTF propulsion system in order to ensure a minimum distance of 1 astronomical unit (AU) from the Sun. Missions longer than 650 days typically resulted in distance less than 1 AU from the Sun resulting in an increase in radiation exposure for the crew. The two magnetoplasmadynamic (MPD) systems included in this TP required mission times well over 1000 days and also required a secondary cargo vehicle to be launched in advanced of the crew vehicle. Also, slightly different setups in VARITOP were required for the two different propulsion systems. It should be noted that a similar study was conducted in 2010 utilizing pulsed z-pinch propulsion for a human piloted Mars mission [20].

2.3.1.1 VARITOP Setup

VARITOP is a two-body analysis tool capable of being used during the heliocentric phase of a spacecraft's trajectory. During this phase, planets are assumed to be massless, but the program is capable of optimizing several variables such as departure date, flight time, and power required. During the planetary capture phase of the trajectory, the program is capable of constructing one spiral maneuver around the target body. Unfortunately, the missions required two spiral trajectories, one around Jupiter and the other around Callisto. The combined ΔV for both the Jupiter and Callisto spiral trajectories was calculated by computing the ΔV value for a spiral trajectory with an altitude slightly lower than Callisto. The slightly lower altitude would result in an equivalent ΔV for the combined spirals. This method was applicable for the two MPD mission but not the much faster MTF missions. A simple graph, shown in Figure 2-6, of the free-space ΔV over the impulse ΔV required versus the thrust-to-weight ratio was used to approximate the ΔV value for the MTF missions as shown in Ref. [21]. The impulsive ΔV can be calculated by knowing the altitude of the

spacecraft above the desired planet; and if the thrust-to-weight ratio of the spacecraft is also known, the [gravity] free-space ΔV value can be approximated from the dimensionless ΔV ratio.

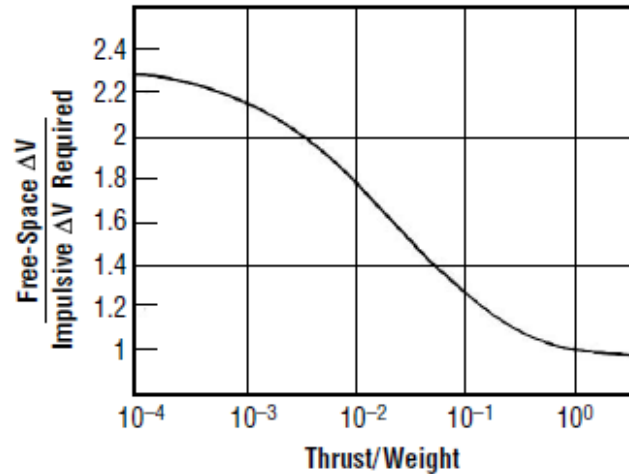


Figure 2-6: ΔV Penalty for Tangentially Directed Thrust to escape from or be captured by Planet [21]

2.3.1.2 Comparison of the MTF propulsion system missions

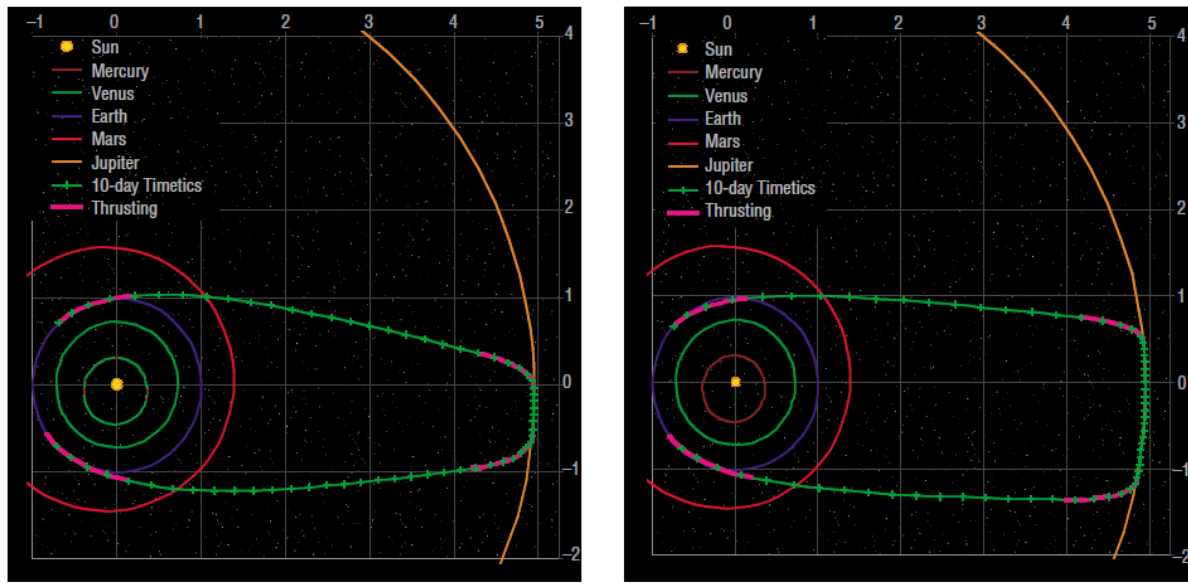
Comparing the two deuterium-deuterium configurations, a 25% decrease in flight time to Callisto will allow the stay time at Callisto to increase by a factor of six and a total “burn” time decrease of 17.8%. Unfortunately, the decrease in ‘burn’ time allowing for a longer stay time causes an increase in propellant due to the larger mass flow rate value required to increase the thrust. An additional propellant mass of 59 mT is required in order to satisfy the increase in thrust. With the increase in mass flow rate, the mass of the propulsion system also increased by more than 5.3 mT and the initial total mass by almost 111 mT. A 111 mT increase in mass may seem like a large increase, but it only increases the total initial mass by 17.2% for an increased stay time of 600%. When comparing the longer stay time of the deuterium–deuterium mission to that of a similar mission with deuterium and helium-3 propellants, configurations values are nearly identical. The total ‘burn’ time increases slightly while masses decrease slightly. Theoretically a MTF propulsion system

utilizing deuterium and helium-3 propellants has slightly better performance characteristics than a MTF propulsion system utilizing deuterium-deuterium propellant, but as previously stated deuterium-deuterium fuses at a much lower temperature than all the other fusion fuels. A MTF deuterium-helium-3 propulsion system could take many more years to develop than a deuterium-deuterium MTF propulsion system. Table 2-3 shows the configuration values for each of the three MTF missions included in this TP and Figure 2-7 shows the 2D trajectories for both MTF D-D missions. The trajectory for the MTF mission utilizing deuterium and helium-3 propellants is nearly identical to the MTF D-D for a 180 day stay time at Callisto.

Table 2-3: MTF Configuration Values

Propellant:	Deuterium-Deuterium	Deuterium-Deuterium	Deuterium-Helium-3
Departure date:	22 April 2045	26 April 2045	27 April 2045
Total Mission time:	654 days	652 days	652 days
Flight to Callisto:	331 days	249 days	249 days
Orbiting Callisto*:	33 days	183 days	183 days
Total "Burn" time:	258 days	212 days	215 days
Initial Mass:	645,173 kg	756,162 kg	691,892 kg
Payload:	163,933 kg	163,933 kg	163,933 kg
Propulsion System:	116,021 kg	121,333 kg	118,4000 kg
Propellant:	106,000 kg	165,000 kg	142,000 kg
Specific Impulse:	70,400 s	70,400 s	77,000 s
Specific Power:	45.45 kW/kg	45.45 kW/kg	51.81 kW/kg

*Orbiting time includes entire time spent in the SOI of Callisto with stay times at 30 and 180 days.



(a) 30 day stay time (b) 180 day stay time
 Figure 2-7: 2D Trajectory of MTF D-D for Earth to Callisto Round Trip Mission [19]

2.4 Continued Development

This document included a brief description on some of the major fusion confinement methods. There are many other confinement methods not mentioned in this document that are being considered for spacecraft propulsion. Also not discussed in this document is nozzle design. Many of the fusion confinement methods rely on a nozzle to expel the exhaust just like chemical propulsion systems. Unfortunately, the exhaust temperature in a fusion system is typically several magnitudes higher than the exhaust temperature in a chemical system. Thus, fusion propulsion systems would cause traditional metal nozzles to ablate much more quickly than the mission duration; so, a fusion propulsion system must rely on a nozzle formed from magnetic field lines [22]. Research and studies on all aspects of fusion propulsion must continue in order to demonstrate its usefulness for traveling great distances in relatively short periods of time. The following chapters of this document discuss one method to illustrate the significance of a fusion propulsion system for an extremely short trip time to Saturn and beyond.

CHAPTER III

GENERAL MISSION ANALYSIS TOOL (GMAT) SOFTWARE

General Mission Analysis Tool (GMAT) is a mission trajectory software tool developed by NASA and the private industry in order to contribute to the mission analysis industry [3]. Other organizations include the Air Force Research Laboratory, Computer Science Corporation, Honeywell Technology Solutions Inc., and Boeing LTS. It is a free and an open source software package available for download at <http://gmat.gsfc.nasa.gov/>. The software can be run on Windows (XP, Vista, 7), Mac OS X (10.6), and Linux operating systems.

3.1 Background History

NASA's Goddard Space Flight Center (GSFC) in part with Thinking Systems, Inc. publicly released GMAT on 24 August 2007. Leading up to the initial public release, GSFC and Thinking Systems were developing the software for over four years. GMAT was released under the NASA Open Source Agreement Version 1.3. Since GMAT's initial release, three other revisions have been released to the general public. The second release occurred just a few months after the initial release on 10 December 2007. The release contained 55 bug fixes, improved error messages, and expanded architectural specifications. On 30 September 2008, the third release of GMAT became available to the general public

fixing 68 bugs, object plug-in capabilities, and more improved error messages. The fourth and current release (as of February 2012) of GMAT was released to the general public on 29 April 2011. This release has over 100,000 lines of code added to the source code, includes 798 bug fixes, and has been through 6216 system test. Also, nine developers contributed to the source code from four organizations. The 2011 release, titled GMAT 2011a, was the first release to include the year and a letter revision in the title. This revision was intended to be the first in a series of releases occurring approximately every six months with either “a” “b” following the year in the title to indicate a fall or spring release. Since GMAT’s last release, the build team at GSFC has been focusing on NASA’s formal certification process in order for GMAT to be used for actual operations. A fifth release, GMAT 2012a, is scheduled for release on 28 May 2012 and will form the baseline tests for the formal certification.

3.2 GMAT Architecture

The program language chosen for the GMAT source code was C++. The advantage of C++ over other programming languages, such as C, is the use of a graphical user interface (GUI) through object-oriented programming. The GMAT architecture is divided into sections called packages and then further divided into subpackages. The package level consists of Program Interfaces, Engine, Model, and Utilities [23]. A flow chart of GMAT’s architecture is shown in Figure 3-1

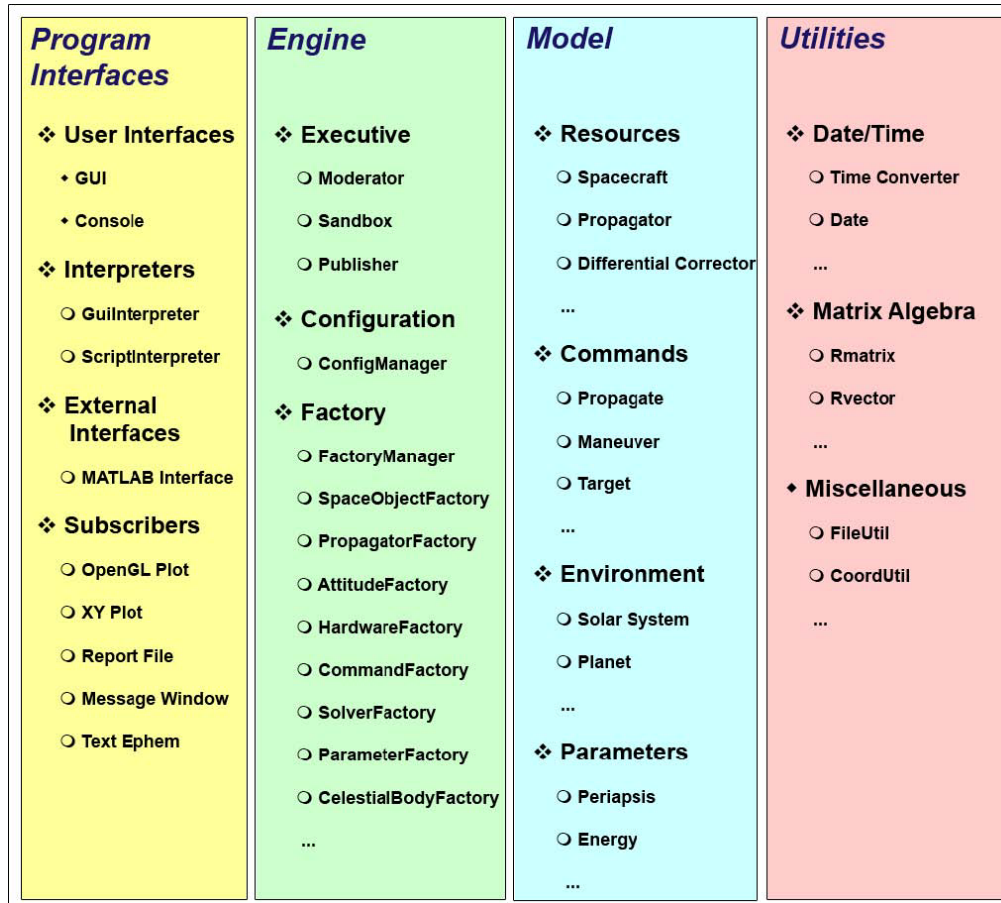


Figure 3-1: GMAT Architecture Flow Chart [23]

3.2.1 Program Interface

The Program Interface package is a two-way communications package between users, external programs, and GMAT. Its subpackages are User Interface, Interpreters, External Interfaces, and Subscribers.

3.2.1.1 User Interfaces

Users access GMAT through the GUI where all the features of GMAT are accessible. GMAT utilizes the wxWidgets cross-platform library allowing the GUI portion of the source code to be compiled over multiple operating systems. Features can also be altered, added, or deleted in the text based script that GMAT creates when a new mission is started. The text based script follows a similar command syntax structure as in MATLAB®. All changes

made in the GUI are stored in the text based script when the User saves the mission. Also, a feature new to GMAT 2011a places GUI/script indicator on the GUI toolbar notifying the User when the GUI settings do not match the settings stored in the script file. Figure depicts the GMAT GUI at startup along with the GMAT Welcome Page.

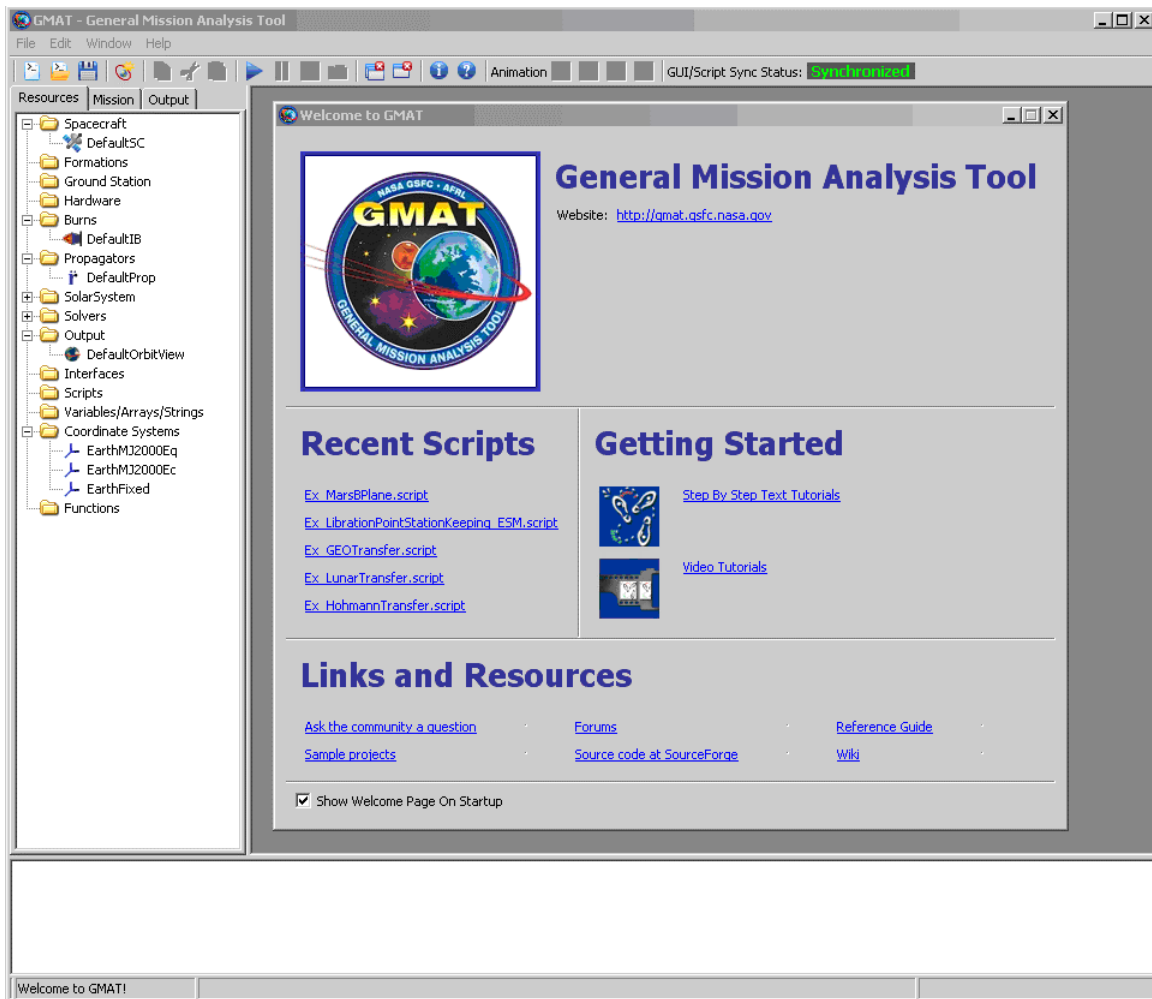


Figure 3-2: Screenshot of GMAT GUI at Startup

GMAT also has a console version that can be used to run multiple scripts at once. Unfortunately, the console version is only used for testing purposes where the GUI is not needed and is not available for public use.

3.2.1.2 Interpreters

The Interpreter subpackage contains two interpreters. The GUI interpreter is designed to communicate messages between the GUI and GMAT engine. The Script interpreter is designed to interpret script files into messages for the engine and serialize the components in the engine into script form in order to save the components to the script file.

3.2.1.3 External Interfaces

GMAT has the ability to communicate to external programs through the External Interfaces subpackage. Currently, the only external interface incorporated into the GMAT source code is an interface for MATLAB®.

3.2.1.4 Subscribers

The Subscriber subpackage contains the elements (subscribers) that Users use to view the results of a mission executed by GMAT. The subscribers include generated views of the spacecraft trajectory (known as OrbitView), plots of mission parameters (known as XYPlot), and reports of mission data in text file form (known as Report).

3.2.2 Engine

The engine controls the model of flight dynamics in GMAT as well as management structures for the program. This package is divided into three subpackages, the executive, configuration, and factory.

3.2.2.1 Executive

The Executive subpackage is composed of three components. The central processing component (known as the Modulator) receives messages containing tasks from the interpreters and determines the actions that need to be taken based on the messages. The Modulator will then send the message to one of the other engine components in order to

accomplish the requested task. A workspace known as the Sandbox is setup by the Modulator in which mission control sequences are run. Data generated by the Sandbox is passed to the Publisher before being sent to one of the corresponding Subscribers previously mentioned in the Subscribers subpackage.

3.2.2.2 Configuration

The configuration is a repository storing model components created by the User. The stored components are accessed by the Configuration Manager only when requested by the Modulator. The Configuration Manager also adds models to the configuration when needed and clears the configuration for a new mission.

3.2.2.3 Factory

The Factory subpackage is responsible for processing requests for new model components before be stored in the configuration. This subpackage contains a factory manager and a collection of factory classes used to create specific types of model components. The Factory Manager receives messages from the Modulator and determines the corresponding factory class in order to create the correct model component. Once the component has been created, the Factory Manager sends the component to the Modulator.

3.2.3 Model

The model package contains the objects that are used to model the elements of the mission simulation. The objects in the model package are available to the User for selection and/or input. The model package is separated into four subpackages, environment, resources, commands, and parameters.

3.2.3.1 Environment

The environment subpackage contains solar system information regarding all nine planets, the Sun, and the Moon which include ephemeris data and atmospheric and gravity models. It can also contain user defined “Special Points” such as Barycenters and Lagrange Points (Liberation Points). Also new to GMAT 2011a, Users can define other celestial bodies such as moons, asteroids and comets. User-defined celestial body ephemeris data are either input by hand or by an existing ephemeris file supplied by JPL from their Navigation and Ancillary Information Facility (NAIF) (<http://naif.jpl.nasa.gov/naif/index.html>). Ephemeris data obtained from NAIF is in the form of a SPICE (Spacecraft Planet Instrument C-matrix Events) file (.bsp file extension). Ephemeris data is just one of many different types of SPICE files (indicated by the name) available to the public from the NAIF. The eleven default celestial bodies in GMAT utilize the de405 (development ephemeris) SPICE file from the NAIF. This SPICE file can be utilized from the year 1600 A.D. to 20 February 2201. See APPENDIX A for more information on SPICE files.

3.2.3.2 Resources

All model objects (excluding environment objects) available on the Resources tab of the GUI are part of the resources subpackage. Once selected by the User, these model objects (resources) are stored in the configuration subpackage. Resources include spacecraft properties (initial orbital elements, attitude, ballistic/mass, fuel tank, and actuator/thruster), propagators, solvers (ordinary differential equation, differential corrector, optimizer, simulator, and estimator), outputs (orbital view, plot, report, ephemeris file), and coordinate systems.

All propagators utilize the same equation of motion. If a term is not utilized in the equation of motion, then its value is set to zero. The equation of motion (acceleration) for a spacecraft in GMAT is depicted in Equation (3-1), and the terms are described in Table 3-1 [24].

$$\begin{aligned} \frac{d^2 \mathbf{r}}{dt^2} = & -\frac{\mu}{r^3} \mathbf{r} + \nabla \phi_{sj}^0 + G \sum_{\substack{k=1 \\ k \neq j}}^n m_k \left(\frac{\mathbf{r}_{ks}}{r_{ks}^3} - \frac{\mathbf{r}_{ks}}{r_{kj}^3} \right) \\ & + \frac{\dot{m}_s}{m_s} \frac{d\mathbf{r}}{dt} - \frac{1}{2} \rho v_{rel}^2 \frac{C_d A}{m_s} \hat{\mathbf{v}}_{rel} + \frac{P_{SR} C_R A_{\odot}}{m_s} \hat{\mathbf{r}}_{s\odot} \end{aligned} \quad (3-1)$$

Table 3-1 Description of Equation of Motion Terms [24]

Term	Description
$-\frac{\mu}{r^3} \mathbf{r}$	Central Body Point Mass
$\nabla \phi_{sj}^0$	Central Body Direct Nonspherical Perturbation
$G \sum_{\substack{k=1 \\ k \neq j}}^n m_k \left(\frac{\mathbf{r}_{ks}}{r_{ks}^3} \right)$	Direct Third Body Point Mass Perturbation
$G \sum_{\substack{k=1 \\ k \neq j}}^n m_k \left(-\frac{\mathbf{r}_{kj}}{r_{kj}^3} \right)$	Indirect Third Body Point Mass Perturbation
$\frac{\dot{m}_s}{m_s} \frac{d\mathbf{r}}{dt}$	Spacecraft Thrust
$-\frac{1}{2} \rho v_{rel}^2 \frac{C_d A}{m_s} \hat{\mathbf{v}}_{rel}$	Atmospheric Drag Perturbation
$\frac{P_{SR} C_R A_{\odot}}{m_s} \hat{\mathbf{r}}_{s\odot}$	Solar Radiation Pressure Perturbation

User inputs are the coefficient of drag (C_d), coefficient of reflectivity (C_R), and the area exposed to the Sun (A_{\odot}). The drag coefficient can be determined experimentally (usually in a wind tunnel with a scaled model), through a computational fluid dynamics computer program, or extrapolated from data of similar spacecrafts. The default value for the drag coefficient in GMAT is 2.2. The coefficient of reflectivity has a value between zero and two; a value of zero indicates the spacecraft is translucent to solar radiation, a value of 1.0

indicates that all of the solar radiation is absorbed by the spacecraft (i.e. black body), and a value of 2.0 indicates that all of the solar radiation is reflected by the spacecraft (i.e. ideal value for solar sail) [25]. Most spacecrafts have a coefficient of reflectivity value between 1.0 and 2.0 and changes slightly over time. The default values in GMAT for the coefficient of reflectivity and the area exposed to the Sun are 1.5 and 1 m^2 and remain constant values because it is virtually impossible to predict when the values will change. The universal gravitational constant (G) has a value of $6.673 \times 10^{-11} \text{ Nm}^2/\text{kg}^2$ [26] or $6.673 \times 10^{-11} \text{ km}^3/\text{kg s}^2$ and knowing the mass of the central body (M), the gravitational parameter (μ) can be calculated by multiplying the two values, as shown in Equation (3-2) [27].

$$\mu = MG \tag{3-2}$$

The central body direct nonspherical perturbation as well as the atmospheric drag perturbation are only utilized when a model is provided for the perturbation. Currently, GMAT has gravity models for the central body direct nonspherical perturbation for the celestial bodies Venus, Earth, Mars, and the Moon and two atmospheric models for the Earth with the option not to use a model. (Note: a gravity model must be selected when Earth is chosen as the primary body.) An atmospheric model provides the value for atmospheric density (ρ) for the atmospheric drag perturbation and is a function of spacecraft position relative to the Earth. The solar radiation pressure perturbation is utilized only when the checkbox is marked GUI window of the propagator or the word “On” appears after “SRP” in the “ForceModel” section of the GMAT script. (“Off” after SRP in the ForceModel section of the script indicates an unchecked box in the propagator window and a value of zero for the solar radiation perturbation in the equation of motion equation.) The equation for solar radiation pressure (P_{SR}) is shown in Appendix C.1.

The Direct and indirect third body perturbations are utilized only when additional point mass bodies are added either through the GUI or by adding PointMases to the ForceModel section of the GMAT script followed by the name or names of the available celestial body enclosed in brackets. The mass flow rate (\dot{m}) for the spacecraft thrust is calculated by dividing the thrust by the specific impulse [24] as shown in Equation (3-3).

$$\dot{m} = \frac{F_T}{V_e} \quad (3-3)$$

Inputting the thrust and specific impulse values into GMAT are discussed in Appendix C.1.

Ordinary differential equation (ODE) solvers are accessible in the integration section of the GUI propagator window or in the propagator section of a GMAT script. These solvers are used to calculate the other state values (velocity and position) for a spacecraft in GMAT. Several methods for solving ODEs are available in GMAT as well as a solver capable of propagating a spacecraft with an attached SPICE when a SPICE file is loaded and the SPK (spacecraft) integrator type is selected. Runge-Kutta 8(9) is the default ODE solver for GMAT. (Note: two digit ODE solvers indicate a variable step size by comparing the solution from two different orders such as the 8th and 9th order of a Runge-Kutta method [28].) SPICE is described in detail in APPENDIX A while the coefficient values for Runge-Kutta 8(9) are shown in Appendix C.3. GMAT also has one differential [predictor-] corrector method, the Adams-Bashforth-Moulton method. A predictor-corrector method is a two step method in which the value(s) is predicted with an equation or series of equations and then is corrected with a second equation or series of equations. The predicted value(s) is always utilized in the correction equation(s). The Adams-Bashforth-Moulton method is a modified version of the multistep Adams-Bashforth method in which a corrector equation has been

added [28][29]. (Note: a multistep method utilizes the results from two or more previous steps vs. a one-step method that only utilizes the previous result. Also, a multistep method is not self-starting and must utilize a one-step method until enough previous results are calculated.) Figure 3-3 shows the propagator window from GMAT with the default settings.

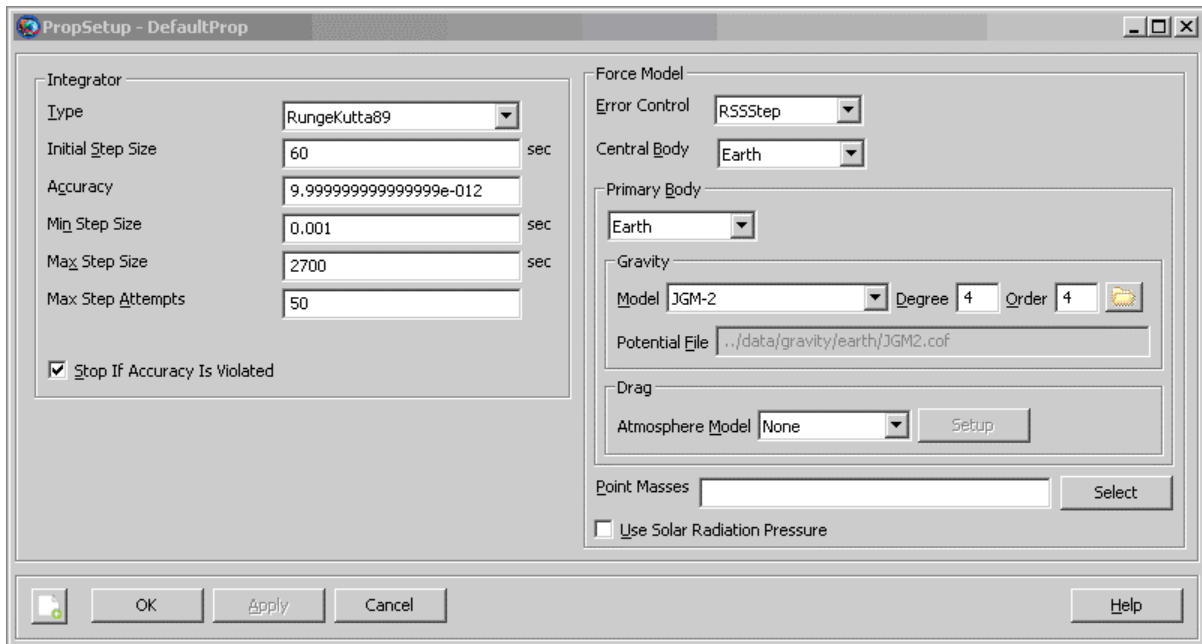


Figure 3-3: Propagator Window with Default Settings

3.2.3.3 Commands

The mission control sequence in GMAT determines how the spacecraft (or spacecrafts) is controlled over time. Commands determine the evolution of the spacecraft(s) and operate in sequential order. Some commands can include nested branching requiring further user input. A single operation command is referred to as a regular command and includes the Propagate and Maneuver commands. Solver commands, such as the Target command, utilize nested branching. Other types of commands available in GMAT are Control Logic commands used to perform control flow operations and Function commands used to call a function in GMAT or a function for an external program such as MATLAB®.

3.2.3.4 Parameters

Parameters are data calculations from the analysis of the spacecraft trajectory, orientation and mission goals. They can be used in Report files or (more importantly) in the Propagate command. Examples of parameters include periapsis, apoapsis, velocity magnitude (VMAG), distance from the center of a celestial body (RMAG), and altitude. The fuel mass left in a fuel tank is also a parameter but has been left out of the default Parameters list when selecting a parameter in a Report File or Propagate command. In order to resolve this issue, a simple solution of just creating a variable called FuelMass in the resource Variables/Arrays/Strings is needed. The FuelMass variable is then used in the on the left side of the Equation command on the mission control sequence with the DefaultSC.FuelTank1.FuelMass on the right side of the Equation command, where DefaultSC is the name of the spacecraft, and FuelTank1 is the name of the fuel tank. Other parameters also may not be included in the parameters list. Gregorian dates cannot be used in the propagator command. If a date is specified as the parameter for a propagator, it must be in the Modified Julian form.

3.2.4 Utilities

The utility package contains subpackages that implement higher level GMAT functions. The subpackages provide basic array computations, core solar system independent calculations, and other low level computations. The utility package contains two subpackages.

3.2.4.1 Date/Time

The date/time subpackage contains a Time Convertor for converting time from coordinated universal time (UTC) to atomic time (TAI, Temps Atomique International) or

vise-versa. It can also convert time into other formats that are available in GMAT. The other formats of time include dynamical times such as terrestrial time (TT), Barycentric Dynamical Time (TDB), and Barycentric Coordinated Time (TCB). GMAT has the ability for Users to input an epoch in Gregorian format or convert an epoch to Gregorian from a Modified Julian date (MJD) as in a Report file. The MJD in GMAT is a reduction of the Julian date (JD) by 2,430,000.0. Other MJDs, such as the MJD from the Smithsonian Astrophysical Observatory (SAO), reduce the JD by another value (SAO uses 2400000.5).

3.2.4.2 Matrix Algebra

This subpackage contains functions for matrixes and vectors needed for calculations in GMAT. Some examples of functions include taking the dot product of a vector, calculating the magnitude of a vector, and multiplying a coordinate system by a rotation matrix.

3.3 GMAT Script Setup

In a GMAT script, the mission problem is defined by the components, which consist of the setup of resources, spacecraft properties, propagators, control system, variables/arrays/strings, and output. The GMAT script was built, mostly, by the GUI. A copy of the GMAT script is provided in APPENDIX B, and a description of the components is given below. Screen shots of the Resource and Mission tabs are shown in Figure 3-4. The spacecraft properties inputted into GMAT are defined in Section 4.1.

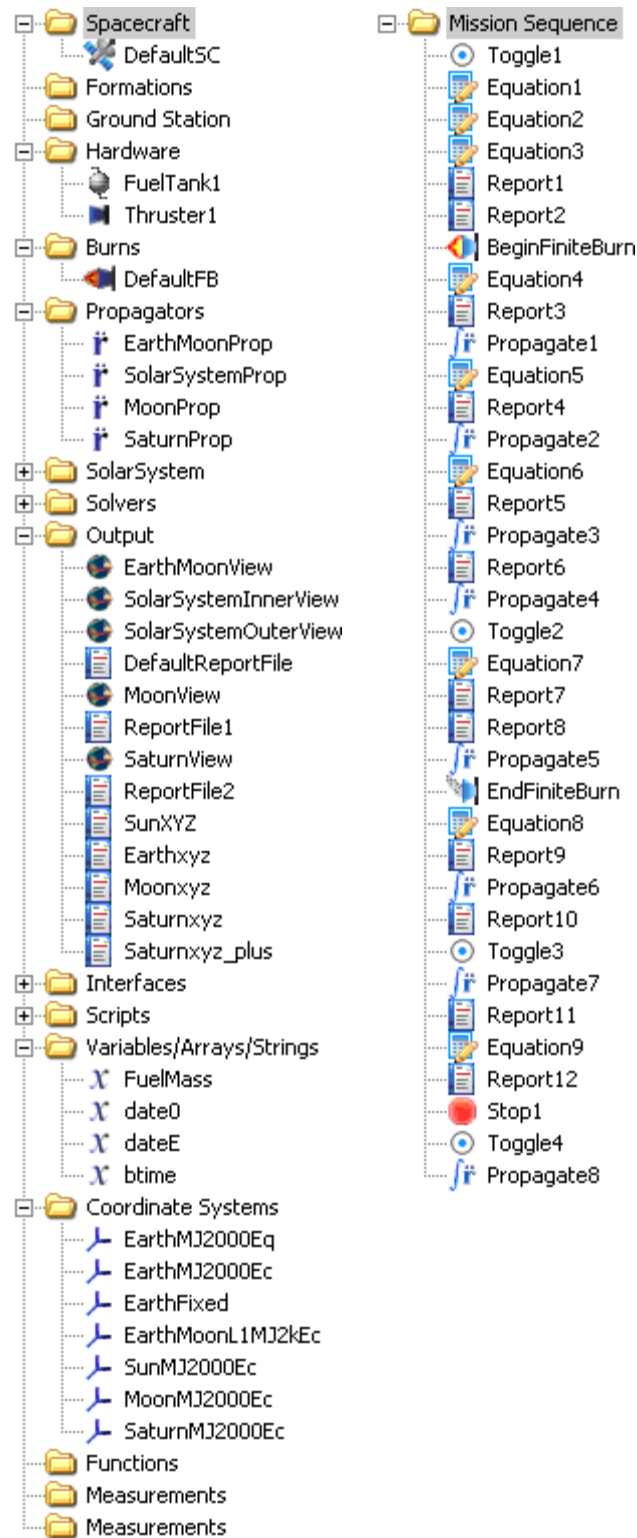


Figure 3-4: Screen shots of Resource and Mission Tabs

3.3.1 Setup of Resources

The Resource tab in GMAT contains all the properties for the spacecraft(s), propagators, output files and views, variables/arrays/strings, and coordinate systems, as well as other resources not used during this mission design. The Mission tab and Output tab rely on the information created on the Resources tab.

3.3.1.1 Spacecraft Properties

Before inputting spacecraft properties into GMAT, the Earth-Moon Lagrange Point 1 was created by adding the Lagrange point (known as Libration Point in GMAT) in the “Special Points” folder inside the “Solar System”. Once the Lagrange Point was added, a coordinate system with the origin located at the Lagrange Point was added in the “Coordinate Systems” folder located on the “Resources” tab. The coordinate system created at the Lagrange Point is a translated coordinate system of the Geocentric J2000.0 [25] ecliptic coordinate system (designated MJ2000 in GMAT). With the coordinate system created, the spacecraft initial orbit properties can be inputted into GMAT.

The initial start date of the mission (epoch) was chosen, after several iterations, to be 06 April 2025 14:04:15.000. The state type was set to Cartesian with each of the six elements (x , y , z , V_x , V_y , and V_z) set to zero kilometers and zero km/s, respectively. The chosen coordinate system was created at the Earth-Moon Lagrange Point 1. On the “Ballistic/Mass” tab of the spacecraft properties window, a value of 49,850 kg was inputted for the dry mass and the rest of settings were on this tab were left at the default settings. Table 3-2 and Table 3-3 list the values of the spacecraft properties that were inputted into GMAT on the spacecraft properties window.

Table3-2: Initial Spacecraft Orbital Elements Input

Epoch	06 April 2025 14:04:15.000		
Coordinate System	Earth-Moon L1 Translated J2000.0 Ecliptic		
State Type	Cartesian		
	X		0
Distance	Y		0
	Z		0
	V _x		0
Velocity	V _y		0
	V _z		0

Table 3-3: Spacecraft Ballistic/Mass Inputs

Dry Mass	49,850 kg	Drag Area	15 m ^{2*}
Coefficient of Drag	2.2	Solar Radiation Pressure Area	1 m ^{2*}
Coefficient of Reflectivity	1.8*		

*Default Value

In order to finish the spacecraft properties, a fuel tank needs to be created before adding a fuel tank to the spacecraft on the “Tanks” tab. Fuel tanks are crated in the “Hardware” folder located on the “Resources” tab. A 10,150 kg value was in was inputted for the fuel mass on the fuel tank properties window. The fuel density value was estimated to be 530 kg/m³ based on the density of lithium, and volume of the fuel tank could be any value larger than the volume of the fuel (fuel mass over fuel density). A value of 20 m³ was used as the input value. Temperature, reference temperature, and pressure were left at the default settings, along with pressure model set to pressure regulated. Altering these values does not have a significant change on the performance of the propulsion system. Finishing the spacecraft properties, the fuel tank is added to the spacecraft on the “Tanks” tab of the spacecraft properties window. Table 3-4 lists the input values for the spacecraft’s fuel tank properties.

Table3-4: Fuel Tank Inputs

Fuel Mass	10,150 kg	Allow Negative Fuel Mass	unchecked
Fuel Density	$530 \frac{\text{kg}}{\text{m}^3}$	Pressure	1500 kPa*
Temperature	20 °C*	Volume	20 m ³
Reference Temperature	20 °C*	Pressure Model	Pressure Regulated*

*Default Value

In order for GMAT to execute a finite burn, a thruster must be created in the “Hardware” folder located on the “Resources” tab. The thruster contains the performance properties of the propulsion system as well as the direction of the thrust created by the thruster. The coordinate system settings on the thruster properties window are left on the default settings with the coordinate system set to local, origin set to Earth, and the axes on VNB (Velocity, Normal, and Binormal). Thrust directions are inputted as a percentage of thrust in decimal form (values must be between 0 and 1). A value of 0.949 was inputted for thrust direction 1 (the Velocity or Tangent direction), and -0.051 for thrust direction 2 (Binormal direction). A negative value is used to indicate the reverse direction. Thus, thrust direction 3 is left with the default value of zero. On the thruster coefficient dialog window, the only coefficient that has a value other than the default value of zero is C1 with 102 newtons (N). Similarly on the impulse coefficient dialog window, K1 has a value of 20,000 seconds and the rest of the coefficients remain at the default value of zero. APPENDIX C shows the thrust and specific impulse equations utilizing the thrust and specific impulse coefficients. Table 3-5 lists the inputs for the spacecraft’s thruster properties.

Table3-5: Thruster Inputs

Coordinate System:	Local	Duty Cycle:	1*
Origin:	Earth	Thrust Scale Factor:	1*
Axes:	VBN	Decrement Mass:	checked
Thrust Direction 1:	0.949	Gravitational Acceleration:	$9.81 \frac{m}{s^2}$
Thrust Direction 2:	-0.051	Thrust Coefficient 1 (C1):	102 N
Thrust Direction 3:	0*	I _{sp} Coefficient 1 (K1):	20,000 seconds

*Default Value

The last step before finishing the spacecraft properties is to associate the spacecraft thruster with a finite burn. Both finite and impulse burns are created in the “Burns” folder located on the “Resources” tab. The only property listed on the finite burns property window is a dropdown menu for all available thrusters created in GMAT. Since the spacecraft only has one thruster, by default thruster 1 is chosen.

3.3.1.2 Propagators

Propagators in GMAT can be separated into two sections. The first section is the integrator. GMAT has many integrators that can be used to solve ordinary differential equations (ODE). The default integrator, Runge-Kutta89, was chosen for all the propagators used in the GMAT script for the Fusion Propulsion spacecraft mission. Other ODE solvers available in GMAT are Prince-Dormand 45 (a very common ODE), Runge-Kutta-Fehberg 56, and Adams Bashforth Moulton predictor-corrector. The coefficients for Runge-Kutta89 are shown in Appendix C.3 [30]. The other integrator settings were also left with the default values. Table 3-6 lists the default settings of the integrator.

Table3-6: List of Runge-Kutta89 Integrator Default Settings

Initial Step Size	60 seconds	Maximum Step Size	2700 seconds
Accuracy	9.999999999999999e-012	Max Step Attempts	50
Minimum Step Size	0.001 seconds	Stop if Accuracy Is Violated	checked

The second section of the propagator is the force model. In the force model section, settings such as central and primary bodies are chosen as well as gravity models and atmospheric models. The control error was one of only two settings that remained constant in the force model section for all propagators created for the GMAT script. The default setting, root sum square (RSS) Step was used for the control error. This measures error with respect to the current step. Other control error choices are RSS state, Largest Step, Largest State. The error is then compared to the accuracy setting under the integrator section. The other constant setting for all force models was the use of solar radiation pressure (SRP). This pressure induced upon a spacecraft by the Sun is typically modeled as a constant and GMAT uses this constant pressure value along with the coefficient of reflectivity and solar radiation pressure area in the spacecraft Ballistics/Mass tab on the spacecraft properties window to determine the force exerted on the spacecraft by solar radiation. Multiple propagators were used in the GMAT script in order to represent the spacecraft's location when inside a particular sphere of influence (SOI). The Earth propagator has the most sophisticated force model since it is the only propagator to include a gravity model in its force model. The other three propagators only have point masses included in the force model because only bodies with gravity models can be used in the "Primary Body" setting of the force model. Table 3-7 lists the force model settings for each propagator.

Table 3-7: Force Model Propagator Settings

Propagator→ Propagator Setting↓	Earth Prop	Moon Prop	Saturn Prop	Solar System Prop
Control Error	RSS Step	RSS Step	RSS Step	RSS Step
Central Body	Earth [*]	Luna	Saturn	Sun
Primary Body	Earth [*]	None	None	None
Gravity Model	JGM-2 [*] Degree: 4 [*] Order: 4 [*]	None	None	None
Atmospheric Model	None [*]	None	None	None
Point Masses	Luna	Luna	Saturn	Earth, Jupiter, Luna, Mars, Neptune, Saturn, Sun, Uranus, Venus
Solar Radiation Pressure	checked	checked	checked	checked

^{*}Default Value

3.3.1.3 Coordinate Systems

As previously discussed, a coordinate system at the Earth-Moon Lagrange Point 1 was created for the spacecraft's initial orbit elements. Other coordinate systems were also created in GMAT for output purposes. The default coordinate systems in GMAT are Geocentric J2000.0 Equatorial (EarthMJ2000Eq), Geocentric J2000.0 Ecliptic (EarthMJ2000Ec), and Earth-Centered Earth-Fixed (EarthFixed). The default coordinate systems cannot be removed from the “Coordinate Systems” folder in GMAT. These coordinate systems are typically used in preprogrammed GMAT equations needed for GMAT to run correctly. The GMAT script also includes a heliocentric ecliptic coordinate system (SunMJ2000Ec), a Moon centered translated J2000.0 ecliptic coordinate system (MoonMJ2000Ec), and a Saturn translated J2000.0 ecliptic coordinate system (SaturnMJ2000Ec).

3.3.1.4 Variables/Arrays/Strings

A variable named date0 was created in order to store the epoch MJD by utilizing the equation command in the mission control sequence. All variables created in GMAT must

contain a value. The equation command can overwrite the variable's value if necessary. The initial value of date0, as well as FuelMass and dateE (the date in which the propulsion system is terminated or ends) is set at a value of zero. The variable btime has a value of 225 representing the amount of time the propulsion system will run or "burn" in days.

3.3.1.5 Output

Several orbit views were created in order to visualize the trajectory of the spacecraft. The default orbit view has the Earth as the view point reference and the view direction along with the EarthMJ2000Eq coordinate system, a view point vector of [3000, 0, 0] km, and a view up direction in the z axis. This view was renamed to EarthMoonView, and the Moon and Sun were to the selected celestial objects list. The coordinate system was changed to the EarthMJ2000Ec, and the view point vector was changed to [0, 0, 1000000] km. The other orbit view major settings, as well as the EarthMoonView settings, are shown in Table 3-8. Minor settings such as drawing options do not affect the location and orientation of the view but can be when interpreting a view. Views can be suppressed or hidden by unchecking the "Show Plot" checkbox. Sometimes the number of steps for "Collect data every" needs to be altered from the default value 1. This is because all orbit views can only support up to 20,000 data points. Once the points start to exceed 20,000, trajectories will start to be erased starting with the oldest data point. This includes spacecraft trajectories as well as celestial bodies. The "Enable Stars" setting is new to GMAT 2011a and could be helpful in determining locations, but it is not needed for this mission and is left unchecked for all orbit views.

Table3-8: Orbit View Major Settings

View→ View Setting↓	Earth Moon View	Moon View	Solar System View	Saturn View
Selected Celestial Objects	Earth, Luna, Sun	Earth, Luna, Sun	Sun, Earth, Mars, Jupiter, Saturn	Sun, Saturn
Coordinate System	EarthMJ2000Ec	MoonMJ2000Ec	SunMJ2000Ec	SaturnMJ2000Ec
View Point Reference	Earth	Luna	Sun	Saturn
View Point Vector	[0, 0, 1000000]	[0, 0, 30000]	[0, 0, 1]	[0, 0, 1000000]
View Scale Vector	1	1	4000000000	1
View Direction	Earth	Luna	Sun	Saturn
View Up Direction	Earth MJ2000Ec.Y	Moon MJ2000Ec.Y	Sun MJ2000Ec.Y	Saturn MJ2000Ec.Y

Also included in the Output folder are report files. In order to output specified parameters during different parts of the mission, a report file is used to record the parameter when commanded by the mission sequence. Several report files were created for this mission, mostly, because the ephemeris file would not operate correctly in MATLAB®. (For MATLAB® to read ephemeris files written in SPICE a plug-in from JPL called MICE is needed. See APPENDIX A for more information on SPICE and MICE.) All figures in Chapter 4 were created in MATLAB® using report files from GMAT for the spacecraft trajectory and MICE to read de405 SPICE file for planetary trajectories. The report files used to create the figures in Chapter 4 are Earthxyz, Moonxyz, SunXYZ, Saturnxyz, and Saturnxyz_plus. The parameters for these report files include the x, y, and z distance in the respective coordinate system as well as the date in both Gregorian and Modified Julian and also the distance and velocity magnitude of the spacecraft in reference to the respective celestial body. When parameters are added to a report file from the Resource tab, the parameter is recorded for every propagation step. Since the SunXYZ report file is the only

report file needed to record the parameters at every propagation step, the toggle command in the mission sequence was used to toggle the other report files off and on when the spacecraft was near the respected celestial body. Two report files were used to record the spacecraft's trajectory around Saturn in order to easily separate the spacecraft's trajectory from "Before closest approach" and "After closest approach". The DefaultReportFile was used to record all other spacecraft parameters and the parameter list was emptied because the report command in the mission sequence was used to write to the file. The column width value for all report files, except the DefaultReportFile, was changed from the default value from 20 spaces to 30 spaces because the Gregorian date parameter utilizes 24 spaces. The DefaultReportFile column width was set to 35 spaces because some of the headers were over 30 spaces long. Also the text file names of the report files were changed to their respected report file names for easy identification. When renaming a report file, GMAT does not automatically change the text file name to match the report file name. The text file name matches the previous name of the report file until the User manually changes the name of the text file. (Note: the text file name does not have to match the report file name. Also, GMAT records over text files every time the mission is run.) Table 3-9 shows the settings and parameters for the five report files that record parameters for every propagation.

Table 3-9: Report File Settings

Report File→ Setting↓	SunXYZ	Earthxyz	Moonxyz	Saturnxyz	Saturnxyz _plus
write headers	unchecked	unchecked	unchecked	unchecked	unchecked
column width	30	30	30	30	30
file name	SunXYZ.txt	Earthxyz.txt	Moonxyz.txt	Saturnxyz .txt	Saturn_ plus.txt
parameters	DefaultSC.Sun MJ2000Ec.X	DefaultSC.Earth MJ2000Ec.X	DefaultSC.Moon MJ2000Ec.X	DefaultSC.Saturn MJ2000Ec.X	
	DefaultSC.Sun MJ2000Ec.Y	DefaultSC.Earth MJ2000Ec.Y	DefaultSC.Moon MJ2000Ec.Y	DefaultSC.Saturn MJ2000Ec.Y	
	DefaultSC.Sun MJ2000Ec.Z	DefaultSC.Earth MJ2000Ec.Z	DefaultSC.Moon MJ2000Ec.Z	DefaultSC.Saturn MJ2000Ec.Z	
	DefaultSC.UTC Gregorian	DefaultSC.UTC Gregorian	DefaultSC.UTC Gregorian	DefaultSC.UTC Gregorian	
	DefaultSC.UTC Gregorian	DefaultSC.UTC Gregorian	DefaultSC.UTC ModJulian	DefaultSC.UTC Gregorian	
	DefaultSC.Sun. RMAG	DefaultSC.Earth. RMAG	DefaultSC.Luna. RMAG	DefaultSC.Saturn. RMAG	

3.3.2 Setup of Mission Sequence

Before beginning the mission sequence command order in GMAT, sphere of influence radius values need to be calculated in order to be used in the propagate command. The SOI for the Earth, Saturn and the Moon were calculated with an equation developed by Laplace. The equation and the values used in the equation for each sphere of influence calculation are shown in APPENDIX D. Table 3-10 shows the calculated values of each SOI used in the propagate commands in GMAT.

Table 3-10: Calculated Radius of Sphere of Influence Values

Celestial Body:	Earth	Saturn	Moon
Radius:	924,217 km	54,796,292 km	66,183 km

The first several commands in the mission sequence are not related to initiating the mission but are needed for logistics and analysis. A toggle command is the first command in the mission sequence. The toggle command toggles off the report files Saturnxyz and

Saturnxyz_plus as well as the orbit view SaturnView. A series of equation commands are next. The first equation command writes the initial fuel mass value to the variable FuelMass. Equation (3-4) depicts the setup of the equation command. This equation is repeated several times throughout the mission sequence in order to record fuel mass left in the tank at periodic stages in the spacecraft's trajectory.

$$\text{FuelMass} = \text{DefaultSC.FuelTank1.FuelMass} \quad (3-4)$$

The next two equations are used for calculating the date and time when the propulsion system is shutdown. At the moment the propulsion system is shutdown, the spacecraft leaves its acceleration phase and enters its cruise phase. The first equation command records the initial epoch in UTC MJD format into the value for the variable date0. The second equation adds the variable value btime (225 days) with the value of date0 and records the calculated value as dateE. Equation (3-5) and Equation (3-6) depict the equation commands for determining the termination date of the propulsion system.

$$\text{date0} = \text{DefaultSC.UTCModJulian} \quad (3-5)$$

$$\text{dateE} = \text{date0} + \text{btime} \quad (3-6)$$

The last command in the mission sequence before initiating the mission is a report command. The report command writes to initial position and velocity of the spacecraft and their respective magnitudes as well as the values of the variables calculated in the previous equation commands. Table 3-11 lists the parameters used in the first report command of the mission sequence. The layout of this parameter list is repeated for every report command used in the mission sequence.

Table 3-11: Parameter List of First Report Command

DefaultSC.Earth.RMAG	DefaultSC.UTCGregorian
DefaultSC.Earth.Altitude	DefaultSC.Sun.RMAG
DefaultSC.EarthMJ2000Ec.X	DefaultSC.SunMJ2000Ec.X
DefaultSC.EarthMJ2000Ec.Y	DefaultSC.SunMJ2000Ec.Y
DefaultSC.EarthMJ2000Ec.Z	DefaultSC.SunMJ2000Ec.Z
DefaultSC.EarthMJ2000Ec.VMAG	DefaultSC.SunMJ2000Ec.VMAG
DefaultSC.EarthMJ2000Ec.VX	DefaultSC.SunMJ2000Ec.VX
DefaultSC.EarthMJ2000Ec.VY	DefaultSC.SunMJ2000Ec.VY
DefaultSC.EarthMJ2000Ec.VZ	DefaultSC.SunMJ2000Ec.VZ
FuelMass	date0
DefaultSC.UTCMODJulian	dateE

The beginning of the actual mission starts with the Begin Finite Burn command and is followed with a propagate command with the propagator set to MoonProp and the parameter set to periapsis of the Moon (DefaultSC.Luna.Periapsis). An equation command utilizing Equation (4-8) is inserted after the first propagate command in order to record the fuel mass left in the fuel tank. A report command follows the equation command with a parameter list similar to the list in Table 3-11. This sequence of propagate command, equation command, and report command is repeated several times until the spacecraft reaches the edge of the Earth's SOI. The second propagate command still utilizes the MoonProp propagator and has a parameter of distance from the center of the Moon (DefaultSC.Luna.RMAG) and a condition value equal to the radius of the SOI of the Moon (66,183 km). The third and fourth propagator commands utilize the EarthMoonProp propagator with a parameter value set to Earth periapsis (DefaultSC.Earth.Periapsis) and distance from the center of the Earth (DefaultSC.Earth.RMAG) with condition value equal to the radius of the SOI of the Earth (924,217 km). After the report command following the fourth propagate command, a toggle command was used to toggle off the Moon orbital view, the EarthMoon orbital view and the report files Earthxyz and Moonxyz.

At this point the spacecraft has left the Earth's SOI and has entered the Sun's SOI. The propagate commands will utilize the SolarSystem Prop propagator until the spacecraft reaches the SOI of Saturn. Before the End Finite Burn command can be utilized, the spacecraft is propagated to the dateE variable value (30997.08628472222 MJD) of 17 Nov 2025 14:04:15.000 UTC in the Gregorian date format. An equation command subsequently records the value of the fuel mass left in the tank and outputs the value in a report command with other spacecraft parameters. This is the last equation command used in the mission sequence. The spacecraft has now entered the cruise phase of its trajectory and the fuel mass left in the tank will remain at 43.57798158902733 kg. A propagate command is then used to move the spacecraft to the edge of Saturn's SOI (54,796,292 km) with a distance from the center of Saturn parameter (DefaultSC.Saturn.RMAG) and condition value equal to 54,796,292 km. A report command then records the spacecraft parameters to the Default Report File. The spacecraft is now inside the SOI of Saturn and will require the SaturnProp propagator to be used with the propagation commands.

The next step in the mission sequence is to toggle on the Saturn orbital view (SaturnView) and the report file Saturnxyz with the toggle command. A propagate command utilizing the Saturn periapsis parameter (DefaultSC.Saturn.Periapsis) propagates the spacecraft to the closest approach (CA) to Saturn. Once again, a report command follows the propagate command to record spacecraft parameters to the Default Report File. This is the end of the fly-by mission to Saturn, but a toggle command and a propagate command were used to toggle on the Saturnxyz_plus report file and move the spacecraft to the edge of Saturn's SOI.

A few additional commands were appended to the end of the mission sequence in order to track the spacecraft to a distance of 1000 AU from the Sun. See Appendix B.1 for the appended commands used to propagate the spacecraft to a distance of 1000 Au from the Sun.

CHAPTER IV

MODELS

4.1 Spacecraft Design

The spacecraft used for all trajectory models developed in GMAT was optimized for a fly-by of Saturn. The planet Saturn was chosen because the spacecraft's trajectory can be compared to the recent and ongoing Cassini-Huygens robotic Saturn mission.

Four main spacecraft parameters were predetermined from reasonable qualities that should be obtainable by the spacecraft's launch date in the year 2025. The first parameter, specific power, is the power output over the mass of the system, usually denoted α . Typical first generation fusion propulsion systems are estimated to be in the 1 to 10 kW per kg range, so 1 kW/kg was chosen to be conservative [2] for the relatively soon launch date of 2025. The second predetermined spacecraft parameter is the payload mass ratio, denoted by λ . The payload mass ratio represents the payload mass divided by the difference of total mass and the payload mass. A value of 0.2 is a typical value used for a fusion propulsion fly-by mission. The other two predetermined spacecraft parameters are mass values. Mass estimates for fusion systems are highly mission dependent and subject to speculation, since there are no working fusion propulsion systems. For this study, 60 mT was set as the mass constraint for the entire vehicle because it could be conceivably deployed in orbit by a single

heavy-lift launch vehicle. For $\lambda = 0.2$, this sets the payload mass at 10 mT. Details of the payload are beyond the scope of this study. We also constrained the propulsion system to 10 mT, leaving 40 mT for structural mass and fuel. The validity of this choice must be reevaluated as the field of fusion propulsion progresses. All the other spacecraft design parameters are derived from these four predetermined spacecraft design parameter values.

The first design parameter calculated was an approximate value for trip time. A field-free space equation was used where only the specific power and payload mass ratio are the spacecraft design parameters needed [2]. Also, the straight-line distance from Earth to Saturn, denoted R, is needed in the equation. The equation used to approximate trip time is

$$t_{\text{trip}} = \frac{3}{2} \left[\frac{2R \sqrt{\frac{1}{2\alpha}}}{1 - \sqrt{\lambda}} \right]^{\frac{2}{3}} \quad (4-1)$$

where

- t_{trip} = total trip time
- R = straight-line distance from Earth to Saturn, 10.58 AU
- α = specific power, 1 kW/kg
- λ = payload mass fraction, 0.2

The straight-line distance includes both the average distances from the Sun to the Earth and the Sun to Saturn. The justification for including both distances is that the Earth will be on the opposite side of the Sun from Saturn's position at closest approach when the spacecraft begins its mission. The approximate trip time calculated by Equation (4-1) is 441 days* and was rounded up to 450 days. An assumption that half of the trip time includes the accelerating phase of the mission was also used in determining the other spacecraft design parameters. With this assumption, the propulsion run time (burn time) becomes 225 days. Knowing the specific power and the burn time, the specific impulse can be calculated.

*Step-by-step calculation is shown in APPENDIX E.

Utilizing the definition for specific power, Equation (4-2), the definition of jet power, Equation (4-3), and the definition of specific impulse, Equation (4-4), an equation for calculating the specific impulse can be developed and is shown in Equation (4-5). This equation has been simplified by allowing the propellant mass, from the definition of mass flow rate, to equal that of the propulsion system mass, 10 mT.

$$\alpha = \frac{P_{\text{jet}}}{m_{\text{ps}}} \quad (4-2)$$

where

α = specific power, W/kg
 P_{jet} = jet power, W
 m_{ps} = propulsion system mass, kg

$$P_{\text{jet}} = \frac{1}{2} \dot{m} V_e^2 \quad (4-3)$$

where

P_{jet} = jet power, W
 \dot{m} = mass flow rate, kg/s
 V_e = exhaust velocity, m/s

$$I_{\text{sp}} = \frac{V_e}{g_0} \quad (4-4)$$

where

I_{sp} = specific impulse, seconds,
 V_e = exhaust velocity, m/s
 g_0 = standard gravity, 9.81 m/s²

Specific impulse (I_{sp}) represents the total impulse per unit mass of the propellant. In rocket propulsion the specific impulse for a spacecraft or launch vehicle is commonly used as a figure of merit analogous to miles per gallon (mpg) in automobiles. The specific impulse is given by:

$$I_{\text{sp}} = \frac{1}{g_0} \sqrt{2\alpha t_b} \quad (4-5)$$

where

- I_{sp} = specific impulse, seconds
- g_0 = standard gravity value, 9.81 m/s^2
- α = specific power, 1 kW/kg
- t_b = burn time, 225 days

The specific impulse value calculated in Equation (4-5) is $20,099.91 \text{ seconds}^*$. This value was rounded down to 20,000 seconds. The exhaust velocity is then the standard gravity multiplied by the specific impulse,

$$V_e = g_0 I_{sp} \quad (4-6)$$

where

- V_e = exhaust velocity, m/s
- g_0 = standard gravity value, 9.81 m/s^2
- I_{sp} = specific impulse, 20,000 s

The exhaust velocity value calculated from Equation (4-6) is $196,200 \text{ m/s}^*$. With an exhaust velocity calculated, the equation for specific power can be rearranged to calculate the mass flow rate.

$$\dot{m} = \frac{2\alpha m_{ps}}{V_e^2} \quad (4-7)$$

where

- \dot{m} = mass flow rate, kg/s
- α = specific power, 1 kW/kg
- m_{ps} = propulsion system mass, 10 mT
- g_0 = standard gravity value, 9.81 m/s^2
- V_e = exhaust velocity, $196,200 \text{ m/s}$

The mass flow rate calculated from Equation (4-7) is $0.000519556 \text{ kg/s}^*$. Next, the value for the thrust produced by the propulsion system is calculated by multiplying the mass flow rate with the exhaust velocity.

*Step-by-step calculation is shown in APPENDIX E.

$$F_T = \dot{m}V_e \quad (4-8)$$

where

$$\begin{aligned} F_T &= \text{thrust, N} \\ \dot{m} &= \text{mass flow rate, } 0.000519556 \text{ kg/s} \\ g_0 &= \text{standard gravity value, } 9.81 \text{ m/s}^2 \\ V_e &= \text{exhaust velocity, } 196,200 \text{ m/s} \end{aligned}$$

The thrust value calculated from Equation (4-8) is 101.937 newtons (N). This value was rounded to 102 N when inputted into GMAT, requiring a slightly corrected mass flow rate of 0.000519878 kg/s*. With the mass flow rate and burn time values determined, the propellant mass can be calculated by multiplying the two values together.

$$m_p = \dot{m}t_b \quad (4-9)$$

where

$$\begin{aligned} m_p &= \text{propellant mass, kg} \\ \dot{m} &= \text{mass flow rate, } 0.000519556 \text{ kg/s} \\ t_b &= \text{burn time, } 225 \text{ days} \end{aligned}$$

The propellant mass calculated by Equation (4-9) is 10106 kg*. This value was rounded up to 10150 kg (10.15 mT). Now that the propellant mass has been calculated, the mass of the spacecraft without propellant and payload (empty mass) can be calculated from the payload mass ratio with help from the mass of the payload and the payload mass fraction.

$$m_e = \frac{1}{\lambda} m_{pl} - m_p \quad (4-10)$$

where

$$\begin{aligned} m_e &= \text{empty mass, mT} \\ \lambda &= \text{payload mass ratio, } 0.2 \\ m_{pl} &= \text{payload mass, } 10 \text{ mT} \\ m_p &= \text{propellant mass, } 10.15 \text{ mT} \end{aligned}$$

*Step-by-step calculation is shown in APPENDIX E.

The empty mass of the spacecraft calculated from Equation (4-10) is 39.85 mT*. If the mass of the payload is added to the empty mass, then the calculated mass is the mass of the spacecraft without propellant. This value is known as the dry mass (m_{dry}) and has a value of 49.85 mT. The structural mass (m_s) of the spacecraft is empty mass minus the propulsion system mass and has a value of 29.85 mT. Finally, the total, or initial, mass of the spacecraft (m_i) can be calculated by summing the dry mass with the propellant mass. The value for the total mass is 60 mT. A conformity check of the mass equations can be done with the definition of the payload mass ratio [31].

$$\lambda = \frac{m_{pl}}{m_i - m_{pl}} \quad (4-11)$$

where

- λ = payload mass ratio
- m_{pl} = payload mass, 10 mT
- m_i = initial mass of spacecraft, 60 mT

The value of the payload mass ratio from Equation (4-11) is equal to 0.2*. This value exactly matches the predetermined value of the payload mass ratio. Thus, all the mass calculations used to determine mass values for the different spacecraft components are consistent. Table 4-1 summarizes the spacecraft mass as well as the rest of the spacecraft design parameters.

*Step-by-step calculation is shown in APPENDIX E.

Table 4-1: Spacecraft Design Parameters

Predetermined Parameters		Propulsion Parameters		Mass Properties	
α	$1 \frac{\text{kW}}{\text{kg}}$	t_b	225 days	m_p	10.15 mT
λ	0.2	I_{sp}	20,000 sec	m_e	39.85 mT
m_{pl}	10 mT	V_e	$196,200 \frac{\text{m}}{\text{s}}$	m_{dry}	49.85 mT
m_{sp}	10 mT	\dot{m}	$0.000519878 \frac{\text{kg}}{\text{s}}$	m_s	29.85 mT
		T	102 N	m_i	60 mT

4.2 Saturn Fly-by

The Fusion Fly-by spacecraft will begin its mission on 06 April 2025 at 14:04:15.000, Coordinated Universal Time (UTC). The spacecraft will depart from the Earth-Moon Lagrange Point 1, and start its fly-by mission to Saturn. As stated in the previous subsection, the spacecraft contains 10.15 metric tons (mT) of propellant and will be propelled by a nuclear fusion main thruster providing 102.0 N of constant thrust at a constant mass flow rate of 0.000519878 kg/s. The direction of the thrust is determined in the Velocity-Normal-Binormal coordinate system relative to the spacecraft and Earth. This type of coordinate system is known as the path coordinate system and the velocity direction is sometimes referred to as the tangential direction [32]. The majority of thrust is directed in the positive velocity direction with 96.798 N of thrust or 94.9% of total thrust. The other 5.1% or 5.202 N of thrust is directed in the negative normal direction to correct the flight for the position of Saturn relative to the J2000.0 Ecliptic plane when the spacecraft travels past the orbit of Saturn. It should be noted that if Saturn is above the ecliptic plane when the spacecraft travels its orbit, then a positive normal thrust direction would be required. The thrust directions are coupled with the epoch, 06 April 2025 at 14:04:15.000 UTC. If the epoch is significantly changed, then the thrust direction percentages must also change in order to fly-by Saturn at the same altitude. The velocity magnitude of the spacecraft relative to an inertial

Earth reference frame (J000.0 Ecliptic) at epoch is 0.856 km/s, and the velocity magnitude relative to the Sun at epoch is 29.9989 km/s. The spacecraft's main thruster will fire for a continuous 225 days during its accelerating phase of the mission.

When the spacecraft main thruster is ignited at epoch, the spacecraft immediately departs the Earth-Moon Lagrange Point 1 located 329,948 km from the center of the Earth, or 58,653 km from the center of the Moon and enters the SOI of the Moon, approximately 66,183 km in radius. The gravitational influence from the Moon combined with the thrust from the main thruster causes the spacecraft to enter a hyperbolic trajectory around the Moon. Closest approach to the Moon occurs on 09 April 2025 09:56:38.763 UTC with an altitude of 7003.5 km. The velocity magnitude of the spacecraft with respect to the Moon at this point is 1.025 km/s. This is an increase of 0.873 km/s from the initial velocity magnitude with respect to the Moon at epoch of 0.152 km/s. When the spacecraft reaches the Moon's SOI on 11 April 2025 05:20:37.931 UTC, the velocity magnitude with respect to the Earth will increase to 1.216 km/s, a 0.360 km/s increase in just over 4.5 days, and the spacecraft will be located 341,578 km from the center of the Earth. On 16 April at about 22:28:54 UTC, the spacecraft will travel past the Earth's orbit relative to the Moon. Figure 4-1 and Figure 4-2 show the trajectory of the spacecraft from epoch to the Earth's orbit with respect to the Moon.

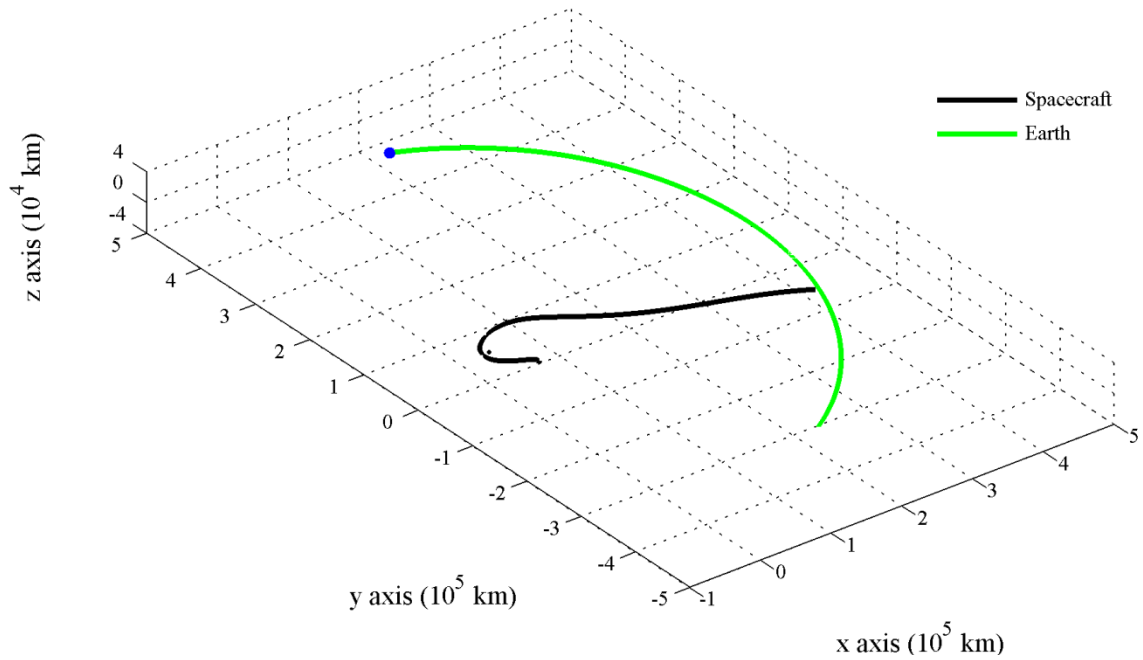


Figure 4-1: 3D Trajectory of Spacecraft from Epoch to Earth Orbit in Moon Centered Translated J2000.0 Ecliptic Frame

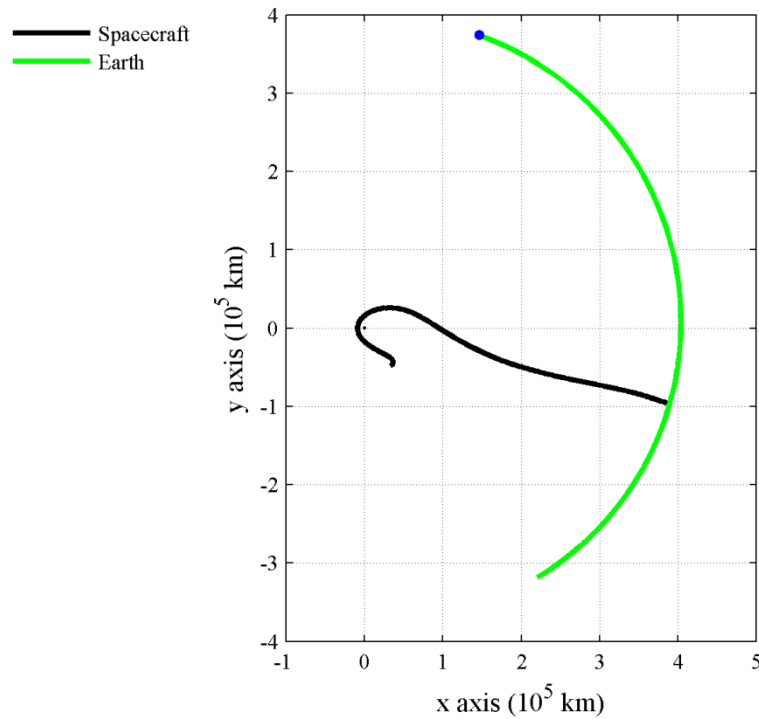


Figure 4-2: 2D Trajectory of Spacecraft from Epoch to Earth Orbit in Moon Centered Translated J2000.0 Ecliptic Frame

Two days after the spacecraft leaves the SOI of the Moon, the spacecraft arrives at its closest approach to the Earth on 13 April 2025 03:22:15.540 UTC. With the help of the Earth, the spacecraft is accelerated farther in the negative J2000.0 Ecliptic z-direction, and

when the spacecraft reaches the edge of the Earth’s SOI at 18:43:51.455 UTC on 19 April 2025, the spacecraft is located at a -80,966 km in the Geocentric J2000.0 Ecliptic z-direction. This is just over 57,000 km difference in the z-direction from epoch. (The location of the spacecraft at epoch in Geocentric J2000.0 Ecliptic coordinates is -187,596 km in the x direction, 270,368 km in the y-direction, and 23,963 km in the z-direction.) The spacecraft is now 924,217 km (radius of Earth SOI) away from the Earth with a velocity magnitude of 2.024 km/s with respect to the Earth and 31.068 km/s with respect to the Sun. The spacecraft has now traveled over 15 and a half days and used 592.648 kg of propellant leaving 9557.3512 km of propellant left inside the main thruster tank. Figure 4-3 and Figure 4-4 show the spacecraft trajectory from epoch to the SOI of the Earth with respect to the Earth.

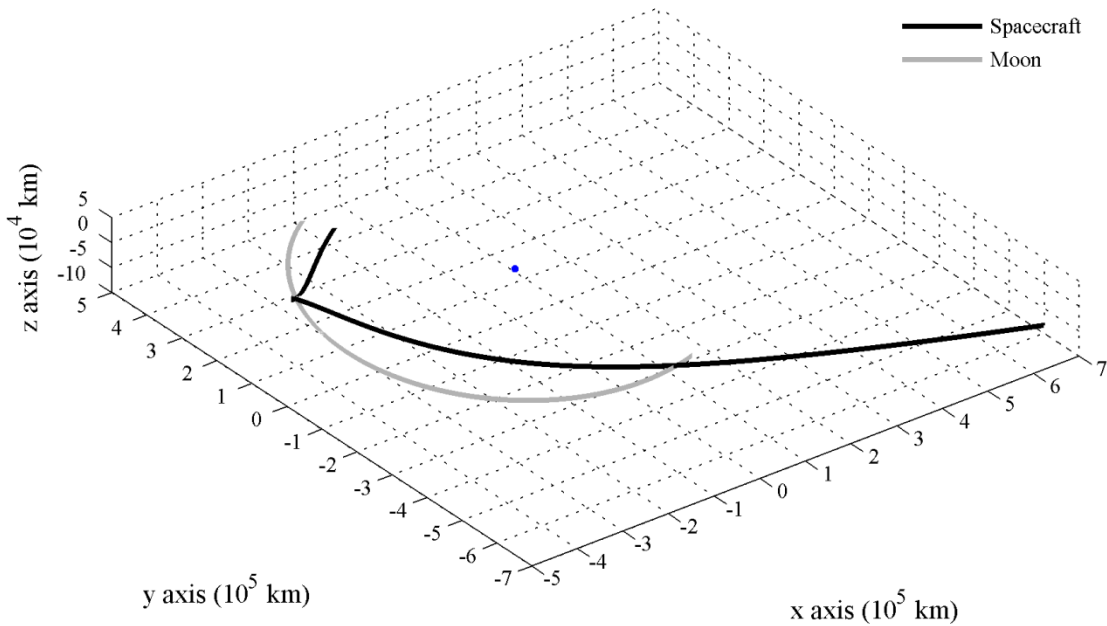


Figure 4-3: 3D Trajectory of Spacecraft from Epoch to the Earth SOI in Geocentric J2000.0 Ecliptic Frame

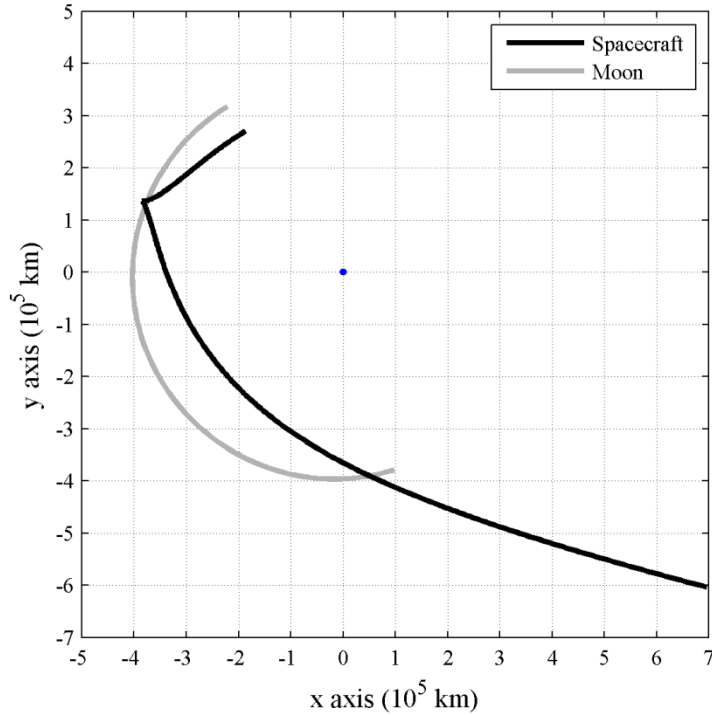


Figure 4-4: 2D Trajectory of Spacecraft from Epoch to the Earth SOI.in Geocentric J2000.0 Ecliptic Fame

For the first time of the spacecrafts' mission, it is no longer just under the gravitational influence of Earth-Moon planetary system. The Spacecraft's main source of gravity from this point on until it reaches the SOI of Saturn will be from the Sun. Even with the spacecraft's main thruster running for another 209 days, the Sun's gravitational influence is still able to shape the spacecraft's trajectory into an elliptical curvature, and this effect is more pronounced when the propulsion system is no longer operating.

After the main thruster is turned off on 17 Nov 2025 at 14:04:15.000 UTC, the main thruster fuel tank will only contain 43.577982 kg of propellant. At this point the spacecraft will be traveling at a velocity magnitude relative to the Earth of 71.742 km/s and 48.711 km/s relative to the Sun. This is the maximum velocity value that the spacecraft will obtain due to the propulsion system. The spacecraft will then enter its coasting phase and decelerate due to the Sun's gravitational influence. The position of the spacecraft in the Heliocentric J2000.0 Ecliptic Coordinates will be 545,683,828 km in the x-direction, -77,847,050 km in the y-

direction, and -18,276,691 km in the z-direction and will be located nearly 503 million km away from Earth. The difference in the z-direction is 71,733,263 km from its initial position of 53,456,572 km in the z-direction. The trajectory of the spacecraft in Heliocentric J2000.0 Ecliptic Coordinates from epoch to the end of the accelerating phase is shown in Figure 4-5 and Figure 4-6.

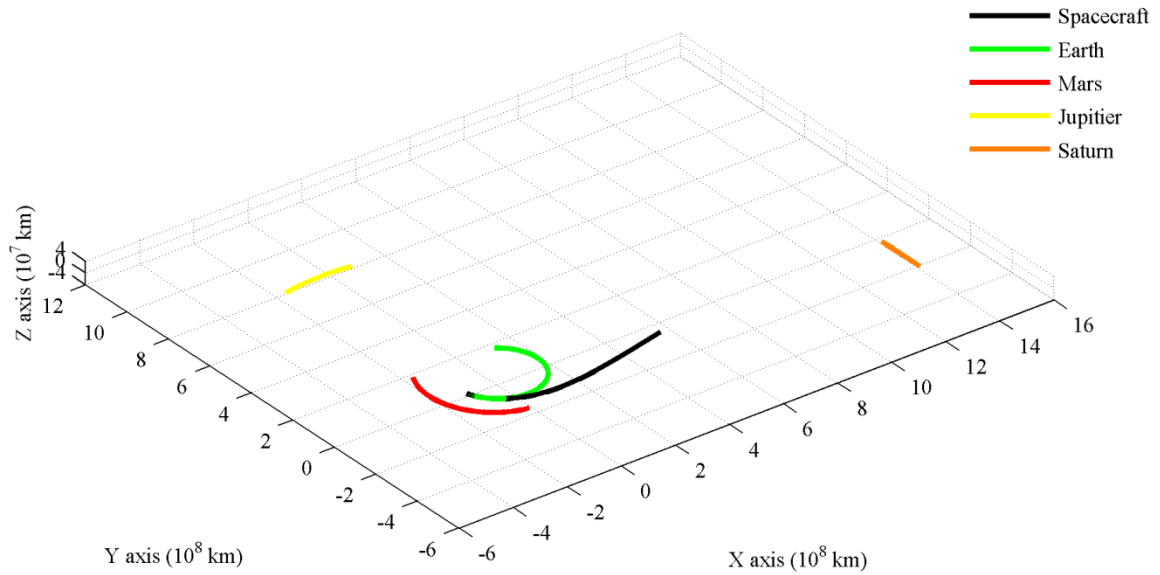


Figure 4-5: 3D Trajectory of Spacecraft during Accelerating Phase in Heliocentric J2000.0 Ecliptic Frame

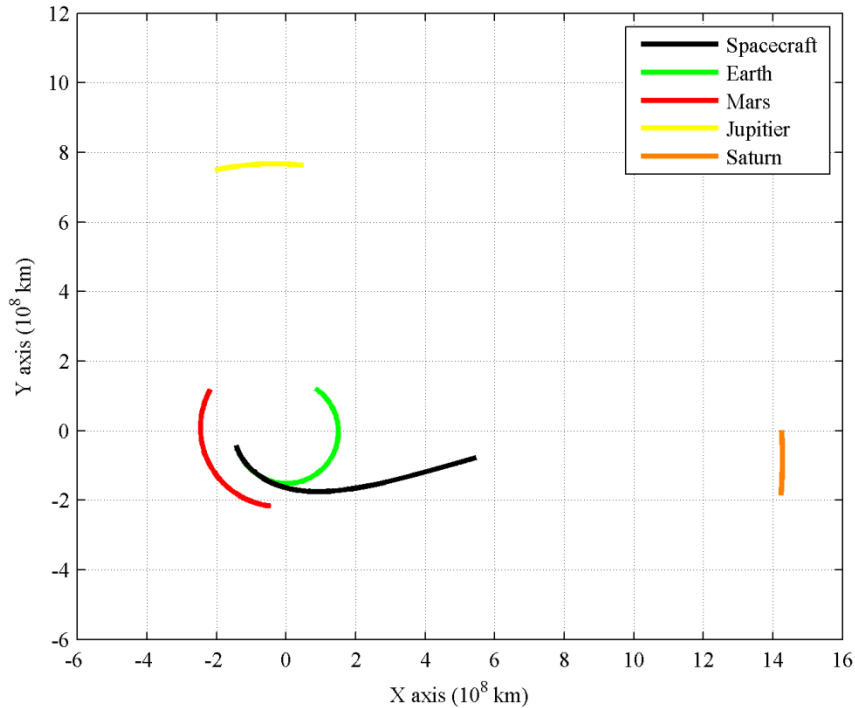


Figure 4-6: 2D Trajectory of Spacecraft during Accelerating Phase in Heliocentric J2000.0 Ecliptic Frame

The spacecraft will remain in the coasting state for the rest of its journey to Saturn and will continue to decelerate until the spacecraft reaches the SOI of Saturn on 14 June 2026 around 00:34 UTC. When the spacecraft enters the SOI of Saturn, its velocity magnitude relative to the Sun will be 45.691 km/s. That is just over a 3 km/s decrease from its maximum velocity of 48.711 km/s at the end of its accelerating phase. The position of the spacecraft in Heliocentric coordinates is 1,349,832,323 km in the x-direction, 169,627,257 in the y-direction, and -56,534,340 km in the z-direction, or in a Saturn centered translated J2000.0 Ecliptic coordinate frame, -54,508,459 km in the x-direction, -5,065,417 in the y-direction, and 2,408,946 km in the z-direction. Also, the velocity magnitude with respect to Saturn at this point is 45.504 km/s, and the distance from Saturn is the radius of Saturn's SOI, 54,796,292 km. The spacecraft is now under the gravitational influence of Saturn and will continue to accelerate towards Saturn until the spacecraft reaches the closest approach to

Saturn's surface. Figure 4-7 and Figure 4-8 show the spacecraft's entire trajectory from epoch to closest approach to Saturn in the Heliocentric J2000.0 Ecliptic coordinate frame.

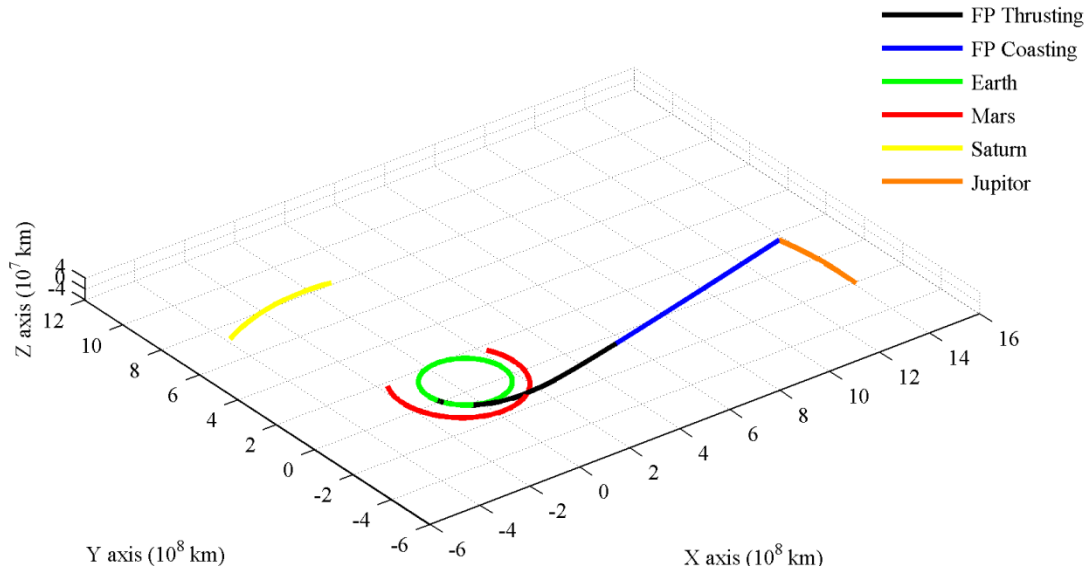


Figure 4-7: 3D Trajectory of Spacecraft from Epoch to Closest Approach of Saturn in Heliocentric J2000.0 Ecliptic Frame

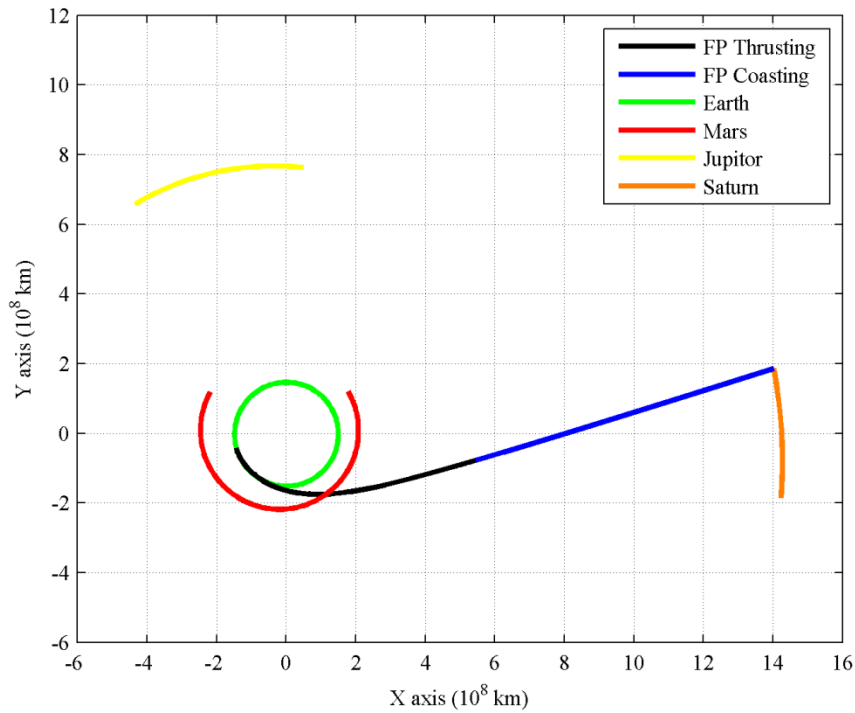


Figure 4-8: 2D Trajectory of Spacecraft from Epoch to Closest Approach of Saturn in Heliocentric J2000.0 Ecliptic Frame

The spacecraft's closest approach with Saturn will occur on 27 June 2026 at 22:30:27.805 UTC with an altitude of 26220 km from the surface of Saturn. This is 447.35

days after epoch on 06 April 2025. The spacecraft approaches Saturn from behind Saturn's trajectory around the Sun. If the epoch date were slightly altered to a later time, for example plus 3 minutes (14:07:15.000 UTC on 06 April 2025), the spacecraft would approach Saturn from the front of Saturn's trajectory on 27 June 2026 22:43:55.873 UTC with an altitude of 12903 km. The difference in arrival time for closest approach is more than the 3 minute difference of the epoch dates. Velocity magnitudes at closest approach are 54.318 km/s with respect to Saturn and 55.916 km/s with respect to the Sun. The velocity of the spacecraft at closest approach with respect to the Sun is 7.205 km/s faster than the spacecraft's velocity at the end of its acceleration phase. This is a significant increase in velocity without the need to utilize the propulsion system. This maneuver, resulting in an increase in velocity from a planetary fly-by is referred to as a gravity assist maneuver, and has been utilized for several previous spacecraft missions. An escape velocity (parabolic orbit velocity) of 13.6923 km/s with respect to the Sun is all that is needed in order for the spacecraft to escape the solar system. Since the velocity magnitude of the spacecraft with respect to the Sun is slightly over 4 times larger than the escape velocity at Saturn, the spacecraft will eventually leave the solar system. The trajectory of the spacecraft as it approaches and flies by Saturn is shown in Figure 4-9 and Figure 4-10. The scale of both figures is set to only include a magnitude of 1 million km before and after closest approach to Saturn. Another visualizing plot that can be helpful in spacecraft trajectory fly-bys, is a B-plane plot (body plane), sometimes referred to as target plane plot [33]. Figure 4-11 shows the plot of the B-plane fly-by of Saturn where the **T** vector is along the equatorial plane of Saturn. The **B·T** and **B·R** calculated by GMAT are -99253 km and 26882 km.

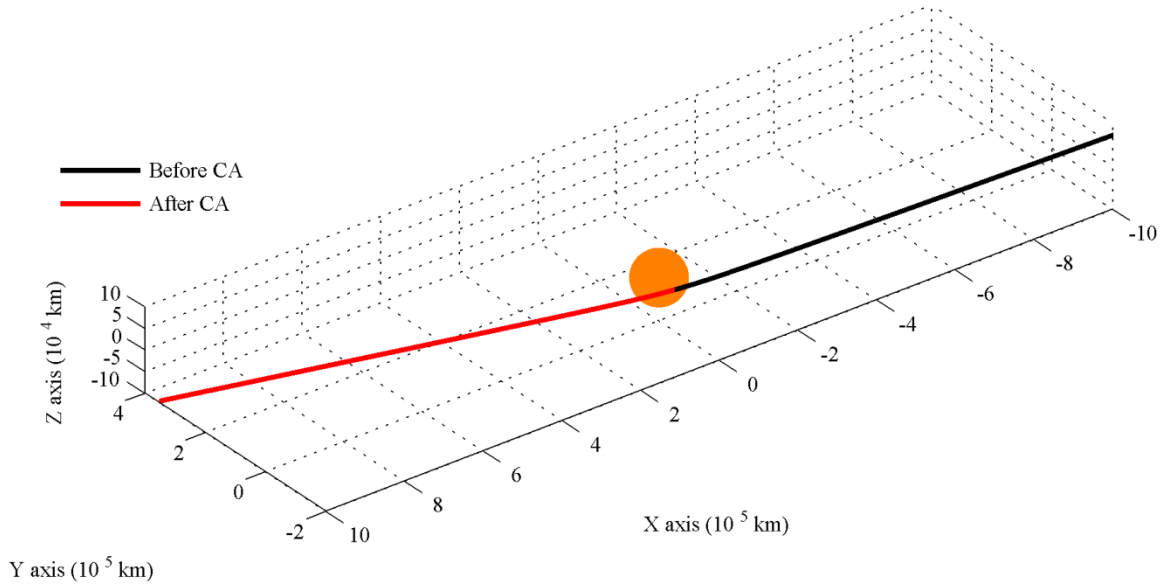


Figure 4-9: 3D Trajectory of Spacecraft Fly-by of Saturn

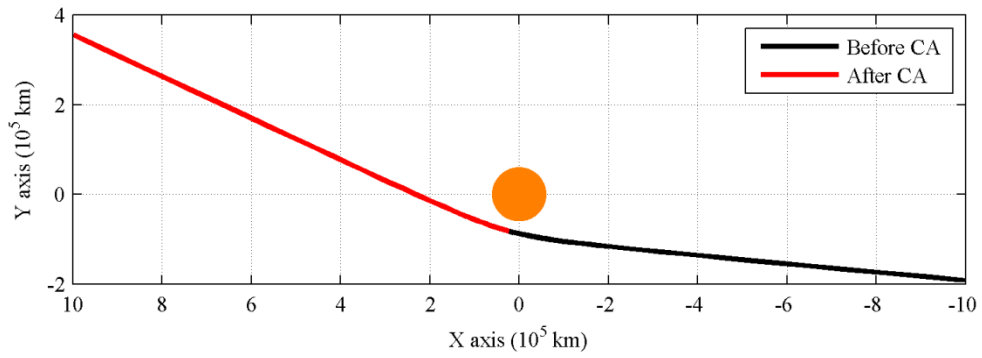


Figure 4-10: 2D Trajectory of Spacecraft Fly-by of Saturn

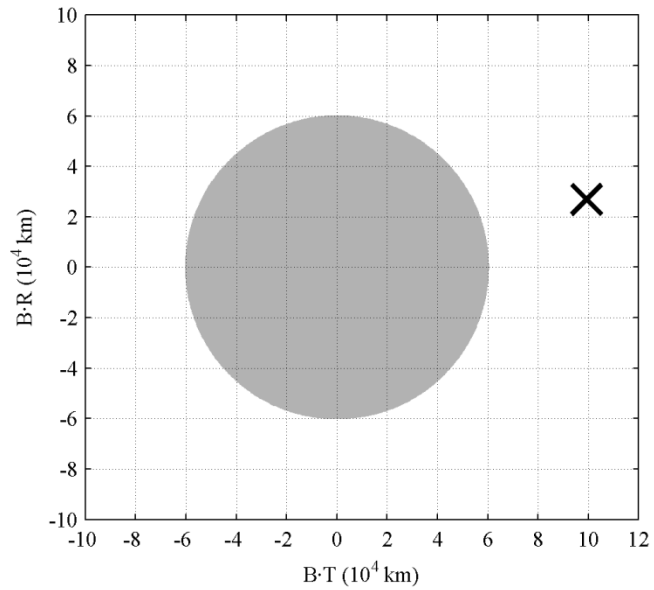


Figure 4-11: Spacecraft B-plane Closest Approach at Saturn (T Vector along Equator)

4.3 Beyond Saturn

Just two weeks after closest approach with Saturn, the spacecraft will leave the sphere of influence of Saturn and reenter a heliocentric orbit. The total time the spacecraft will spend inside the SOI of Saturn is approximately four weeks. The spacecraft entered Saturn's SOI with a velocity magnitude with respect to Saturn of 45.691 km/s and will leave Saturn's SOI with the same velocity magnitude with respect to Saturn, but the spacecraft entered the SOI with velocity magnitude of 45.691 km/s with respect to the Sun and will leave Saturn's SOI with a velocity magnitude of 48.761 km/s with respect to the Sun. This increase in the spacecraft's velocity has already been affected by the gravitational influence from the Sun because the spacecraft's velocity magnitude with respect to the Sun at closest approach was 54.318 km/s and has since slowed down 7.155 km/s. The spacecraft will continue to decelerate at an exponential rate (see Figure 4-15 or Figure 4-16) under the Sun's gravitational influence, but the velocity magnitude of the spacecraft will never fall below the escape velocity needed to leave the solar system. After leaving Saturn, the spacecraft will be able to get a glimpse of Neptune when it reaches the closest distance to the planet on 24 Apr 2028, just over 3 years since the spacecraft began its journey. The spacecraft will be approximately 10.75 AU away from the planet and over 10 AU away from the SOI of Neptune, thus Neptune will not cause any significant changes to the spacecraft's trajectory path as it enters the Kuiper Belt. One or more Kuiper Belt Objects (KBO) can be chosen for study while the spacecraft is inside the Kuiper Belt. Just over five years after epoch, the spacecraft will leave the Kuiper Belt around 15 August 2030 when it is 50 Au away from the Sun. Its velocity magnitude will decrease to 47.246 km/s with respect to the Sun. Since leaving Saturn's SOI, the spacecraft's velocity has only decreased about 1.5 km/s in a

distance of about 40 AU. Figure 4-12 and Figure 4-13 show the spacecraft trajectory from Epoch to the edge of the Kuiper Belt in the Heliocentric J2000.0 Ecliptic Coordinate Frame.

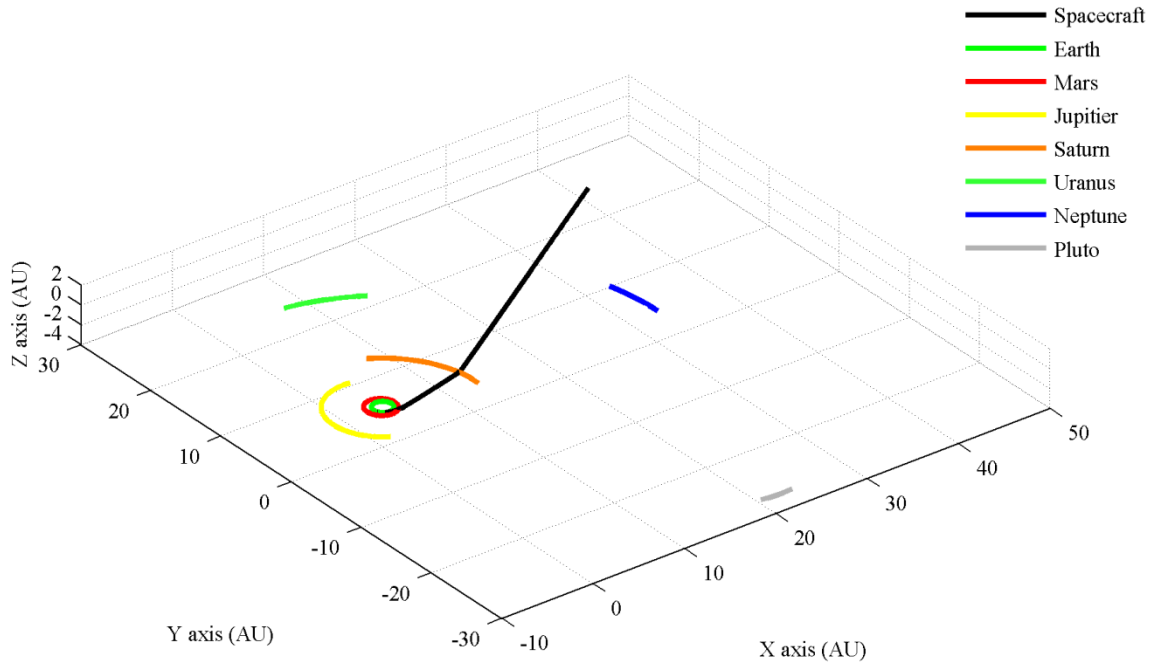


Figure 4-12: 3D Trajectory of Spacecraft from Epoch to Edge of Kuiper Belt in Heliocentric J2000.0 Ecliptic Frame

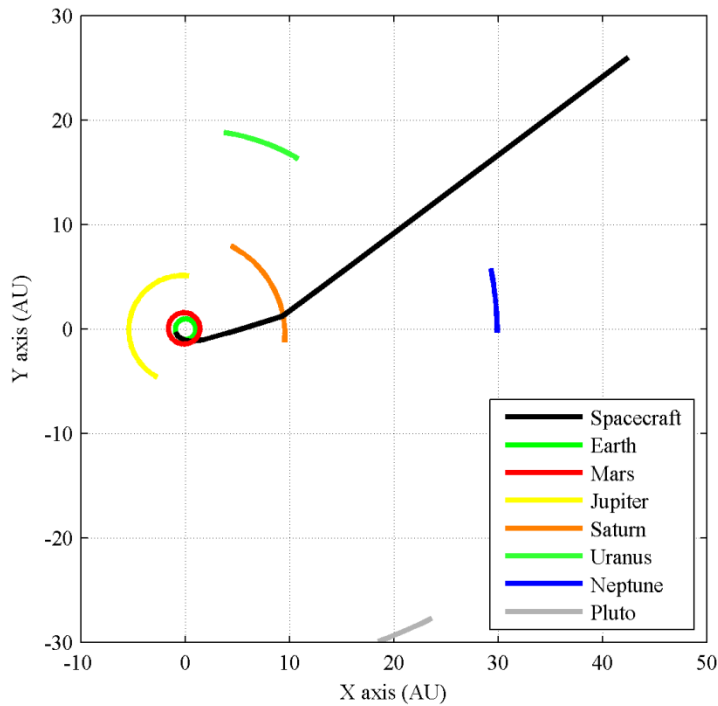


Figure 4-13: 2D Trajectory of Spacecraft from Epoch to Edge of Kuiper Belt in Heliocentric J2000.0 Ecliptic Frame

After leaving the Kuiper Belt, the spacecraft will eventually leave the solar system thousands of years after epoch. After one hundred years from epoch, the spacecraft will be nearly 1000 AU from the Sun (the spacecraft will actually reach 1000 Au in 101 years). The velocity magnitude will start to stabilize at 46.891 km/s as the gravitational influence of the Sun and rest of the planets become negligible Figure 4-14 shows the distance the spacecraft will travel in 100 years from epoch. Figure 4-15 shows a plot of the spacecraft velocity magnitude with respect to the Sun verses time from epoch to 100 years, whereas Figure 4-16 shows a closer look at the velocity magnitude of the spacecraft with respect to the Sun in the first 10 years since epoch.

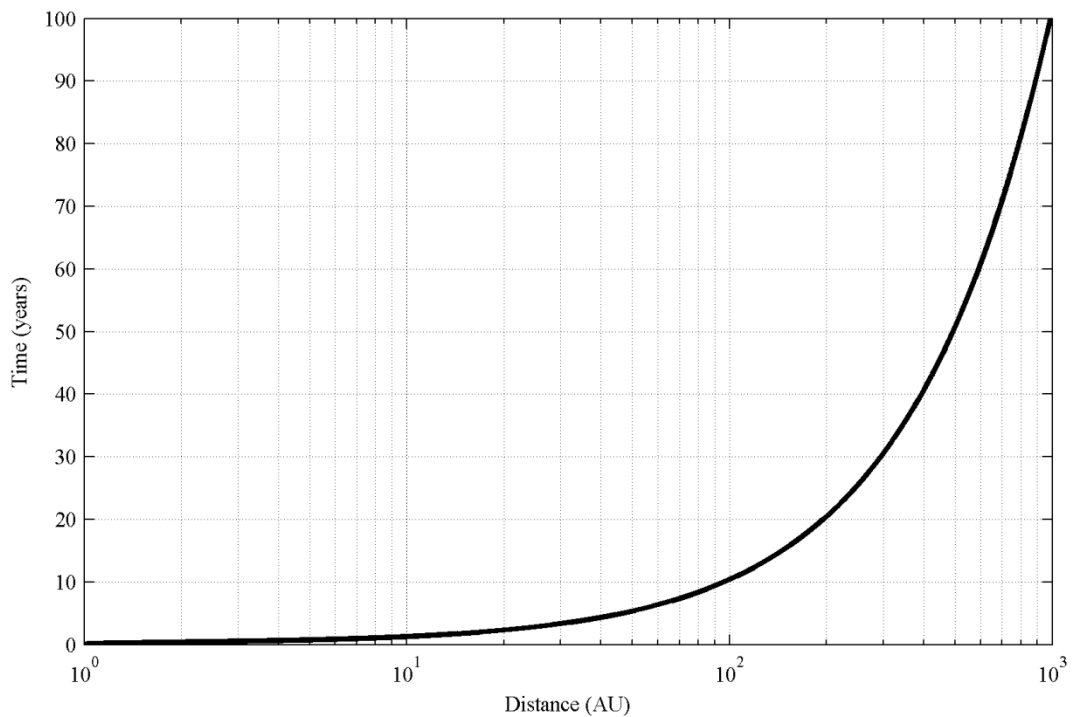


Figure 4-14: Plot of Spacecraft Distance verses Time from epoch to 100 years

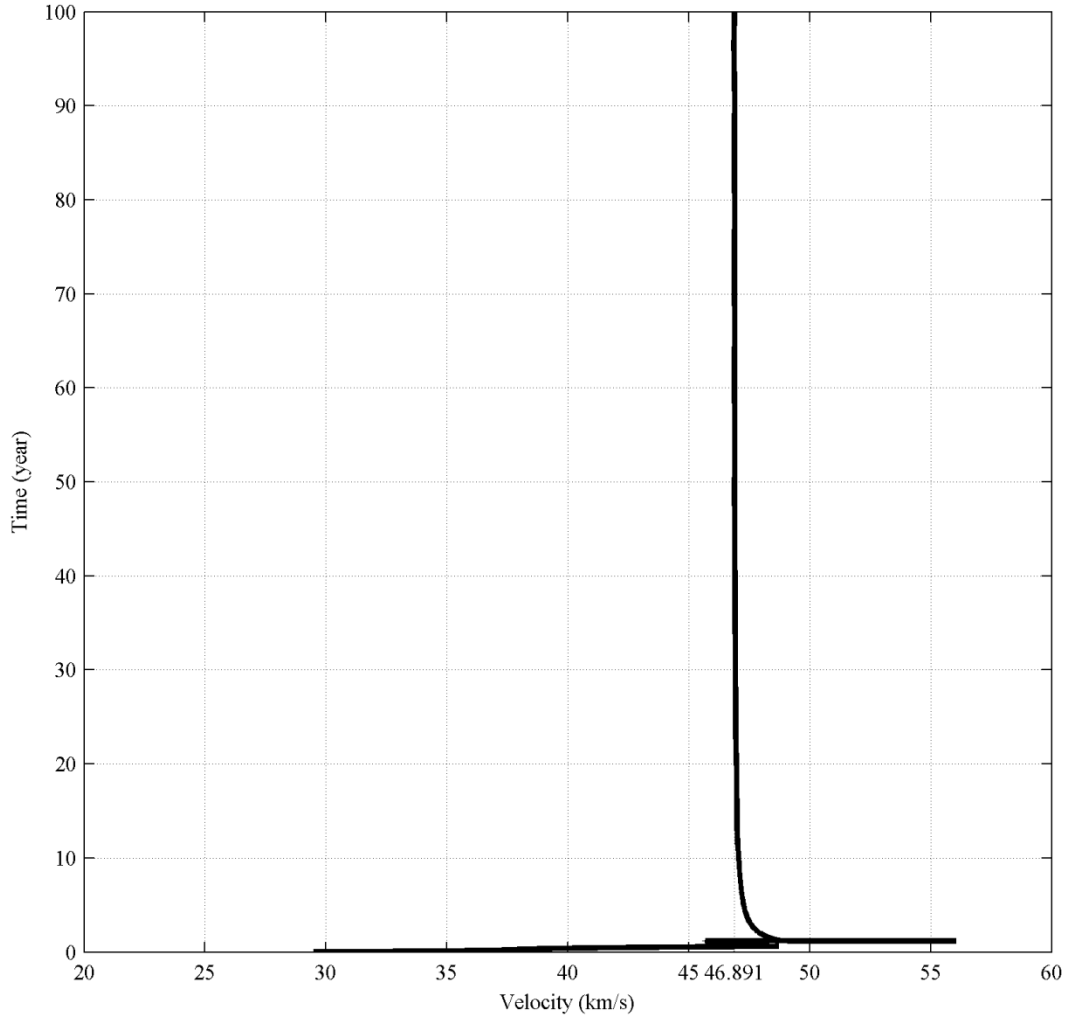


Figure 4-15: Plot of Spacecraft Velocity Time from Epoch to 100 years with respect to the Sun versus

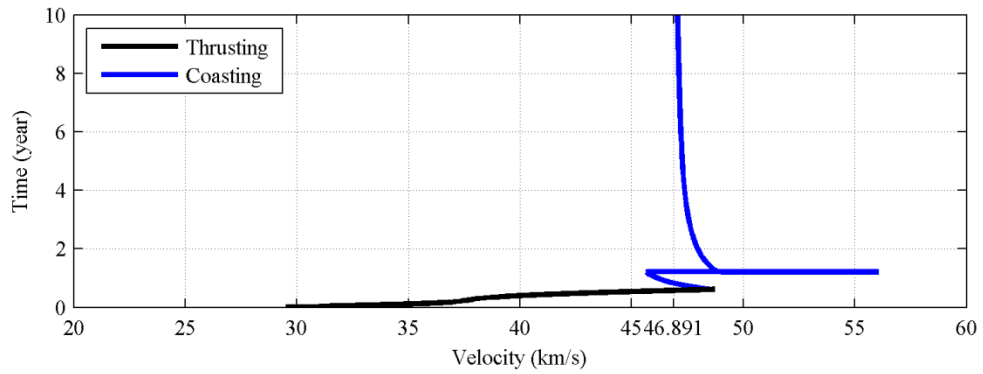


Figure 4-16: Plot of Spacecraft Velocity versus Time from Epoch to 10 years with respect to the Sun

4.4 Gravity Free and Central-Body only Models

The gravity free approximation in the field-free space equation, Equation (4-1), calculates an approximation of the trip based on the straight-line distance, the specific power, and the payload mass fraction. Even though the equation does not calculate the spacecrafts acceleration, gravity mostly due to the Sun is still accounted in the equation. This can be shown by using Equation (2-1), the ideal rocket equation, to determine the total trip time. Using the spacecraft design parameters from Section 4.1, the change in velocity during the accelerating phase of the spacecraft's trajectory can be calculated in gravity free space.

$$\Delta V = V_e \ln\left(\frac{m_i}{m_f}\right) = 196.2 \frac{\text{km}}{\text{s}} \ln\left(\frac{60}{49.85}\right) = 36.361 \frac{\text{km}}{\text{s}} \quad (4-12)$$

Then adding the change in velocity of the spacecraft to the initial velocity of the spacecraft will calculate the spacecraft's velocity at the end of the acceleration phase of its trajectory. This velocity value will also be the constant velocity value for the spacecraft during the coasting phase of its trajectory. The initial velocity of the spacecraft with respect to the Sun will have approximately the same velocity of the Earth. If the Earth is assumed to be in a circular orbit at a radius distance of 1 AU from the Sun, then the velocity of the Earth and the initial velocity of the spacecraft can be calculated from Equation (4-13).

$$V_{\text{earth}} = \sqrt{\frac{\mu_{\text{sun}}}{r_{\oplus}}} \quad (4-13)$$

where

$$\begin{aligned} V_{\text{earth}} &= \text{circular velocity of Earth, km/s} \\ \mu_{\text{sun}} &= \text{gravitational parameter for the Sun, } 132,712,439,935.5 \text{ km}^3/\text{s}^2 \\ r_{\oplus} &= \text{trajectory radius of Earth, 1 AU} \end{aligned}$$

The velocity of the Earth, and thus the initial velocity of the Fusion propulsion spacecraft are approximately 29.785 km/s with respect to the Sun. Adding the gravity free

change in velocity determines that the velocity of the spacecraft at the end of the accelerating phase and during the coasting phase of the trajectory will be 66.146 km/s with respect to the Sun. If one time step were taken (i.e. the time step value is equal to the propulsion operation time of 225 days), the distance traveled during the accelerating phase can be calculated by multiplying the final velocity at the end of the accelerating phase with the change in time, as shown in Equation (4-14).

$$r_{acc} = V_{sp} dt \quad (4-14)$$

where

- r_{acc} = distance traveled during accelerating phase, km
- V_{sp} = velocity of spacecraft at end of accelerating phase, 66.146 km/s
- dt = change in time during accelerating phase, 225 day

The distance that the spacecraft travels during the accelerating phase of the trajectory is 8.596 AU when gravitational influences are excluded. Utilizing the same radius magnitude value (straight-line distance from Earth to Saturn) of 10.58 AU, the distance the spacecraft will travel during the coasting phase of the trajectory would be simply the difference between the two distances. Now knowing the distance traveled and velocity during the coasting phase, the time the spacecraft accumulates during the coasting phase can be calculated by dividing the distance the spacecraft travels during the coasting phase by the coasting phase velocity. This value is 51.95 days. Adding this value to the propulsion operation time of 225 days gives a total trip time of 276.95 days. This method for calculating trip time is a very poor approximation method and is easily shown when comparing the result to the trip time calculated from Equation (3-1) and the trip time determined by GMAT. To increase the accuracy of this gravity free approximation method a much smaller step size should be used. A MATLAB® script provided in APPENDIX F uses a time step of 1 hour

and calculates a total trip time of 341.26 days for a gravity free approximation utilizing the ideal rocket equation.

Another method for modeling the trajectory of the Fusion Propulsion spacecraft in GMAT only included the central body gravitational acceleration in the equation of motion. This was done by only including the central body point mass for each propagator. Table 4-2 shows the point mass setting for each propagator.

Table 4-2: Force Model Propagator Point Mass Setting

Propagator:	Earth Prop	Moon Prop	Saturn Prop	Solar System Prop
Point Mass:	Earth	Luna	Saturn	Sun

Using the same epoch of 06 April 2025 14:04:15.000 UTC, the Fusion Propulsion spacecraft reaches Saturn two days earlier than in the original GMAT script, but the altitude at closest approach has increase by more than a factor of 150. This value is to be expected since an epoch of 06 April 2025 14:04:15.000 UTC was chosen in order to have a reasonable altitude from Saturn at closest approach. This was conducted by running the GMAT script through several iterations with varying epochs. If the epoch for this patched conic central body only point mass method was slightly altered than the altitude from Saturn at closest approach would have a reasonable value. Figure 4-17 shows a plot of magnitude distance from the Sun verses time for each method and Figure 4-18 shows a plot of both GMAT scripts with respect to Saturn.

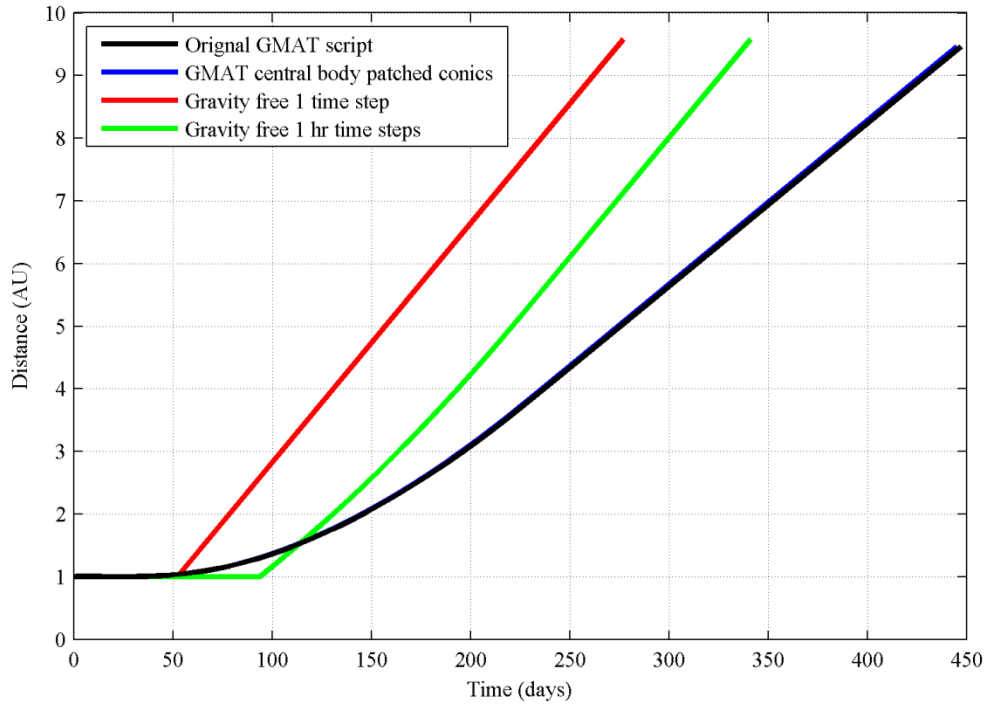


Figure 4-17: Comparison of Trajectory Methods

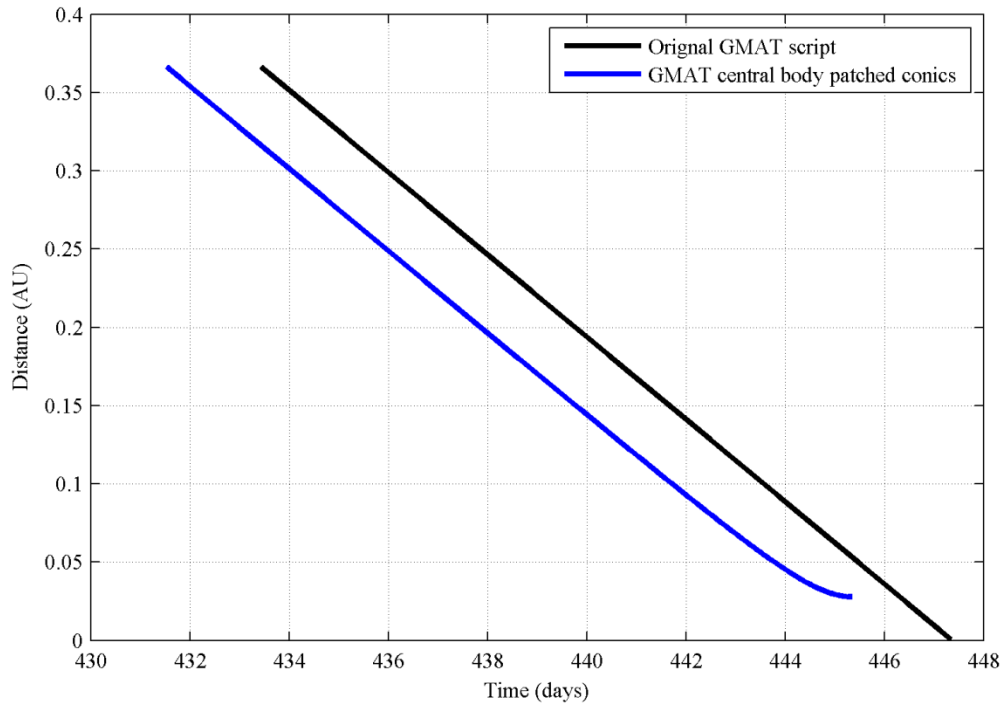


Figure 4-18: Comparison of GMAT scripts with respect to Saturn

CHAPTER V

COMPARISON TO OTHER TYPES OF PROPULSION MISSIONS

Since fusion reactors have yet to exceed breakeven, a mission utilizing fusion propulsion has not been conducted by NASA or nay any other Space agency/company to facilitate comparisons. This chapter will instead compare the previously discussed modeled mission to past and current interplanetary missions performed by spacecrafts with other types of propulsion systems.

5.1 Chemical Propulsion

In chemical propulsion chemical reactions (combustion) between two or more elements occur resulting in energetic gases that are exhausted through a rocket nozzle in order to produce thrust.

5.1.1 Chemical Propulsion Background

Chemical propulsion was the first type of propulsion system used and has become the de facto choice for almost all spacecraft missions, both Earth orbiting and interplanetary missions and the only type of propulsion type used in launch vehicles. Chemical propulsion can be classified into three main branches in regards to the type of propellant being used, Liquid, Solid, and a combination of Liquid and Solid propellants called a Hybrid.

5.1.1.1 Liquid Propellants

Liquid propulsion can be further classified as either monopropellant or bipropellants [34]. Monopropellants have been the ideal choice for a spacecraft's main propulsion systems for decades because they are able to be stored for long periods of time and do not need the extensive hardware associated with bipropellants. Hydrazine is typically chosen as the monopropellant used on a spacecraft. Other types of monopropellants include "cold" and "warm" gaseous propellants. Gaseous propellants are rarely used in the spacecraft's main propulsion system but have been used for attitude changes and corrections in the spacecraft's reaction control system (RCS). Bipropellants offer greater propulsion performance than monopropellants but require a more complex feed system that can result in an increase for failure. Larger spacecrafts utilize a bipropellant propulsion system rather than a monopropellant propulsion system and typically contain mono-methyl hydrazine (MMH) as the fuel and nitrogen tetroxide (NTO) for the oxidizer. Cryogenic fuels and oxidizers require specific storage temperatures and pressures and are not normally chosen as spacecraft propellants but have better performance characteristics than storable bipropellants making them very useful in Launch vehicles. Large launch vehicles employ liquid oxygen and liquid hydrogen because of very high performance characteristics and the non-toxic exhaust (water vapor).

5.1.1.2 Solid Propellants

Unlike liquid engines, solid rocket motors involve few to no moving parts. The propellant is stored inside the motor's combustion chamber, and the combustion takes place at the propellant surface [34]. Burning rate and grain configuration are two key design parameters for motor performance. The burning rate is the rate of regression of the solid

propellant and is measured in regression distance per time (cm/s, mm/s, or in./s). Chemical composition of the solid propellant is the major contributor to the burning rate; while operating chamber pressure and ambient grain temperature can slightly alter the burning rate. The grain of a solid propellant describes the chemical composition as well as the configuration (shape) of the propellant. The grain configuration can have almost as much of an effect on performance as chemical composition. Configuration is classified into three types. A progressive grain increases the thrust and chamber pressure by increasing the burning surface. It is the easiest configuration to manufacture because the port cavity can be a simple cylindrical hole down the center of the grain. A neutral grain holds the thrust and chamber pressure nearly constant by maintaining a constant burn area throughout operation. Star, wagon wheel, and slots with tubs are some common regressive grain shapes. The last configuration type is regressive where the thrust and chamber pressure decrease with time as the burn surface decreases in area. Regressive grains are the most complex grains to manufacture because the port cavity must shrink in size. The simplest regressive design is a cylindrical or spherical shape with the port cavity between the grain and motor case. Regressive burn configurations would be the ideal grain configurations for launch vehicles if manufacturing was not so complex because the thrust would decrease along with gravity as the attitude increases. This would result in a constant or nearly constant gravitational force (g force) being exerted on the launch vehicle.

5.1.1.3 Hybrid Rockets

Hybrid rockets consist of systems utilizing both solid and liquid propellants simultaneously. A typical hybrid rocket consists of a liquid oxidizer and a solid fuel [34]. The most common oxidizer is liquid oxygen (LOX), and hydroxyl-terminated polybutadiene

(HTPB) is the most common fuel. Other configurations include the inverse configuration, where the rocket contains a liquid fuel and solid oxidizer and the mixed hybrid configuration where a small amount of oxidizer has been imbedded into the solid fuel in order to increase the burning rate. Hybrid rockets are ideally suited for missions requiring throttle control (thrust varying), shutdown and restarts, and long duration missions requiring storable propellants. In a hybrid rocket, the solid fuel must vaporize before mixing with the liquid oxidizer. This causes the grain configuration to be more complex than for solid rockets. Additional port cavities are needed to increase the burning rate of the solid fuel in order to achieve the correct mixture ratio. Achieving the correct mixture ratio in a hybrid rocket is difficult because a hybrid rocket suffers from a turbulent mixing environment that can result in unreacted fuel and oxidizer being expelled from the rocket. Multiple combustion ports can decrease the amount of unreacted propellant by mixing with the fuel before being expelled from the rocket. More research and development is needed before hybrid rockets can be utilized effectively.

5.1.2 Cassini-Huygens

The Cassini-Huygens mission utilized a launch vehicle with both liquid and solid chemical propellants and the spacecraft's propulsion system consists of both a bipropellant and monopropellant system. The spacecraft was launched on 15 October 1997 at 08:43:00 UTC (04:43:00 EDT) from Cape Canaveral, Florida onboard a Titan IVB launch vehicle with a Centaur upper stage. The Titan IVB used to launch the Cassini-Huygens spacecraft utilized two solid rocket motor (SRM) boosters, liquid bipropellant engines for the first and second stage, and a Centaur third stage [35] (401B configuration [36]). The SRM boosters consist of 88% solid loading (fuel and oxidizer percentage) and 12% HTPB binder [37]. The first and

second stage engines use Aerozine 50 (50/50 mixture of hydrazine and unsymmetrical dimethyldiazine [38]) as the fuel with NTO as the oxidizer. The Centaur engine uses liquid hydrogen as the fuel and liquid oxygen as the oxidizer [35]. The spacecraft's primary thruster utilizes a bipropellant of MMH and NTO; while the RCS utilizes a hydrazine monopropellant [39]. With the help of a complex trajectory involving multiple gravity assists, the 5,574 kg (mass of spacecraft after Centaur separation) Cassini-Huygens spacecraft was able to be inserted into an orbit around Saturn.

5.1.2.1 Cassini-Huygens Trajectory and Mission

After 43 minutes from initial launch time, the Centaur stage separated from Cassini, but before separating the Centaur stage placed Cassini into a fly-by orbit with its first celestial body, Venus, in order to conduct a gravity assist maneuver. The launch from the Titan IVB rocket was so successful that the first and second trajectory correct maneuvers (TCM) were reduced to ΔV values of 2.7 m/s and 0.2 m/s with respect to the Earth allowing TCM 3, the maneuver before first Venus closest approach, and TCM 4, the maneuver after first Venus closest approach, to be cancelled [40]. Since TCM 2 had a very small ΔV , the RCS was used instead of the thruster main engine. The near perfect launch from the Titan IVB rocket resulted in a spacecraft propellant savings allowing Cassini to be involved in not one but two extended missions around Saturn. The first Venus fly-by occurring on 26 April 1998 at an altitude of 284 km imparted a 7.055 km/s increase in velocity. On 03 December 1998, Cassini performed an 88 minute thruster main engine burn to execute the Deep Space Maneuver in order to reduce the spacecraft's velocity by 450 m/s. This decrease in velocity allowed Cassini to fly-by Venus for a second time which would place the spacecraft in a fly-by trajectory with Earth. TCM 6 and TCM 7 occurred before the second Venus fly-by but

only required a ΔV of 11.6 m/s from the thruster main engine and 0.2 m/s from the RCS respectively. TCM 8 scheduled for 03 June 1999 was a bias clean-up TCM with an anticipated ΔV of 50 mm/s and was deemed unnecessary after reviewing the results from TCM 7 and if cancelled would lower the ΔV value for TCM 9. The second Venus fly-by occurred on 24 June 1999 at an altitude of 603 km and imparted a ΔV increase of 6.690 km/s. Four more TCMs (TCM 9, TCM 10, TCM 11, and TCM 12) utilizing the thruster main engine occurred before the Earth fly-by causing ΔV values of 43.5 m/s, 5.1 m/s, 36.3 m/s, 12.3 m/s respectively. The Earth fly-by on 18 August 1999 at an altitude of 1175 km imparted a ΔV increase of 5.477 km/s onto the Cassini spacecraft. This increase in velocity was sufficient in ensuring a fly-by of Jupiter, which was needed in order for the spacecraft to reach its final destination of Saturn. TCM 13 on 31 August 1999 with a ΔV of 6.7 m/s concluded the inner planetary cruise portion of Cassini's trajectory. The other six TCMs, the Jupiter fly-by, and the Saturn orbit insertion maneuver made up the outer planetary cruise portion of Cassini's trajectory.

TCM 14 was executed on 14 June 2000, just 288 days after TCM 13, to comply with the requirement of at least a five second duration thruster main engine burn every 400 days or less (a.k.a "flushing maneuver). The "flushing" maneuvers must occur in order to ensure that the small orifices of the feed system valves do not get plugged by oxidation from iron alloys in the bipropellant aboard the Cassini spacecraft. TCM 14 increased the velocity of spacecraft by 0.6 m/s. TCM 15 and TCM 16 were cancelled because TCM 14 placed Cassini-Huygens spacecraft in a very similar trajectory as the reference trajectory. Closest approach to Jupiter occurred on 30 December 10:12 UTC. The fly-by of Jupiter imparted a positive ΔV of 2.218 km/s at an altitude of 9,723,890 km. TCM 17 was executed on 28

February 2001 in order to realign the spacecraft's trajectory with a Saturn rendezvous. A 1.0 m/s ΔV was all that was needed to correct the spacecraft's trajectory. TCM 18 and TCM 19 were also "flushing" maneuvers executed on 3 April 2002, 399 days since TCM 17, and 01 May 2003, 393 days since TCM 18. Only TCM 18 required the use of the thruster main engine increasing the velocity by 1.2 m/s. TCM 19 was executed by the RCS and increased the velocity by 0.5 m/s. TCM 20 executed on 27 May 2004, 392 days since TCM 19, was the first pressurized maneuver since TCM 9. All the other trajectory correction maneuvers utilizing the thruster main engine were conducted in a blow-down system manner. TCM 20 increased the Cassini-Huygens spacecraft's velocity by 35 m/s and aligned the spacecraft with a fly-by trajectory of Saturn's largest irregular moon, Phoebe. Closest approach to Phoebe occurred on 11 June 2004 at an altitude of 2000 km. Five days after the Phoebe fly-by on 16 June 2004 TCM 21 was executed with a ΔV of 5.5 m/s in order to have Cassini-Huygens pass through the F and G rings of Saturn where the debris hazard is expected to be minimal. Finally on 1 July 2004 the Saturn orbit insertion was executed in order to place Cassini-Huygens into an elliptical orbit around Saturn. The thruster main engine ran for 1 hour and 36 minutes to decrease the spacecraft's velocity by 633 m/s. Figure 5-1 and Figure 5-2 show the trajectory of the Cassini-Huygens spacecraft from launch to Saturn Orbital Insertion.

After a Probe Release Maneuver (PRM) on 23 August 2004, the Huygens probe was release from the Cassini spacecraft on 25 December 2004 and landed on Titan's surface on 14 January 2005. On 30 June 2008 Cassini finished its primary mission of a 4 year tour around the Saturnian System and started its first extended mission, Cassini Equinox Mission.

The Cassini Equinox Mission ran from 01 July 2008 to 30 September 2010 and included Saturn's equinox in August of 2009. The spacecraft was able to study the seasonal changes on Saturn and Titan and explore the cryovolcanic plumes of ice on Saturn's six largest moon Enceladus. On 1 October 2010, the Cassini spacecraft entered its second extended mission named Cassini Solstice Mission. This mission will run until September 2017, a few months beyond Saturn's summer solstice in May 2017. The second extended mission also has Cassini flying between Saturn and its rings in a near polar orbit in order to study the internal structure of Saturn and the mass of its rings. After finishing the solstice mission, Cassini's fuel tanks will be depleted and the spacecraft will be sent into Saturn where it will be disintegrated by the temperature and pressure of Saturn's atmosphere to ensure no biological contamination on any of the Saturnian moons [41].

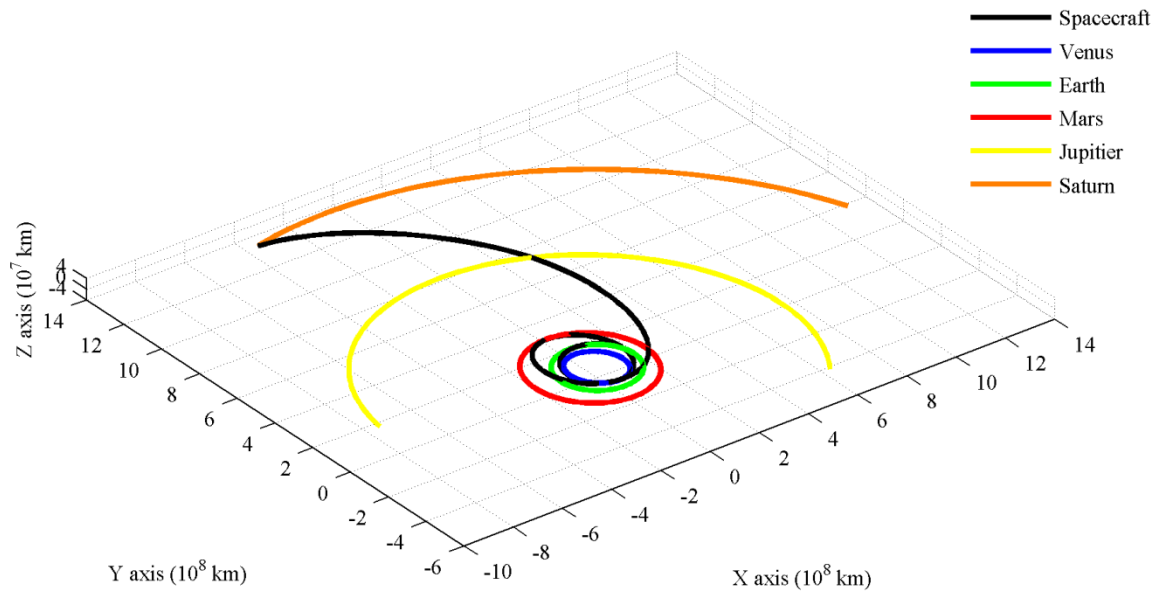


Figure 5-1: 3D Trajectory of Cassini-Huygens from Launch to Saturn in Heliocentric J2000.0 Ecliptic Frame

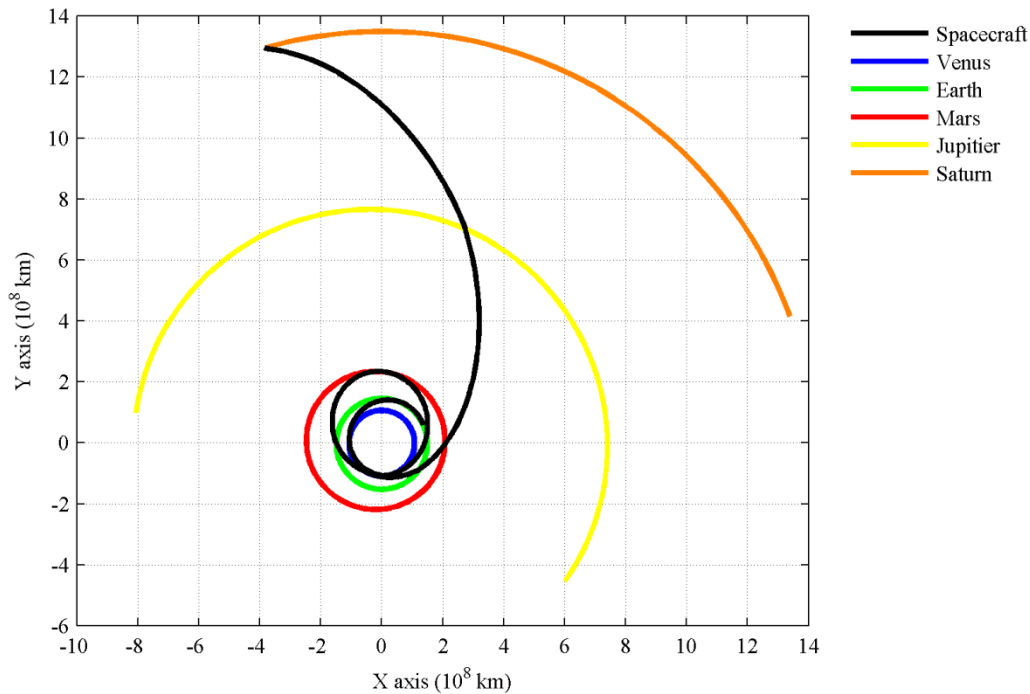


Figure 5-2: 2D Trajectory of Cassini-Huygens from Launch to Saturn in Heliocentric J2000.0 Ecliptic Frame

5.1.2.2 Comparison to Cassini-Huygens Mission

The most obvious comparison between the Fusion Propulsion Mission and Cassini-Huygens Mission to Saturn is the trip time. The Cassini-Huygens spacecraft reached Saturn in 2451 days (6.71 years) from launch on 15 October 1997 where as the Fusion Propulsion spacecraft will fly-by Saturn in 447 days (1.22 years) from leaving the Earth-Moon Lagrange Point 1 on 06 April 2025, about 18.25% of the Cassini-Huygens. The Fusion Propulsion spacecraft will reach Saturn in about 18.25% of the time that the Cassini-Huygens used to reach Saturn. This trip time savings would result in a reduced fiscal budget for the trip and would reduce the overall mission fiscal budget significantly.

The complexity of the Cassini-Huygens trajectory to Saturn was due to its mass being launched from the surface of the Earth. The Cassini-Huygens spacecraft is the largest spacecraft (by size and mass) to leave the inner solar system with a mass of 5,574 kg. Without the gravity assists maneuvers from Venus, Earth, and Jupiter the Titan IVB launch

vehicle would not have been able to send Cassini-Huygens to Saturn. Even though the Fusion Propulsion spacecraft is more than 10 times as massive as the Cassini-Huygens spacecraft, the Fusion Propulsion spacecraft's trajectory is not nearly as complex as the Cassini-Huygens spacecraft's trajectory because of the Fusion Propulsion spacecraft's initial launch location, the Earth-Moon Lagrange Point 1, and an acceleration phase from constant continuous thrust provided the fusion propulsion system. Also, the preliminary trajectory for the Fusion Propulsion spacecraft is adjusted continuously via thrust vectoring during the accelerating phase, which replaces the short duration trajectory correction maneuvers of Cassini.

5.1.3 New Horizons

New Horizons is a NASA mission to study the dwarf planet Pluto and its moons Charon, Nix, and Hydra. This is the first NASA mission to study the dwarf planet and its moons. NASA also plans to include an extended mission to reach one or more of the Kuiper Belt Objects. New Horizons is the first mission in NASA's New Frontiers program, a medium-cost (not to exceed \$700 million) series of space missions [42]. The New Horizons spacecraft was launched on January 19, 2006 at 19:00 UTC (14:00 EST) aboard an Atlas V 551 rocket with an ATK Star 48B SRM third stage on launch complex 41 at the Kennedy Space Center in Cape Canaveral, Florida [43]. The Atlas V 551 utilizes 5 SRM boosters, a liquid bipropellant first stage, and a Centaur second stage [36]. The first stage engine is the RL-180 engine burning liquid oxygen and rocket propellant 1 (kerosene, a.k.a. RP-1). The SRM boosters consist of 87% solid loading (68% Ammonium Perchlorate and 19% Aluminum) and 13% HTPB binder [34]. The Star 48B SRM consists of 89% solid loading (71% Ammonium Perchlorate and 18% Aluminum) and 11% HTPB binder [44].

The propulsion system and attitude control system for the New Horizons spacecraft share a monopropellant blowdown system. The propellant is liquid hydrazine and the pressurant is gaseous helium. Both the propellant and pressurant are stored in one titanium tank [42]. The spacecraft will travel approximately 3 billion miles in almost 10 years to reach the dwarf planet Pluto with reconnaissance of the planet beginning on April 12, 2015 and the closest approach occurring on July 14, 2015.

5.1.3.1 New Horizons Trajectory and Mission

When the New Horizons spacecraft was launched on January 19, 2006, it left the Earth's orbit with an escape velocity of 16.2 km/s [43], making it the fastest human-made object to leave Earth's orbit. The high escape velocity allowed the spacecraft to reach lunar orbit in approximately nine hours [42]. For a comparison, the Apollo astronautics spent 3 days traveling in space before reaching lunar orbit. The spacecraft needed to be launched before February 3, 2006 in order to take advantage of a Jupiter gravity assist. The gravity assist from Jupiter is a very important maneuver for the New Horizons trajectory. Without the gravity assist, the trip time to Pluto would have to be extended three to five more years. The New Horizons spacecraft reached the closet point to Jupiter on February 28, 2007 and was about 1.4 million miles from the center of the gas giant. This distance is about three times closer than the closest distance the Cassini spacecraft was to Jupiter in late 2000. New Horizons left Jupiter with a heliocentric velocity of 22.85 km/s increasing its velocity by 3.89 km/s. On June 8, 2008, the spacecraft crossed over Saturn's orbit with a slower heliocentric velocity of 18.26 km/s due to the Sun's gravitational acceleration. The spacecraft crossed over Uranus's orbit on March 18, 2011, and will cross Neptune's orbit on August 24, 2014. When New Horizons reaches Pluto on July 14, 2015, the spacecraft's velocity will be

decreased to about 14 km/s. On February 25, 2010 the spacecraft reached half the total travel distance from Earth to Pluto, and is currently (March 2012) in a spin-stabilized “hibernation mode”. Having the New Horizons spacecraft “sleep” during this period reduces wear and tear on the spacecrafts electronics. Only crucial systems will continue to operate during this time and a beacon through the medium gain antenna will broadcast weekly updates back to Earth. Trajectory correction maneuvers along with other system checks and instrument calibrations are performed once a year and the first annual system check occurred six months after the Jupiter flyby. “Hibernation mode” will last until about six months before closest approach to Pluto. Figure 5-3 and Figure 5-4 show New Horizons trajectory from launch to Pluto in Heliocentric J2000.0 Ecliptic Coordinate Frame.

The spacecraft’s closest approach distance to Pluto will be about 6,200 miles (10,000 kilometers) away from the planet’s surface, and 14 minutes later it will reach the closest approach to Charon at 16,800 miles (27,000 kilometers) away. In order to complete all of the scientific objectives for the mission, the spacecraft must be rotated in various orientations during the Pluto flyby. Without rotating the spacecraft, some of the scientific instruments could not do their assigned tasks or at the very least would not be able to collect sufficient data. Unfortunately, these rotations will point the spacecraft’s antenna away from Earth causing limited communication to the spacecraft during this critical time. In order to overcome the obstacle of not having continuous communication from Earth during the Pluto flyby, the entire sequence for the encounter of Pluto will be pre-programmed into all of New Horizons flight path computers. The spacecraft will fly between Charon’s orbit and Pluto and then continue its journey into the Kuiper Belt. Like the Pioneer and Voyager spacecraft, New Horizons is in a hyperbolic trajectory and will eventually escape the solar system.

When New Horizons successfully completes all of its mission objectives, the spacecraft will conduct similar reconnaissance on one or two KBOs. The extended mission will begin just two weeks after the flyby of Pluto and will require the thrusters to be fired in order to set a trajectory toward the first KBO. The farthest KBO that will be chosen to study will not be more than 55 AU, because that is the maximum operating range for the New Horizons' antennas due to the reduction in power from its power supply, a radioisotope thermal generator (RTG). Propellant will be minimized by having the spacecraft take long range pictures of KBO as early as possible. The spacecraft will reach the first KBO in about two to three years after the Pluto encounter. The mission will continue until about 2021 when the spacecraft will no longer be able to send communication signals back to Earth.

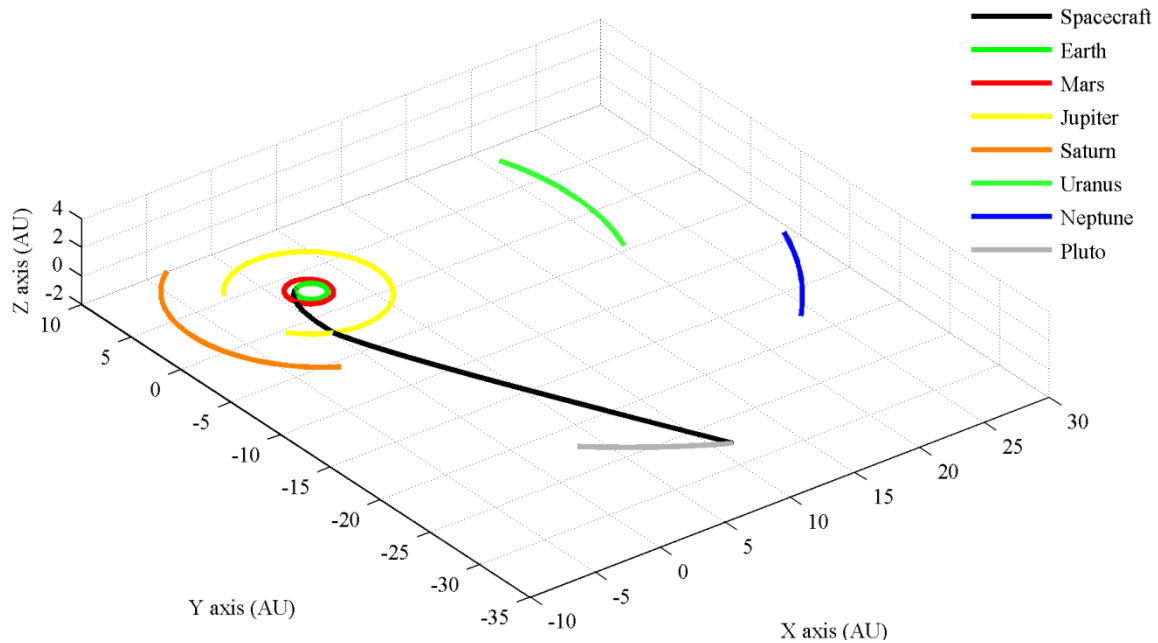


Figure 5-3: 3D Trajectory of New Horizons from Launch to Pluto in Heliocentric J2000.0 Ecliptic Frame

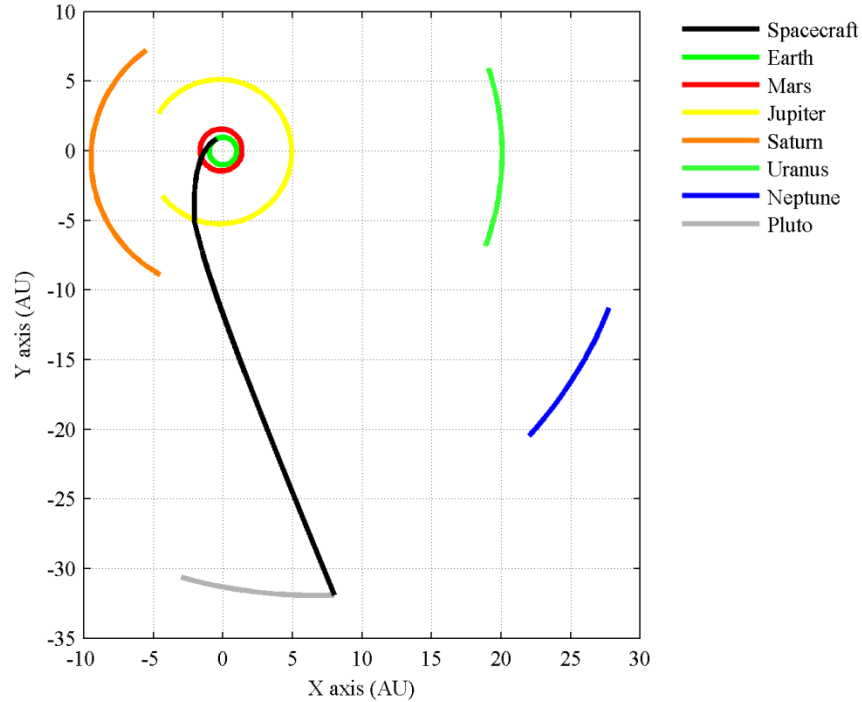


Figure 5-4: 2D Trajectory of New Horizons from Launch to Pluto in Heliocentric J2000.0 Ecliptic Frame

5.1.3.2 Comparison to New Horizons

Unlike the New Horizons spacecraft, the Fusion Propulsion spacecraft requires a significantly larger amount of time in order to reach the minimum escape velocity from the Earth. The New Horizons spacecraft reached a velocity of 16.26 km/s when the Star 48B burned out 47 minutes after launch, and this velocity was approximately 6 km/s more than the required velocity to escape the Earth’s gravitational influence at that altitude. When the Fusion Propulsion spacecraft starts its propulsion system, the spacecraft will be traveling 0.856 km/s with respect to the Earth at an altitude of 323,573 km above the surface of the Earth. The minimum escape velocity at this altitude is 1.554 km/s. If the Fusion propulsion spacecraft were to escape the gravitational influence of the Earth at this altitude, then the spacecraft would have to almost double its velocity instantaneously. It will take the Fusion Propulsion spacecraft almost seven days after epoch to reach the minimum escape velocity from the Earth’s gravitational influence with a velocity magnitude of 1.692 km/s with respect

to the Earth and will occur just hours after its closest approach to the Earth on 13 April 2025. On 19 July 2025 the Fusion Propulsion spacecraft will match the escape velocity of the New Horizons spacecraft (16.26 km/s), but unlike the New Horizons spacecraft continuously decreasing in velocity until its Jupiter fly-by, the Fusion Propulsion spacecraft will continue to accelerate until 17 Nov 2025 and reach a velocity of 71.742 km/s with respect to the Earth.

When the New Horizons spacecraft finishes its extended mission in 2021, the spacecraft will be about 55 AU away from the Earth and the entire mission will have lasted for about 15 years. The Fusion Propulsion spacecraft, however, will reach the same distance in about 5 years and nearly double the distance in 10 years. It could have the same limitations on communication unless a more powerful antenna is included in the payload package, and sufficient power is available. Such details are beyond the scope of this thesis.

5.2 Electrical Propulsion

In electrical propulsion the propellant is either heated by an electrical system or is ejected from the spacecraft due to electrical properties.

5.2.1 Electrical Propulsion Background

Electrical Propulsion (EP) was envisioned by the same founding fathers of modern day chemical propulsion, Tsiolkovsky, Goddard, Oberth, and et al. [45], but took a back seat to chemical propulsion for many years until Ernst Stuhlinger's first published paper on the subject entitled "Possibilities of Electric Space Ship Propulsion" for the 5th International Astronautical Congress in 1954 [46]. The paper showed specific power (α) as an essential parameter to EP and ion propulsion could be used for low-thrust applications. By the 1990's EP had been utilized in 100's of missions. The variants of EP that had emerged can be

classified according to the primary acceleration mechanism: electrothermal, electrostatic, and electromagnetic. For completeness, these are discussed below.

5.2.1.1 Electrothermal

Electrothermal devices simply heat the propellant (typically a gas, sometimes a liquid) electrically before being expelled at supersonic speeds out of a rocket nozzle. The two most common electrothermal thrusters are resistojets and arcjets. Resistojets are the simplest EP thruster to design and manufacture because the propellant is heated by flowing over an electrically heated metal surface such as coils of wires. Resistojets have specific impulse values similar to chemical rockets, but offer the advantage of using many different types of propellants for the same resistojet design including waste products (e.g. H₂O and CO₂) from manned missions. The slightly more complex arcjet heats the propellant with an arc of electricity before the propellant passes through the nozzle throat. The propellant can be heated to a temperature of 20,000 K or more resulting in a more energetic propellant entering the nozzle [47].

5.2.1.2 Electrostatic

Electrostatic devices accelerate charged particles with an electrostatic field. The thrusters can only operate in a vacuum or near vacuum environment. Electrons, due to their mass can be accelerated to nearly the speed of light, but the momentum created by electrons is relatively negligible due to their small mass. Heavier positively charged particles (typically Xenon ions) are used as the propellant for generating useful thrust. The source of the positively charged particle can be categorized into two types. Electron bombardment produces positive ions in a gas by bombarding the gas with electrons usually emitted from a cathode [47]. In field emission electric propulsion (FEEP) positive ions are produced from a

liquid metal source subjected to an electric field [34]. Many electric bombardment electrostatic thrusters are in the operational status were as the FEEP system is in the qualified status [34].

5.2.1.3 Electromagnetic

Electromagnetic thrusters accelerate a charge-neutral plasma via the interaction of currents with magnetic fields ($\mathbf{j} \times \mathbf{B}$ Lorentz force) [48]. The Lorentz force accelerates the propellant before being exhausted from the spacecraft. Electromagnetic thrusters are characterized into three types, magnetoplasmadynamic (MPD), pulsed-plasma, and Hall-effect. A magnetoplasmadynamic thruster can be constructed by applying a magnetic field to an arcjet or by creating a self-induced magnetic field from the current flow through a gas. Pulsed-plasma thrusters (PPTs) utilize a self-induced magnetic field with the help of a capacitor charged by the spacecraft power supply and operate in a pulse-state in order for the capacitor to recharge. Solid propellant, such as Teflon [34], can be used by ablating the surface of a Teflon block with an arc of electricity discharged from the capacitor. The discharge ablates, vaporizes, and ionizes a small amount of Teflon and the Lorent force accelerates this plasma away from the Teflon block. It should be mentioned that a large component of the thrust in this device is actually due to thermal expansion after the discharge has ended. Hall-effect thrusters rely on the Hall-effect when particle densities are low or when magnetic fields are high. The Hall-effect occurs when a voltage difference (Hall voltage) is transverse to the current and the current is perpendicular to the magnetic field. A Hall-effect thruster (Hall thruster) is sometimes referred to as a gridless ion thruster and can also be classified as an electrostatic device [47].

5.2.2 Dawn

Dawn is a NASA mission to study the asteroids Vesta and Ceres and is the first spacecraft to orbit more than one celestial body. It is the ninth project in NASA's Discovery Program, a low-cost series of missions within NASA's Science Mission Directorate in which the scientific community proposes missions and is lead by a scientific principle investigator (PI). The Dawn spacecraft was launched on 27 September 2007 at 11:34:00 UTC (07:34:00 EDT) aboard a Delta II rocket with nine SRM boosters on launch complex 17B at the Kennedy Space Center in Cape Canaveral, Florida [49]. The Delta II rocket is a conventional chemically powered launch vehicle with liquid engines for the first and second stage and an optional SRM for the third stage. The first stage engine is a Boeing/Rocketdyne RS-27A gas generator using liquid oxygen and RP-1; while the second stage is an Aerojet AJ10-118K utilizing Aerozine-50 and NTO. An ATK Star 48B SRM was also included for the third stage of the launch vehicle [36]. The nine SRM boosters are ATK GEM-46 boosters where GEM stands for graphite epoxy motor indicating a composite motor case and 46 is the motor case diameter in inches. The SRM boosters consist of 87% solid loading and 13% HTPB binder [37]. The propulsion system aboard the Dawn spacecraft is a xenon ion propulsion system (XIPS) utilizing 3 NSTAR (NASA Solar Technology Application Readiness) thrusters. (An NSTAR thruster was first used aboard the Deep Space 1 spacecraft to explore the asteroid Braille and then the comet Borrelly) [34]. The RCS thrusters utilize hydrazine and produce 0.9 N of thrust per thruster [50]. Dawn was captured into Vesta's orbit on 16 July 2011 03:48 UTC and will orbit Vesta until July 2012. The spacecraft will then travel to Ceres arriving in February 2015 and end its mission in July 2015.

5.2.2.1 Dawn Trajectory and Mission

The Dawn spacecraft separated from the Star motor at 12:36 UTC (8:36 EST) on 27 September 2007, just over an hour after launching from complex 17B at the Kennedy Space Center. After many extensive tests and checklists, the ion propulsion system (IPS) was fired on 6 October 2007. Before the spacecraft entered the long-term cruise to fly-by Mars, the IPS was fired for a total testing time of 11 hours 14 minutes from 16 starts over the month of October and November. Further testing of other spacecraft subcomponents along with software upgrades occurred until 17 December 2007. At approximately 20:00 UTC 17 December 2007, the spacecraft entered long-term cruise to Mars with the IPS running during most of the cruise. On 31 October 2008, the acceleration phase of the long-term cruise to Mars was terminated with the Dawn spacecraft in a trajectory path to fly-by Mars in February 2009. The IPS was fired for a total time of 270 days equally about 85% of the long-term cruise time with periodic coasting accounting for the rest of the time. Only 72 kg from the initial 450 kg of xenon propellant had been expelled from the spacecraft when the acceleration phase ended on 31 October 2008, and imparted a ΔV of 1.81 km/s since the acceleration phase started on 17 December 2007. The Dawn spacecraft conducted its first trajectory correction maneuver, TCM 1, on 20 November 2008. The maneuver started at 12:31 UTC and lasted for slightly more than two hours, ending at 14:42 UTC. TCM 1 only changed the speed of the spacecraft by 60 cm/s even though the spacecraft was already traveling at 22.5 km/s relative to the Sun, but the maneuver was required in order to obtain the correct altitude needed for the Mars fly-by. TCM 2 was scheduled for an undetermined date in January of 2009, but because of the success of TCM 1, TCM 2 was deemed unnecessary and was cancelled. Closest approach to Mars occurred on 18 February 2009 at

00:28:58 UTC (17 February 19:28:58 EST) with an altitude of 542 km. The altitude at closest approach was only 42 km from the target altitude of 500 km and was well within the altitude range of 300 km to 750 km. The gravity assist from Mars imparted a ΔV of 3.188 km/s, the minimum ΔV needed from the gravity assist was calculated to be 2.6 km/s, and a turning angle of 78 degrees.

During the coasting phase after the Mars fly-by, another software upgrade (flight software 8.0) was sent to the Dawn spacecraft on 13 April 2009 and was fully functional three days later. On 27 April 2009, pre-start thrusting procedures began with a four hour test of thruster 2 of the IPS. While thruster 1 and thruster 3 had already accumulated 123 days and 158 days respectively, thruster 3 had only operated for 22 hours at this point in Dawn's mission. A second test was conducted on 01 May 2009 and confirmed that flight software 8.0 was capable of piloting the spacecraft. The longest coasting phase of the Dawn mission ended on 8 June 2009 when the IPS was started. This acceleration phase of the mission was much longer than the first acceleration phase between Earth and Mars and lasted until the Dawn spacecraft reached the asteroid Vesta in July of 2011. During this accelerating phase, the spacecraft's velocity increased by an average of 7 m/s per day while only using 0.26 kg per day, and when the spacecraft reached Vesta, approximately half of the 378 kg of xenon propellant that was in the tank before the acceleration phase was still left.

The approach phase to Vesta began three months before orbiting Vesta when the Dawn spacecraft reached 1.21 million km from Vesta. At this distance optical navigation was available for use providing an additional resource to the navigation system which previously only consisted of radio navigation. The Dawn spacecraft was captured into Vesta's gravity on 16 July 2011 at 03:48 UTC when the spacecraft was approximately

16,000 km from Vesta. The approach phase continued for almost three weeks after capture when the spacecraft reached an altitude of 2,700 km on 02 August 2011 at 07:07 UTC. Fine tune orbit adjustments occurred at this altitude until 11 August 16:13 UTC at which time the spacecraft started the survey phase of Vesta. The survey phase orbit had a 69 hour period in which the spacecraft provided images of Vesta about 150 times sharper than from the Hubble telescope. After seven orbits the Dawn spacecraft first entered the High Altitude Mapping Orbit, HAMO, before decreasing its altitude to the Low Altitude Mapping Orbit, LAMO. HAMO was reached on 18 September 2011 at an altitude of 680 km and an orbital period of 12.3 hours. The primary goals of HAMO were to map Vesta's illuminated surface in color, provide stereo data, and obtain visible and infrared mapping spectrometer data. The Dawn spacecraft orbited Vesta at HAMO for a total of 60 orbits before descending to LAMO. On 12 December 2011, the spacecraft reached LAMO altitude of 210 km (average). At this altitude the spacecraft has an average period of 4 hours 21 minutes. The primary mission objective at LAMO was to collect data for the gamma ray and neutron detector and measure the gravitational force in order to determine the composition of the asteroid. Originally scheduled for 70 days, LAMO was extended an additional 40 days and ended on 01 April 2012. The Dawn spacecraft is currently (15 April 2012) on its way to the second high altitude mapping orbit, HAMO2, with the same 680 km altitude as the first HAMO and is scheduled to depart Vesta in June 2012 in which the spacecraft will enter the cruise phase to Ceres.

The cruise phase from Vesta to Ceres will last almost 2.5 years with the majority of time spent in the acceleration phase. Ceres approach is scheduled to start in November 2014 when the spacecraft is approximately three month from reaching Ceres and ends when the

Dawn spacecraft achieves its first science observation orbit around Ceres in February 2015. Just as in orbiting Vesta, the spacecraft will operate at different orbits around Ceres for predetermined periods of time in order to conduct different types of scientific measurements of the asteroid. At the end of Dawn's primary mission, the spacecraft will be sent to an average altitude of 700 km to ensure that the spacecraft will not impact the surface of Ceres for at least a half century. Figure 5-5 and Figure 5-6 show the trajectory of the Dawn spacecraft from Earth to Ceres.

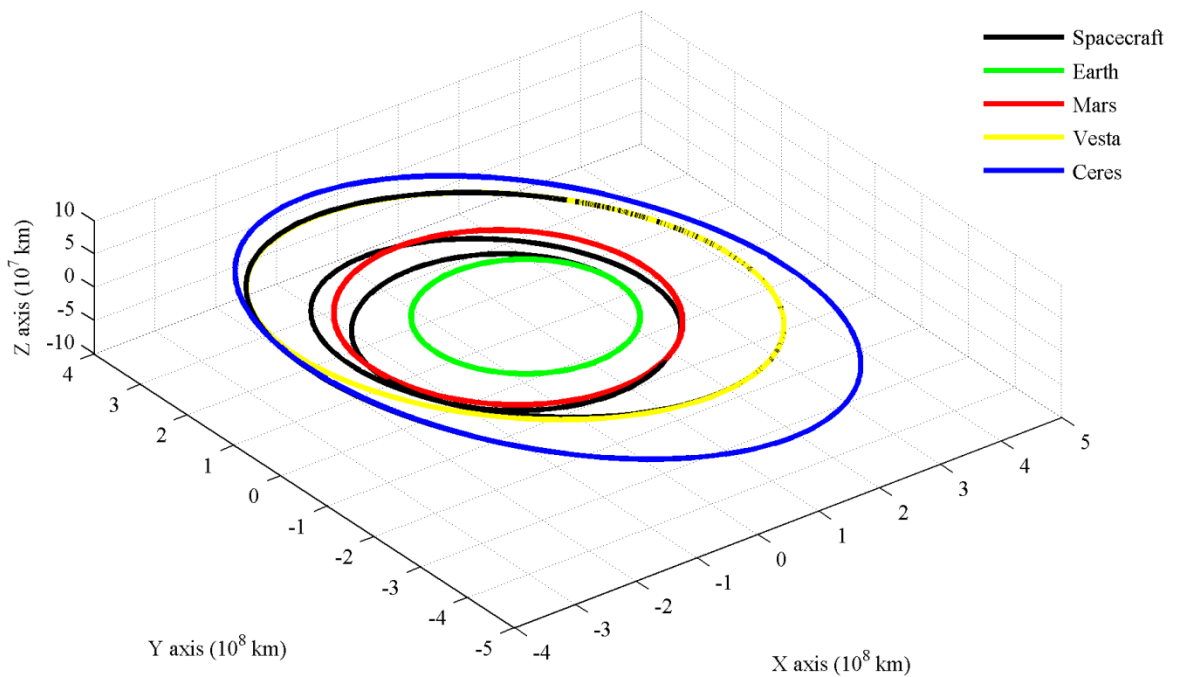


Figure 5-5: 3D Trajectory of Dawn in Heliocentric J2000.0 Coordinates from Earth to Ceres

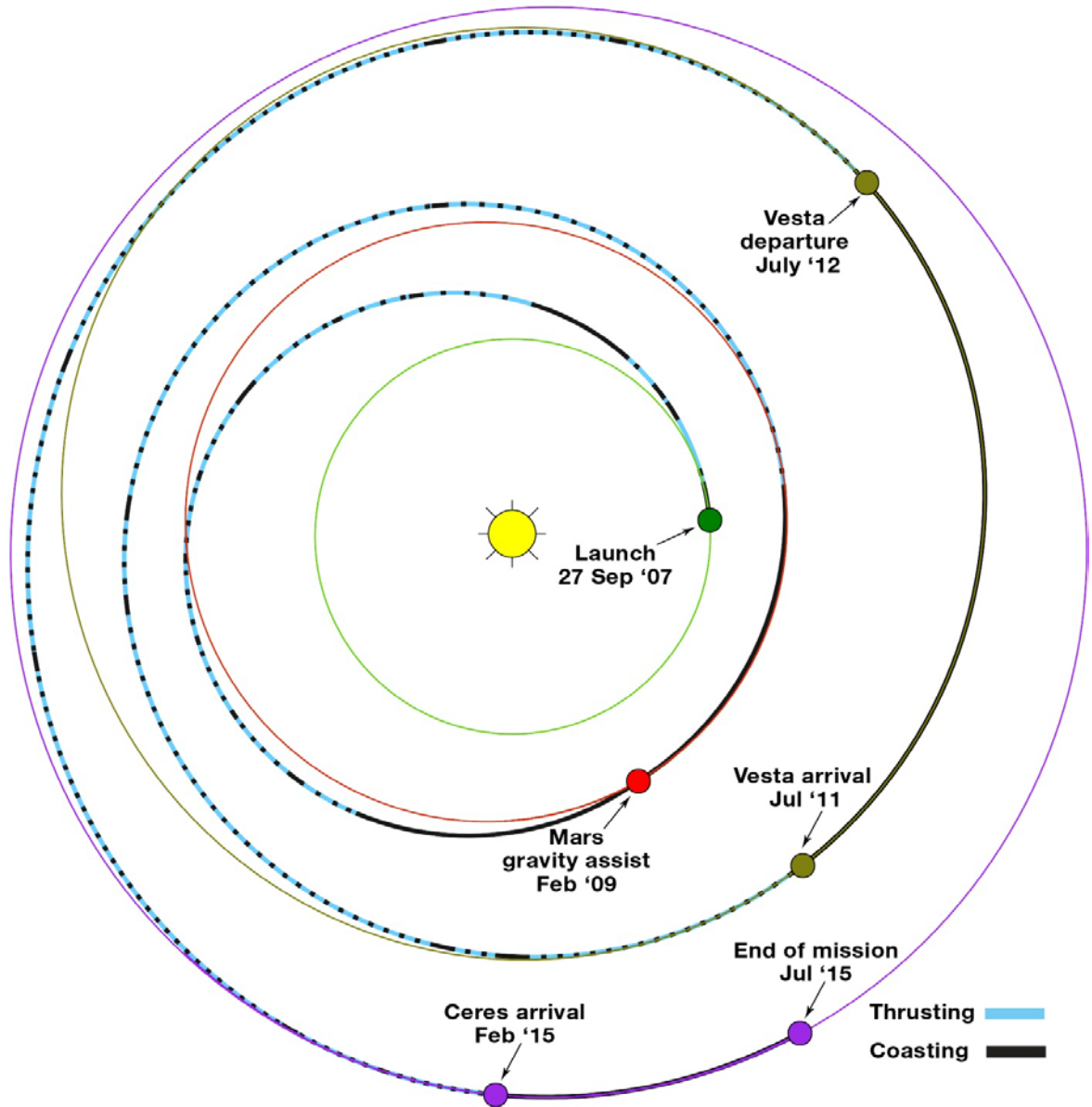


Figure 5-6: 2D Trajectory of Dawn showing acceleration and coasting phases from Earth to Ceres [50]

5.2.2.2 Comparison to Dawn

Just like the Dawn Spacecraft, the Fusion Propulsion spacecraft utilizes longer burn times and lower thrust than conventional chemical propulsion. Unlike the Dawn spacecraft, the Fusion Propulsion Spacecraft does not require the extremely long burn time of the Dawn spacecraft in order to cover the same distance. When the Dawn Spacecraft reached Vesta, the IPS had a total run time of almost 3 years, and when the spacecraft finishes its mission in

July 2015, the IPS will accumulate nearly 6.5 years of run time. Ceres orbits the Sun at a distance of 2.767 AU (average), and if the Fusion Propulsion spacecraft were to flyby Ceres, the spacecraft would reach the asteroid in just over a half year utilizing less than 10% of Dawn's thrust time. The significant decrease in burn time not only results in a shorter length in the mission operation time but also a significant decrease in monetary fund for the overall operational budget.

The Dawn spacecraft is also limited (mostly) to the inner solar system because of its power source that all of the spacecraft's components use to operate. The Dawn spacecraft's power source consists of two 18 m² solar panels able to provide the spacecraft with enough power throughout the entire mission. Unfortunately, power degrades as the life of a solar panel increases as well as when the spacecraft increase its distance from the Sun. At the start of the Dawn mission, the solar panels aboard the spacecraft supplied 10.3 kW of power, and at the end of mission, the solar panels will only be able to supply 1.3 KW of power. At the maximum thrust of 92 mN for the IPS, 2.6 kW of power is required by the IPS. Thus the maximum thrust amount cannot be utilized during the entire mission. Fortunately the IPS can run at a variable thrust rate, and at the minimum thrust of 19 mN, the IPS only requires 0.5 kW allowing the rest of the power from the degraded solar panels to be used on other spacecraft components. The Fusion Propulsion spacecraft has a constant thrust of 101.937 N throughout its entire acceleration phase of its trajectory and has a large enough power source to supply the required power to the fusion reactor as well as the scientific payload aboard the spacecraft. With a much higher constant thrust, the Fusion Propulsion spacecraft can reach the same distance as the Dawn spacecraft in a significantly shorter time span with a

significantly larger payload as well, and if the Fusion propulsion spacecraft were to flyby Ceres, a gravity assist maneuver from Mars would not be necessary.

5.3 Conclusion

The Fusion Propulsion spacecraft would be the most massive and fastest human-made object to travel through the solar system. This is easily shown in Figure 5-7 where the Fusion Propulsion spacecraft's magnitude distance from the Sun is plotted versus trip time with the maximum distance shown at 40 AU (just beyond Pluto's aphelion) along with each previously discussed spacecraft (including the New Horizons spacecraft which is currently the fastest human-made object to leave Earth). If the plot in Figure 5-7 were tremendously enlarged at the Earth's trajectory, the plot would clearly show that the Fusion Propulsion spacecraft actually takes more time initially to cover the same distance as the other three spacecrafts but then quickly overtakes the Cassini and Dawn spacecraft within the first two months of the trip time before overtaking the New Horizons spacecraft in slightly over the first half year of the mission trip time.. A plot of the velocity for each spacecraft versus trip time would look similar to the plot of spacecrafts' magnitude distance from the Sun versus trip time shown in Figure 5-7; where the Fusion Propulsion spacecraft's velocity would initially be slower than the other three spacecrafts' velocities but would quickly overtake the other spacecrafts' velocities in a relatively short period of time. This is mostly due to the fact that the other spacecrafts' velocities are continually decreasing (unless a gravity assist maneuver is conducted) while the Fusion Propulsion spacecraft's velocity is increasing for the first 225 days of its trip time. A similar comparison of the Fusion Propulsion spacecraft to the current spacecrafts escaping the solar system is shown in Figure 5-8 where the

spacecrafts' magnitude distance from the Sun are plotted versus the actual date in years with a maximum distance of 300 AU (inside the Interstellar Medium).

Starting with the New Horizons spacecraft, the Fusion Propulsion spacecraft reaches the same magnitude distance from the Sun at 87.243 AU on 17 May 2034, less than ten years from epoch (06 April 2025 at 14:04:15.000), when the New Horizons spacecraft will have been traveling for more than 28 years. After passing the New Horizons spacecraft, the Fusion Propulsion spacecraft will reach the same magnitude distance from the Sun as the Pioneer 11 spacecraft at 150.44 AU in 2040 and will reach the Pioneer 10 spacecraft's magnitude distance of 185.46 AU from the Sun in 2044. (These dates are estimates based on the last known positions and velocities of both Pioneer spacecrafts. Last contact with Pioneer 10 was on 23 January 2003 due to loss of spacecraft power, and last contact with Pioneer 11 was September 1995 because the spacecraft's antenna could no longer point towards Earth. Pioneer 10 was launched on March 02 1972 01:49:00 UTC and Pioneer 11 was launched 06 April 1973 02:11:00 UTC.) When the Fusion Propulsion spacecraft reaches a magnitude distance of 206.48 AU from the Sun on 30 May 2046, the spacecraft will be at the same magnitude distance of the Voyager 2 spacecraft launched on 20 Aug 1977 14:29:00 UTC. Then on 23 December 2051 at a magnitude distance of 261.60 AU from the Sun, the Fusion Propulsion spacecraft will reach the same magnitude distance as the Voyager 1 spacecraft launched 05 September 1977 12:56:00 UTC and will become the farthest human-made object from Earth. Table 5-1 shows the date and distance of when the Fusion Propulsion spacecraft will reach the magnitude distance of each escaping spacecraft.

When the Fusion Propulsion spacecraft passes both Voyager spacecrafts, the Voyager spacecrafts should no longer be capable of transmitting radio signals because both

spacecrafts are expected to lose the capability of transmitting around the year 2025 (nearly 50 years of communication with the Earth) due to insufficient power from their RTG power sources. Fortunately, the Fusion Propulsion spacecraft will have a mission trip time of about 25.5 years compared to 74 years for the Voyager 1 spacecraft when the Fusion Propulsion spacecraft passes Voyager 1, and if the Fusion propulsion spacecraft is designed with a sufficient power source capable of providing communication with the Earth for the first 50 years of its mission, then the spacecraft would be able to transmit data to the Earth from a distance of about 500 AU (not shown in Figure 5-8) well within the Interstellar Medium. If the Fusion Propulsion spacecraft has a longer lived power source, it will be able to provide valuable scientific information about the Interstellar Medium, including information about the nearest Oort cloud objects at approximately 2,000 AU from the Sun.

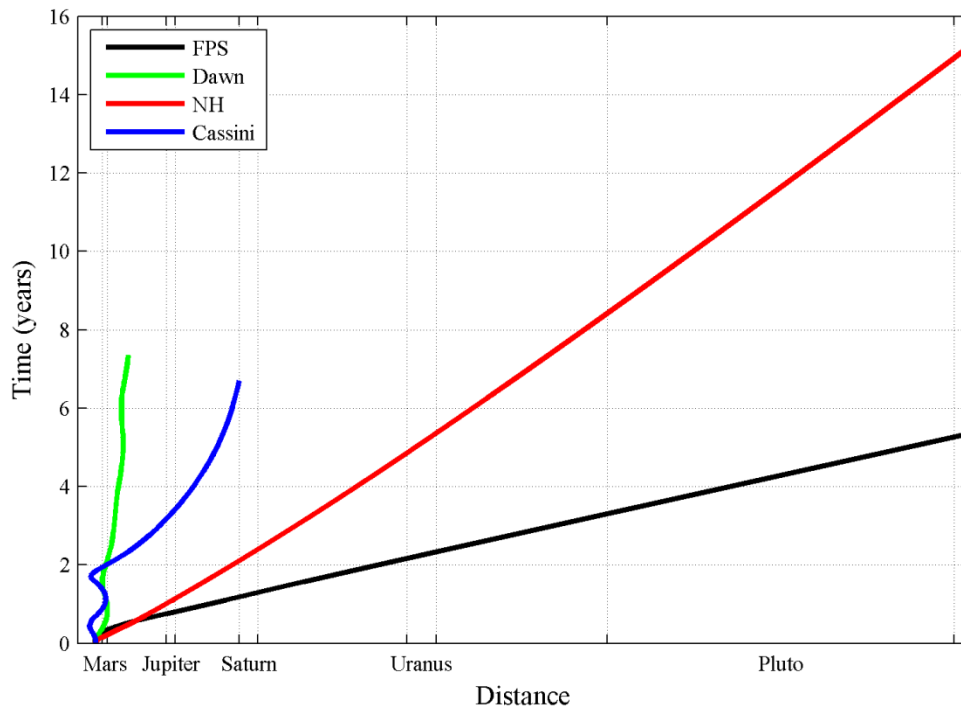


Figure 5-7: Plot of Spacecraft's Magnitude Distance from the Sun versus Trip Time

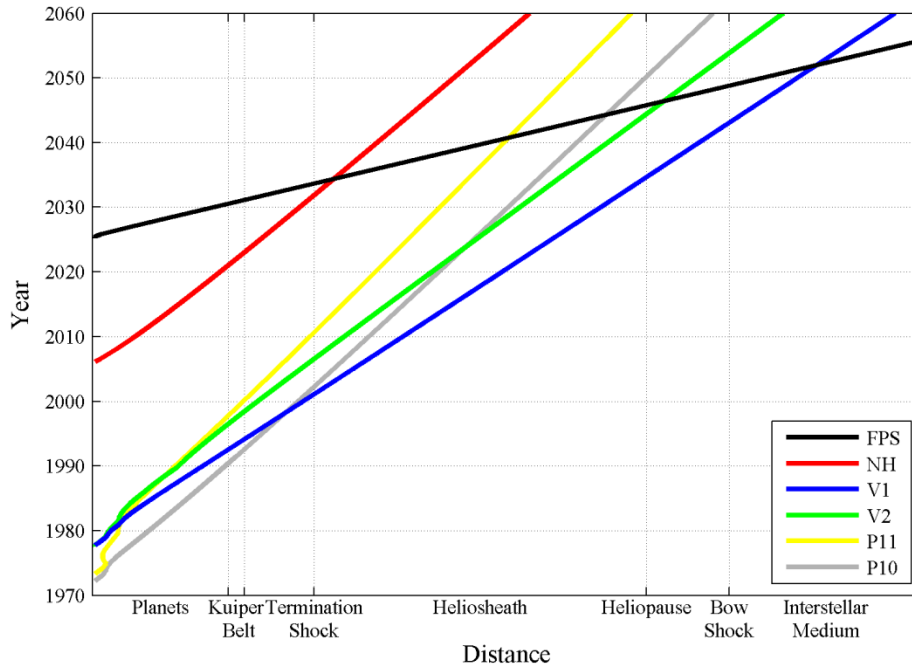


Figure 5-8: Plot of Spacecraft's Magnitude Distance from the Sun versus Year

Table 5-1: Date when Fusion Propulsion Spacecraft will reach Escaping Spacecraft same Magnitude Distance

Spacecraft	Date	Distance (AU)
New Horizons	17 May 2034	87.243
Pioneer 11	01 October 2040	150.44
Pioneer 10	15 April 2044	185.45
Voyager 2	30 May 2046	206.48
Voyager 1	23 December 2051	261.60

CHAPTER VI

CONCLUDING REMARKS

Fusion propulsion has the potential to revolutionize exploration of celestial bodies in the solar system. In this thesis, a hypothetical fusion propulsion system with an initial mass of 60 mT, a specific impulse of 20,000 seconds and a 102 N of thrust were utilized in a robotic flyby mission of Saturn and beyond. GMAT, a trajectory analysis tool, was utilized to conduct the trajectory analysis for this mission. Then the hypothetical mission was compared to existing spacecraft mission with similar characteristics. The comparisons demonstrated that fusion propulsion spacecrafts are desirable for traveling great distances in approximately one third the time of currently utilized chemical propulsion systems. The gravity free method for estimating trip time was shown to give a great departure from the more accurate GMAT tool which includes the asymmetric gravitational and N-body perturbations. The patched conic method gave a trajectory which was very close to that of the GMAT model which included the gravity and N-body terms, but the point of closest approach at Saturn was considerably different.

6.1 Additional Fly-by Missions

The fusion propulsion spacecraft designed for this thesis was optimized for a Saturn fly-by, but the spacecraft could be used for many other planetary fly-bys with little to no

design modifications to the spacecraft. For instance if the initial epoch of 06 April 2025 at 14:04:15.000 was altered to a slightly earlier date, or much later date, the spacecraft could be able to fly-by both Jupiter and Saturn. Other fly-by missions that could be conducted with the same or a slightly altered spacecraft design include fly-by missions to Uranus, Neptune, or Pluto. Multi-planetary fly-by missions such as Jupiter/Uranus or Saturn/Neptune can also be conducted utilizing the fusion propulsion spacecraft design and would not result in a significant increase in mission trip time. Slightly more complex trajectory analysis is needed for multi-planetary fly-by missions compared to single planetary fly-by missions.

6.2 Rendezvous and Return Missions

Initially, rendezvous (orbit capture) and round trip missions were intended to be explored as part of the work. Unfortunately after many trials and iterations, a conclusion was established indicating NASA's General Mission Analysis Tool (GMAT) was not the ideal software package available for medium-thrust (i.e. fusion propulsion) rendezvous missions. While this could be accomplished in an approximate way with patched conics and spiral trajectories, it was preferred to retain the high fidelity of GMAT's gravitational models and N-body physics and focus on a fly-by mission. For medium-thrust rendezvous inter-planetary missions, low-thrust trajectory tools (LTTT) maybe the closest ideal software package currently available. NASA currently utilizes several LTTT software packages such as Mystic for the Dawn spacecraft trajectory. Unfortunately, most LTTT from NASA are only available to NASA employees, but some LTTT such as the Mission Analysis Low-Thrust Optimization (MALTO) tool are available to academia or to the industry through commercial licensing. LTTT typically rely on the ability to solve nonlinear optimization problems. A medium-thrust spacecraft inter-planetary rendezvous mission would have a

similar trajectory as a low-thrust (i.e. electric propulsion) spacecraft inter-planetary rendezvous mission except thrusting would occur continuously during the acceleration and deceleration phases (See Dawn trajectory in Figure 5-6 for example of a low-thrust spacecraft inter-planetary rendezvous mission trajectory). Return missions to Earth such as manned missions to other planets and moons are simply multi-rendezvous missions and would require additional trajectory analyses for the return trip back to Earth.

6.3 Precision of Trajectory Analysis

Many trajectory tools are rated with a precision level ranging from very low fidelity to extremely high fidelity. GMAT's precision rating is based mostly on user inputs and settings rather than the mathematical expressions written in the source code. The user inputs and settings used in GMAT for the trajectory analysis of the Fusion Propulsion spacecraft described in this thesis would most likely have a rating between low and medium fidelity. The rating is based on the inputs and settings for each propagator. Settings such as the atmospheric and gravity model are only available for the primary body, and GMAT's default source code only has these models for Venus, Earth and Mars and a gravity model for the moon. All other celestial bodies must be selected as a point mass, unless an external atmospheric or gravity model is provided for GMAT.

Also, the propagator used in the propagation command was determined by the location of the spacecraft relative to the primary body. Once the magnitude distance of the spacecraft equaled the radius of the sphere of influence, the propagation was terminated in order to select a new propagator (Patched Conic Method). Radius values for each SOI were calculated with Laplace's equation. Unfortunately, the equation developed by Laplace is only approximating the radius value for the SOI based on the mass of the planet, the mass of

the Sun, and the mean orbital distance between the Sun and planet (see APPENDIX D for Laplace's equation). GMAT could increase its precision by allowing more than one planet per propagator to utilize an atmospheric model (if necessary) and gravity model, thus eliminating the need to calculate the radius of the SOI for each planet. This would allow just one propagator to be used for all propagations and would eliminate the Patched Conic method by replacing it with the N-body method. Other settings in the integrator section of the propagator can also be altered to increase GMAT's precision. For instance, decreasing the minimum step size value or accuracy value may result in a more precise simulation. Also, more accurate integrators could be added to GMAT to increase precision.

6.4 Remarks on Future Work

The fly-by mission studied in this thesis was a first step towards understanding fusion propulsion utilization for space travel using high fidelity models. Initially, it was desired to study a rendezvous (orbit insertion at Saturn) maneuver and possibly the two-burn maneuver discussed by Adams [51]. However, it was realized that GMAT requires alterations in its source code in order to add additional commands for finite burn targeting. The additional commands allow GMAT to pass user-defined data to a plug-in in which a targeting solution can be calculated. Without the additional commands and plug-in, GMAT is only suitable for fly-by missions when utilizing long durations of finite burning. The fly-by mission discussed in this document is, to the author's knowledge, the first attempt at a detailed mission analysis utilizing nuclear fusion as viable propulsion system beyond the approximations made in gravity free and patched conic methods. The rapid trip times enabled by fusion propulsion merit further mission analysis for rendezvous, round trip, and multiple celestial body exploration missions.

APPENDICES

APPENDIX A

SPICE

A.1 History

A report from the Committee on Data Management and Computation within the National Research Council was released in 1982, and inside the report a detailed list of problems with archiving data from NASA Space Science Missions was addressed [52]. A Planetary Data Workshop was formed in response to the problem listed in the report. The workshop was lead by Dr. Hugh Kieffer from the Astrogeology Branch of the United States Geological Survey. During this workshop scientists and engineers outlined their requirements for archiving ancillary information obtained by space missions [53]. During several months after the workshop, Dr. Kieffer worked with Charles Acton, the leader of the Pilot Planetary Data System, to refine the archival system. After which, Dr. Kieffer coined the acronym “SPICE” in order to identify the major components of the archival system [54].

Proof of concept was first demonstrated on ancillary data from scientific instruments aboard the Voyager spacecrafts. The formats used for archiving the ancillary data from the Voyager spacecrafts helped design the modern SPICE kernels. The Magellan spacecraft mission to Venus was the first official use of the current SPICE kernels. The archival data included spacecraft trajectory information stored in the spacecraft/planet kernel (SPK).

Following the success of archiving data from the Magellan spacecraft, SPICE was used to archive both the Mars Observer and Galileo spacecraft data. In doing so, SPICE was determined to be sufficient in replacing the previous archival system labeled Supplemental Experiment Data Records [54].

A.2 Concept

SPICE is controlled by the Navigation and Ancillary Information Facility (NAIF) under the Planetary Science Division of NASA located at the Jet Propulsion Laboratory (JPL). Initially developed for ancillary data archiving, SPICE is now utilized in all levels of spacecraft missions. Other government agencies, including foreign, as well as private and academic institutions are also utilizing SPICE. SPICE stores its information in the form of kernels. In order to access the stored information in one or more SPICE kernels, a toolkit must be utilized. A toolkit is a file or set of files that contain subroutines needed to read kernel files. The first SPICE Toolkit was available for ANSI FORTRAN 77, but now toolkits are available for C, IDL, and MATLAB® programming as well. (Note: the MATLAB® SPICE Toolkit labeled Mice was used to create the 2D and 3D trajectory figures in this document.). All SPICE Toolkits and documentation with tutorials, lessons, and examples are available from the NAIF free to the public. Many trajectory analysis programs now have the option of outputting ephemeris data in the form of one or more SPICE kernels.

The NAIF maintains a database available to the public for accessing information from NASA spacecrafts in the form of SPICE kernels which includes many past missions as well as current and future missions. Spacecraft information regarding future missions or future parts of a current mission located in the database has SPICE kernel files labeled in a fashion indicating a prediction. Spacecraft information from past missions in which the information

was obtained from the spacecraft are labeled in a fashion to indicate the kernel file was produced by reconstructing the data from the spacecraft. The database is updated as spacecraft information becomes available to the public and kernels can be created from reconstructed spacecraft data.

A.3 Summary of Kernels

Each SPICE kernel is briefly described below as stated directly from [55].

S- Spacecraft ephemeris, given as a function of time.

P- Planet, satellite, comet, or asteroid ephemerides, or more generally, location of any target body, given as a function of time.

The P kernel also logically includes certain physical, dynamical and cartographic constants for target bodies, such as size and shape specifications, and orientation of the spin axis and prime meridian.

I- Instrument description kernel, containing descriptive data peculiar to a particular scientific instrument, such as field-of-view size, shape and orientation parameters.

C- Pointing kernel, containing a transformation, traditionally called the C-matrix, which provides time-tagged pointing (orientation) angles for a spacecraft structure upon which science instruments are mounted. May also include angular rate data.

E- Events kernel, summarizing mission activities - both planned and unanticipated. Events data are contained in the SPICE EK file set, which consists of three components: Science Plans, Sequences, and Notes.

Some additional data products are also important components of the SPICE system, even if not contained in the "SPICE" acronym.

A "frames kernel" (FK file) contains specifications for the assortment of reference frames that are typically used by flight projects. This file also includes mounting alignment information for instruments, antennas and perhaps other structures of interest. Spacecraft clock (SCLK) and leapseconds (LSK) files are also part of SPICE; these are used in converting time tags between various time measurement systems.

APPENDIX B

GMAT SCRIPT

```
%General Mission Analysis Tool(GMAT) Script  
%Created: 2011-09-19 01:28:56
```

```
%-----  
%----- Calculated Points  
%-----
```

```
Create LibrationPoint EarthMoonL1;  
GMAT EarthMoonL1.Primary = Earth;  
GMAT EarthMoonL1.Secondary = Luna;  
GMAT EarthMoonL1.Point = L1;
```

```
%-----  
%----- Spacecraft  
%-----
```

```
Create Spacecraft DefaultSC;  
GMAT DefaultSC.DateFormat = UTCGregorian;  
GMAT DefaultSC.Epoch = '06 Apr 2025 14:04:15.000';  
GMAT DefaultSC.CoordinateSystem = EarthMoonL1MJ2kEc;  
GMAT DefaultSC.DisplayStateType = Cartesian;  
GMAT DefaultSC.X = 0;  
GMAT DefaultSC.Y = 0;  
GMAT DefaultSC.Z = 0;  
GMAT DefaultSC.VX = 0;  
GMAT DefaultSC.VY = 0;  
GMAT DefaultSC.VZ = 0;  
GMAT DefaultSC.DryMass = 49850;  
GMAT DefaultSC.Cd = 2.2;  
GMAT DefaultSC.Cr = 1.8;  
GMAT DefaultSC.DragArea = 15;  
GMAT DefaultSC.SRPArea = 1;
```

```

GMAT DefaultSC.Tanks = {FuelTank1};
GMAT DefaultSC.Thrusters = {Thruster1, Thruster2};
GMAT DefaultSC.NAIFId = -12345678;
GMAT DefaultSC.NAIFIdReferenceFrame = -12345678;
GMAT DefaultSC.Id = 'SatId';
GMAT DefaultSC.Attitude = CoordinateSystemFixed;
GMAT DefaultSC.ModelFile = '../data/vehicle/models/aura.3ds';
GMAT DefaultSC.ModelOffsetX = 0;
GMAT DefaultSC.ModelOffsetY = 0;
GMAT DefaultSC.ModelOffsetZ = 0;
GMAT DefaultSC.ModelRotationX = 0;
GMAT DefaultSC.ModelRotationY = 0;
GMAT DefaultSC.ModelRotationZ = 0;
GMAT DefaultSC.ModelScale = 3;
GMAT DefaultSC.AttitudeDisplayStateType = 'Quaternion';
GMAT DefaultSC.AttitudeRateDisplayStateType = 'AngularVelocity';
GMAT DefaultSC.AttitudeCoordinateSystem = 'EarthMJ2000Eq';
GMAT DefaultSC.Q1 = 0;
GMAT DefaultSC.Q2 = 0;
GMAT DefaultSC.Q3 = 0;
GMAT DefaultSC.Q4 = 1;
GMAT DefaultSC.EulerAngleSequence = '321';
GMAT DefaultSC.AngularVelocityX = 0;
GMAT DefaultSC.AngularVelocityY = 0;
GMAT DefaultSC.AngularVelocityZ = 0;

```

```

%-----
%----- Hardware Components
%-----

```

```

Create FuelTank FuelTank1;
GMAT FuelTank1.AllowNegativeFuelMass = false;
GMAT FuelTank1.FuelMass = 10150;
GMAT FuelTank1.Pressure = 1500;
GMAT FuelTank1.Temperature = 20;
GMAT FuelTank1.RefTemperature = 20;
GMAT FuelTank1.Volume = 40;
GMAT FuelTank1.FuelDensity = 530;
GMAT FuelTank1.PressureModel = PressureRegulated;

```

```

Create Thruster Thruster1;
GMAT Thruster1.CoordinateSystem = Local;
GMAT Thruster1.Origin = Earth;
GMAT Thruster1.Axes = VNB;
GMAT Thruster1.ThrustDirection1 = 0.949;
GMAT Thruster1.ThrustDirection2 = -0.051;

```

```

GMAT Thruster1.ThrustDirection3 = 0;
GMAT Thruster1.DutyCycle = 1;
GMAT Thruster1.ThrustScaleFactor = 1;
GMAT Thruster1.DecrementMass = true;
GMAT Thruster1.Tank = {FuelTank1};
GMAT Thruster1.GravitationalAccel = 9.81;
GMAT Thruster1.C1 = 102;
GMAT Thruster1.C2 = 0;
GMAT Thruster1.C3 = 0;
GMAT Thruster1.C4 = 0;
GMAT Thruster1.C5 = 0;
GMAT Thruster1.C6 = 0;
GMAT Thruster1.C7 = 0;
GMAT Thruster1.C8 = 0;
GMAT Thruster1.C9 = 0;
GMAT Thruster1.C10 = 0;
GMAT Thruster1.C11 = 0;
GMAT Thruster1.C12 = 0;
GMAT Thruster1.C13 = 0;
GMAT Thruster1.C14 = 0;
GMAT Thruster1.C15 = 0;
GMAT Thruster1.C16 = 0;
GMAT Thruster1.K1 = 20000;
GMAT Thruster1.K2 = 0;
GMAT Thruster1.K3 = 0;
GMAT Thruster1.K4 = 0;
GMAT Thruster1.K5 = 0;
GMAT Thruster1.K6 = 0;
GMAT Thruster1.K7 = 0;
GMAT Thruster1.K8 = 0;
GMAT Thruster1.K9 = 0;
GMAT Thruster1.K10 = 0;
GMAT Thruster1.K11 = 0;
GMAT Thruster1.K12 = 0;
GMAT Thruster1.K13 = 0;
GMAT Thruster1.K14 = 0;
GMAT Thruster1.K15 = 0;
GMAT Thruster1.K16 = 0;

%-----
%----- ForceModels
%-----

Create ForceModel EarthMoonProp_ForceModel;
GMAT EarthMoonProp_ForceModel.CentralBody = Earth;
GMAT EarthMoonProp_ForceModel.PrimaryBodies = {Earth};

```

```

GMAT EarthMoonProp_ForceModel.PointMasses = {Luna};
GMAT EarthMoonProp_ForceModel.Drag = None;
GMAT EarthMoonProp_ForceModel.SRP = On;
GMAT EarthMoonProp_ForceModel.ErrorControl = RSSStep;
GMAT EarthMoonProp_ForceModel.GravityField.Earth.Degree = 4;
GMAT EarthMoonProp_ForceModel.GravityField.Earth.Order = 4;
GMAT EarthMoonProp_ForceModel.GravityField.Earth.PotentialFile = 'JGM2.cof';
GMAT EarthMoonProp_ForceModel.SRP.Flux = 1367;
GMAT EarthMoonProp_ForceModel.SRP.Nominal_Sun = 149597870.691;

```

```

Create ForceModel SolarSystemProp_ForceModel;
GMAT SolarSystemProp_ForceModel.CentralBody = Sun;
GMAT SolarSystemProp_ForceModel.PointMasses = {Earth, Jupiter, Luna, Mars, Neptune,
Saturn, Sun, Uranus, Venus};
GMAT SolarSystemProp_ForceModel.Drag = None;
GMAT SolarSystemProp_ForceModel.SRP = On;
GMAT SolarSystemProp_ForceModel.ErrorControl = RSSStep;
GMAT SolarSystemProp_ForceModel.SRP.Flux = 1367;
GMAT SolarSystemProp_ForceModel.SRP.Nominal_Sun = 149597870.691;

```

```

Create ForceModel MoonProp_ForceModel;
GMAT MoonProp_ForceModel.CentralBody = Luna;
GMAT MoonProp_ForceModel.PointMasses = {Luna};
GMAT MoonProp_ForceModel.Drag = None;
GMAT MoonProp_ForceModel.SRP = On;
GMAT MoonProp_ForceModel.ErrorControl = RSSStep;
GMAT MoonProp_ForceModel.SRP.Flux = 1367;
GMAT MoonProp_ForceModel.SRP.Nominal_Sun = 149597870.691;

```

```

Create ForceModel SaturnProp_ForceModel;
GMAT SaturnProp_ForceModel.CentralBody = Saturn;
GMAT SaturnProp_ForceModel.PointMasses = {Saturn};
GMAT SaturnProp_ForceModel.Drag = None;
GMAT SaturnProp_ForceModel.SRP = On;
GMAT SaturnProp_ForceModel.ErrorControl = RSSStep;
GMAT SaturnProp_ForceModel.SRP.Flux = 1367;
GMAT SaturnProp_ForceModel.SRP.Nominal_Sun = 149597870.691;

```

```

%-----
%----- Propagators
%-----

```

```

Create Propagator EarthMoonProp;
GMAT EarthMoonProp.FM = EarthMoonProp_ForceModel;
GMAT EarthMoonProp.Type = RungeKutta89;
GMAT EarthMoonProp.InitialStepSize = 60;

```

```
GMAT EarthMoonProp.Accuracy = 9.999999999999999e-012;
GMAT EarthMoonProp.MinStep = 0.001;
GMAT EarthMoonProp.MaxStep = 2700;
GMAT EarthMoonProp.MaxStepAttempts = 50;
GMAT EarthMoonProp.StopIfAccuracyIsViolated = true;
```

```
Create Propagator SolarSystemProp;
GMAT SolarSystemProp.FM = SolarSystemProp_ForceModel;
GMAT SolarSystemProp.Type = RungeKutta89;
GMAT SolarSystemProp.InitialStepSize = 60;
GMAT SolarSystemProp.Accuracy = 9.999999999999999e-012;
GMAT SolarSystemProp.MinStep = 0.001;
GMAT SolarSystemProp.MaxStep = 2700;
GMAT SolarSystemProp.MaxStepAttempts = 50;
GMAT SolarSystemProp.StopIfAccuracyIsViolated = true;
```

```
Create Propagator MoonProp;
GMAT MoonProp.FM = MoonProp_ForceModel;
GMAT MoonProp.Type = RungeKutta89;
GMAT MoonProp.InitialStepSize = 60;
GMAT MoonProp.Accuracy = 9.999999999999999e-012;
GMAT MoonProp.MinStep = 0.001;
GMAT MoonProp.MaxStep = 2700;
GMAT MoonProp.MaxStepAttempts = 50;
GMAT MoonProp.StopIfAccuracyIsViolated = true;
```

```
Create Propagator SaturnProp;
GMAT SaturnProp.FM = SaturnProp_ForceModel;
GMAT SaturnProp.Type = RungeKutta89;
GMAT SaturnProp.InitialStepSize = 60;
GMAT SaturnProp.Accuracy = 9.999999999999999e-012;
GMAT SaturnProp.MinStep = 0.001;
GMAT SaturnProp.MaxStep = 2700;
GMAT SaturnProp.MaxStepAttempts = 50;
GMAT SaturnProp.StopIfAccuracyIsViolated = true;
```

```
%-----
%----- Burns
%-----
```

```
Create FiniteBurn DefaultFB;
GMAT DefaultFB.Thrusters = {Thruster1};
```

```
Create FiniteBurn FiniteBurn1;
GMAT FiniteBurn1.Thrusters = {Thruster2};
```

```

%-----
%----- Arrays, Variables, Strings
%-----
Create Variable FuelMass date0 dateE btime daysf daysE I btime_half bday_half datef;
Create Variable Kuiper_end AU_1000;
GMAT FuelMass = 0;
GMAT date0 = 0;
GMAT dateE = 0;
GMAT btime = 225;
GMAT Kuiper_end = 0;
GMAT AU_1000 = 0;

```

```

%-----
%----- Coordinate Systems
%-----

```

```

Create CoordinateSystem EarthMoonL1MJ2kEq;
GMAT EarthMoonL1MJ2kEq.Origin = EarthMoonL1;
GMAT EarthMoonL1MJ2kEq.Axes = MJ2000Eq;

```

```

Create CoordinateSystem EarthMoonL1MJ2kEc;
GMAT EarthMoonL1MJ2kEc.Origin = EarthMoonL1;
GMAT EarthMoonL1MJ2kEc.Axes = MJ2000Ec;

```

```

Create CoordinateSystem SunMJ2000Ec;
GMAT SunMJ2000Ec.Origin = Sun;
GMAT SunMJ2000Ec.Axes = MJ2000Ec;

```

```

Create CoordinateSystem MoonMJ2000Ec;
GMAT MoonMJ2000Ec.Origin = Luna;
GMAT MoonMJ2000Ec.Axes = MJ2000Ec;

```

```

Create CoordinateSystem SaturnMJ2000Ec;
GMAT SaturnMJ2000Ec.Origin = Saturn;
GMAT SaturnMJ2000Ec.Axes = MJ2000Ec;

```

```

%-----
%----- Subscribers
%-----

```

```

Create OrbitView EarthMoonView;
GMAT EarthMoonView.SolverIterations = Current;
GMAT EarthMoonView.Add = {DefaultSC, Earth, Luna, Sun};
GMAT EarthMoonView.DrawObject = [ true true true true ];
GMAT EarthMoonView.OrbitColor = [ 255 32768 8421504 8454143 ];

```

```

GMAT EarthMoonView.TargetColor = [ 8421440 0 4227327 0 ];
GMAT EarthMoonView.CoordinateSystem = EarthMJ2000Ec;
GMAT EarthMoonView.ViewPointReference = Earth;
GMAT EarthMoonView.ViewPointVector = [ 0 0 1000000 ];
GMAT EarthMoonView.ViewDirection = Earth;
GMAT EarthMoonView.ViewScaleFactor = 1;
GMAT EarthMoonView.ViewUpCoordinateSystem = EarthMJ2000Ec;
GMAT EarthMoonView.ViewUpAxis = X;
GMAT EarthMoonView.CelestialPlane = Off;
GMAT EarthMoonView.XYPlane = On;
GMAT EarthMoonView.WireFrame = Off;
GMAT EarthMoonView.Axes = Off;
GMAT EarthMoonView.Grid = Off;
GMAT EarthMoonView.SunLine = Off;
GMAT EarthMoonView.UseInitialView = On;
GMAT EarthMoonView.DataCollectFrequency = 1;
GMAT EarthMoonView.UpdatePlotFrequency = 50;
GMAT EarthMoonView.NumPointsToRedraw = 0;
GMAT EarthMoonView.StarCount = 7000;
GMAT EarthMoonView.EnableStars = Off;
GMAT EarthMoonView.EnableConstellations = On;
GMAT EarthMoonView.ShowPlot = true;

```

```

Create OrbitView SolarSystemInnerView;
GMAT SolarSystemInnerView.SolverIterations = Current;
GMAT SolarSystemInnerView.Add = {DefaultSC, Earth, Jupiter, Mars, Sun};
GMAT SolarSystemInnerView.DrawObject = [ true true true true true ];
GMAT SolarSystemInnerView.OrbitColor = [ 255 32768 1743054 128 1743054 ];
GMAT SolarSystemInnerView.TargetColor = [ 8421440 0 4227327 4227327 4227327 ];
GMAT SolarSystemInnerView.CoordinateSystem = SunMJ2000Ec;
GMAT SolarSystemInnerView.ViewPointReference = Sun;
GMAT SolarSystemInnerView.ViewPointVector = [ 0 0 1 ];
GMAT SolarSystemInnerView.ViewDirection = Sun;
GMAT SolarSystemInnerView.ViewScaleFactor = 350000000;
GMAT SolarSystemInnerView.ViewUpCoordinateSystem = SunMJ2000Ec;
GMAT SolarSystemInnerView.ViewUpAxis = X;
GMAT SolarSystemInnerView.CelestialPlane = Off;
GMAT SolarSystemInnerView.XYPlane = On;
GMAT SolarSystemInnerView.WireFrame = Off;
GMAT SolarSystemInnerView.Axes = On;
GMAT SolarSystemInnerView.Grid = Off;
GMAT SolarSystemInnerView.SunLine = Off;
GMAT SolarSystemInnerView.UseInitialView = On;
GMAT SolarSystemInnerView.DataCollectFrequency = 1;
GMAT SolarSystemInnerView.UpdatePlotFrequency = 50;
GMAT SolarSystemInnerView.NumPointsToRedraw = 0;

```



```

GMAT SolarSystemInnerView.StarCount = 7000;
GMAT SolarSystemInnerView.EnableStars = Off;
GMAT SolarSystemInnerView.EnableConstellations = On;
GMAT SolarSystemInnerView.ShowPlot = false;

Create OrbitView SolarSystemOuterView;
GMAT SolarSystemOuterView.SolverIterations = Current;
GMAT SolarSystemOuterView.Add = {DefaultSC, Earth, Sun, Jupiter, Saturn, Mars,
Uranus, Neptune, Pluto};
GMAT SolarSystemOuterView.DrawObject = [ true true true true true true true true ];
GMAT SolarSystemOuterView.OrbitColor = [ 255 32768 1743054 1743054 4227327 128
65280 16744448 8421504 ];
GMAT SolarSystemOuterView.TargetColor = [ 8421440 0 4227327 4227327 4227327
4227327 4227327 4227327 4227327 ];
GMAT SolarSystemOuterView.CoordinateSystem = SunMJ2000Ec;
GMAT SolarSystemOuterView.ViewPointReference = Sun;
GMAT SolarSystemOuterView.ViewPointVector = [ 0 0 1 ];
GMAT SolarSystemOuterView.ViewDirection = Sun;
GMAT SolarSystemOuterView.ViewScaleFactor = 10000000000;
GMAT SolarSystemOuterView.ViewUpCoordinateSystem = SunMJ2000Ec;
GMAT SolarSystemOuterView.ViewUpAxis = Z;
GMAT SolarSystemOuterView.CelestialPlane = Off;
GMAT SolarSystemOuterView.XYPlane = On;
GMAT SolarSystemOuterView.WireFrame = Off;
GMAT SolarSystemOuterView.Axes = Off;
GMAT SolarSystemOuterView.Grid = Off;
GMAT SolarSystemOuterView.SunLine = Off;
GMAT SolarSystemOuterView.UseInitialView = On;
GMAT SolarSystemOuterView.DataCollectFrequency = 10;
GMAT SolarSystemOuterView.UpdatePlotFrequency = 500;
GMAT SolarSystemOuterView.NumPointsToRedraw = 0;
GMAT SolarSystemOuterView.StarCount = 7000;
GMAT SolarSystemOuterView.EnableStars = Off;
GMAT SolarSystemOuterView.EnableConstellations = On;
GMAT SolarSystemOuterView.ShowPlot = true;

Create OrbitView MoonView;
GMAT MoonView.SolverIterations = Current;
GMAT MoonView.Add = {DefaultSC, Earth, Luna, Sun};
GMAT MoonView.DrawObject = [ true true true true ];
GMAT MoonView.OrbitColor = [ 255 32768 1743054 4227327 ];
GMAT MoonView.TargetColor = [ 8421440 0 4227327 0 ];
GMAT MoonView.CoordinateSystem = MoonMJ2000Ec;
GMAT MoonView.ViewPointReference = Luna;
GMAT MoonView.ViewPointVector = [ 0 0 30000 ];
GMAT MoonView.ViewDirection = Luna;

```

```

GMAT MoonView.ViewScaleFactor = 1;
GMAT MoonView.ViewUpCoordinateSystem = MoonMJ2000Ec;
GMAT MoonView.ViewUpAxis = Z;
GMAT MoonView.CelestialPlane = Off;
GMAT MoonView.XYPlane = On;
GMAT MoonView.WireFrame = Off;
GMAT MoonView.Axes = Off;
GMAT MoonView.Grid = Off;
GMAT MoonView.SunLine = On;
GMAT MoonView.UseInitialView = On;
GMAT MoonView.DataCollectFrequency = 1;
GMAT MoonView.UpdatePlotFrequency = 50;
GMAT MoonView.NumPointsToRedraw = 0;
GMAT MoonView.StarCount = 7000;
GMAT MoonView.EnableStars = Off;
GMAT MoonView.EnableConstellations = On;
GMAT MoonView.ShowPlot = true;

```

```

Create OrbitView SaturnView;
GMAT SaturnView.SolverIterations = Current;
GMAT SaturnView.Add = {DefaultSC, Saturn, Earth, Sun, Neptune};
GMAT SaturnView.DrawObject = [ true true true true true ];
GMAT SaturnView.OrbitColor = [ 255 1743054 32768 8454143 16744448 ];
GMAT SaturnView.TargetColor = [ 8421440 4227327 0 0 4227327 ];
GMAT SaturnView.CoordinateSystem = SaturnMJ2000Ec;
GMAT SaturnView.ViewPointReference = Saturn;
GMAT SaturnView.ViewPointVector = [ 0 0 1000000 ];
GMAT SaturnView.ViewDirection = Saturn;
GMAT SaturnView.ViewScaleFactor = 1;
GMAT SaturnView.ViewUpCoordinateSystem = SaturnMJ2000Ec;
GMAT SaturnView.ViewUpAxis = X;
GMAT SaturnView.CelestialPlane = Off;
GMAT SaturnView.XYPlane = On;
GMAT SaturnView.WireFrame = Off;
GMAT SaturnView.Axes = Off;
GMAT SaturnView.Grid = Off;
GMAT SaturnView.SunLine = On;
GMAT SaturnView.UseInitialView = On;
GMAT SaturnView.DataCollectFrequency = 1;
GMAT SaturnView.UpdatePlotFrequency = 50;
GMAT SaturnView.NumPointsToRedraw = 0;
GMAT SaturnView.StarCount = 7000;
GMAT SaturnView.EnableStars = Off;
GMAT SaturnView.EnableConstellations = On;
GMAT SaturnView.ShowPlot = true;

```

```
Create ReportFile SunXYZ;
GMAT SunXYZ.SolverIterations = Current;
GMAT SunXYZ.Filename = 'SunXYZ4_cont.txt';
GMAT SunXYZ.Precision = 16;
GMAT SunXYZ.Add = {DefaultSC.UTCGregorian, DefaultSC.UTCModJulian,
DefaultSC.Sun.RMAG, DefaultSC.SunMJ2000Ec.VMAG};
GMAT SunXYZ.WriteHeaders = Off;
GMAT SunXYZ.LeftJustify = On;
GMAT SunXYZ.ZeroFill = Off;
GMAT SunXYZ.ColumnWidth = 30;
GMAT SunXYZ.WriteReport = true;
```

```
Create ReportFile ReportFile1;
GMAT ReportFile1.SolverIterations = Current;
GMAT ReportFile1.Filename = 'ReportFile1.txt';
GMAT ReportFile1.Precision = 16;
GMAT ReportFile1.WriteHeaders = On;
GMAT ReportFile1.LeftJustify = On;
GMAT ReportFile1.ZeroFill = Off;
GMAT ReportFile1.ColumnWidth = 25;
GMAT ReportFile1.WriteReport = true;
```

```
Create ReportFile ReportFile2;
GMAT ReportFile2.SolverIterations = Current;
GMAT ReportFile2.Filename = 'ReportFile2.txt';
GMAT ReportFile2.Precision = 16;
GMAT ReportFile2.WriteHeaders = On;
GMAT ReportFile2.LeftJustify = On;
GMAT ReportFile2.ZeroFill = Off;
GMAT ReportFile2.ColumnWidth = 40;
GMAT ReportFile2.WriteReport = true;
```

```
Create ReportFile Earthxyz;
GMAT Earthxyz.SolverIterations = Current;
GMAT Earthxyz.Filename = 'Earthxyz4.txt';
GMAT Earthxyz.Precision = 16;
GMAT Earthxyz.Add = {DefaultSC.EarthMJ2000Ec.X, DefaultSC.EarthMJ2000Ec.Y,
DefaultSC.EarthMJ2000Ec.Z, DefaultSC.UTCGregorian, DefaultSC.UTCModJulian,
DefaultSC.Earth.RMAG, DefaultSC.EarthMJ2000Ec.VMAG};
GMAT Earthxyz.WriteHeaders = Off;
GMAT Earthxyz.LeftJustify = On;
GMAT Earthxyz.ZeroFill = Off;
GMAT Earthxyz.ColumnWidth = 30;
GMAT Earthxyz.WriteReport = true;
```

```

Create ReportFile Moonxyz;
GMAT Moonxyz.SolverIterations = Current;
GMAT Moonxyz.Filename = 'Moonxyz4.txt';
GMAT Moonxyz.Precision = 16;
GMAT Moonxyz.Add = {DefaultSC.MoonMJ2000Ec.X, DefaultSC.MoonMJ2000Ec.Y,
DefaultSC.MoonMJ2000Ec.Z, DefaultSC.UTCGregorian, DefaultSC.UTCModJulian,
DefaultSC.Luna.RMAG, DefaultSC.MoonMJ2000Ec.VMAG};
GMAT Moonxyz.WriteHeaders = Off;
GMAT Moonxyz.LeftJustify = On;
GMAT Moonxyz.ZeroFill = Off;
GMAT Moonxyz.ColumnWidth = 30;
GMAT Moonxyz.WriteReport = true;

```

```

Create ReportFile Saturnxyz;
GMAT Saturnxyz.SolverIterations = Current;
GMAT Saturnxyz.Filename = 'Saturnxyz.txt';
GMAT Saturnxyz.Precision = 16;
GMAT Saturnxyz.Add = {DefaultSC.SaturnMJ2000Ec.X, DefaultSC.SaturnMJ2000Ec.Y,
DefaultSC.SaturnMJ2000Ec.Z, DefaultSC.UTCGregorian, DefaultSC.UTCModJulian,
DefaultSC.Saturn.RMAG, DefaultSC.SaturnMJ2000Ec.VMAG};
GMAT Saturnxyz.WriteHeaders = Off;
GMAT Saturnxyz.LeftJustify = On;
GMAT Saturnxyz.ZeroFill = Off;
GMAT Saturnxyz.ColumnWidth = 30;
GMAT Saturnxyz.WriteReport = true;

```

```

Create ReportFile Saturnxyz_plus;
GMAT Saturnxyz_plus.SolverIterations = Current;
GMAT Saturnxyz_plus.Filename = 'Saturn_plus.txt';
GMAT Saturnxyz_plus.Precision = 16;
GMAT Saturnxyz_plus.Add = {DefaultSC.SaturnMJ2000Ec.X,
DefaultSC.SaturnMJ2000Ec.Y, DefaultSC.SaturnMJ2000Ec.Z, DefaultSC.UTCGregorian,
DefaultSC.UTCModJulian, DefaultSC.Saturn.RMAG,
DefaultSC.SaturnMJ2000Ec.VMAG};
GMAT Saturnxyz_plus.WriteHeaders = Off;
GMAT Saturnxyz_plus.LeftJustify = On;
GMAT Saturnxyz_plus.ZeroFill = Off;
GMAT Saturnxyz_plus.ColumnWidth = 30;
GMAT Saturnxyz_plus.WriteReport = true;

```

```

%-----
%----- Mission Sequence
%-----

```

```

BeginMissionSequence;
Toggle SaturnView Saturnxyz Saturnxyz_plus Off;

```

```

GMAT FuelMass = DefaultSC.FuelTank1.FuelMass;
GMAT date0 = DefaultSC.UTCModJulian;
GMAT btime_half = btime/2;
GMAT bday_half = date0+btime_half;
GMAT dateE = date0+btime;
Report ReportFile2 DefaultSC.Earth.RMAG DefaultSC.Earth.Altitude
DefaultSC.EarthMJ2000Ec.X DefaultSC.EarthMJ2000Ec.Y DefaultSC.EarthMJ2000Ec.Z
DefaultSC.EarthMJ2000Ec.VMAG DefaultSC.EarthMJ2000Ec.VX
DefaultSC.EarthMJ2000Ec.VY DefaultSC.EarthMJ2000Ec.VZ FuelMass
DefaultSC.UTCModJulian DefaultSC.UTCGregorian DefaultSC.Sun.RMAG
DefaultSC.SunMJ2000Ec.X DefaultSC.SunMJ2000Ec.Y DefaultSC.SunMJ2000Ec.Z
DefaultSC.SunMJ2000Ec.VMAG DefaultSC.SunMJ2000Ec.VX
DefaultSC.SunMJ2000Ec.VY DefaultSC.SunMJ2000Ec.VZ date0 dateE;
Report ReportFile1 DefaultSC.Luna.RMAG DefaultSC.Luna.Altitude
DefaultSC.UTCGregorian DefaultSC.MoonMJ2000Ec.VMAG
DefaultSC.MoonMJ2000Ec.VX DefaultSC.MoonMJ2000Ec.VY
DefaultSC.MoonMJ2000Ec.VZ FuelMass;
BeginFiniteBurn DefaultFB(DefaultSC);
GMAT FuelMass = DefaultSC.FuelTank1.FuelMass;
Report ReportFile2 DefaultSC.Luna.RMAG DefaultSC.Luna.Altitude
DefaultSC.UTCGregorian DefaultSC.MoonMJ2000Ec.VMAG
DefaultSC.EarthMJ2000Eq.VMAG DefaultSC.SunMJ2000Ec.VMAG FuelMass;
Propagate MoonProp(DefaultSC) {DefaultSC.Luna.Periapsis};
GMAT FuelMass = DefaultSC.FuelTank1.FuelMass;
Report ReportFile1 DefaultSC.Luna.RMAG DefaultSC.Luna.Altitude
DefaultSC.MoonMJ2000Ec.VMAG DefaultSC.MoonMJ2000Ec.VX
DefaultSC.MoonMJ2000Ec.VY DefaultSC.MoonMJ2000Ec.VZ FuelMass
DefaultSC.UTCModJulian DefaultSC.UTCGregorian DefaultSC.SunMJ2000Ec.VMAG
DefaultSC.EarthMJ2000Ec.VMAG;
Propagate MoonProp(DefaultSC) {DefaultSC.Luna.RMAG = 66183};
GMAT FuelMass = DefaultSC.FuelTank1.FuelMass;
Report ReportFile1 DefaultSC.Luna.RMAG DefaultSC.Luna.Altitude
DefaultSC.MoonMJ2000Ec.VMAG DefaultSC.MoonMJ2000Ec.VX
DefaultSC.MoonMJ2000Ec.VY DefaultSC.MoonMJ2000Ec.VZ FuelMass
DefaultSC.UTCModJulian DefaultSC.UTCGregorian DefaultSC.SunMJ2000Ec.VMAG
DefaultSC.EarthMJ2000Ec.VMAG DefaultSC.Earth.RMAG;
Propagate EarthMoonProp(DefaultSC) {DefaultSC.Earth.Periapsis};
Report ReportFile1 DefaultSC.Earth.RMAG DefaultSC.Earth.Altitude
DefaultSC.EarthMJ2000Ec.VMAG DefaultSC.EarthMJ2000Ec.VX
DefaultSC.EarthMJ2000Ec.VY DefaultSC.EarthMJ2000Ec.VZ FuelMass
DefaultSC.UTCModJulian DefaultSC.UTCGregorian DefaultSC.SunMJ2000Ec.VMAG;
Propagate EarthMoonProp(DefaultSC) {DefaultSC.Earth.RMAG = 924217, StopTolerance =
1e-006};
Toggle EarthMoonView Earthxyz MoonView Moonxyz Off;
GMAT FuelMass = DefaultSC.FuelTank1.FuelMass;

```

```

Report ReportFile1 DefaultSC.Earth.RMAG DefaultSC.Earth.Altitude
DefaultSC.EarthMJ2000Ec.VMAG DefaultSC.EarthMJ2000Ec.VX
DefaultSC.EarthMJ2000Ec.VY DefaultSC.EarthMJ2000Ec.VZ FuelMass
DefaultSC.UTCModJulian DefaultSC.UTCGregorian DefaultSC.SunMJ2000Ec.VMAG
DefaultSC.EarthMJ2000Ec.Z DefaultSC.SunMJ2000Ec.Z DefaultSC.EarthMJ2000Eq.Z;
Report ReportFile2 date0 dateE daysE btime daysf FuelMass;
Propagate SolarSystemProp(DefaultSC) {DefaultSC.UTCModJulian = dateE};
EndFiniteBurn DefaultFB(DefaultSC);
GMAT FuelMass = DefaultSC.FuelTank1.FuelMass;
Report ReportFile1 DefaultSC.Earth.RMAG DefaultSC.Earth.Altitude
DefaultSC.EarthMJ2000Ec.VMAG DefaultSC.EarthMJ2000Ec.VX
DefaultSC.EarthMJ2000Ec.VY DefaultSC.EarthMJ2000Ec.VZ FuelMass
DefaultSC.UTCModJulian DefaultSC.UTCGregorian DefaultSC.Sun.RMAG
DefaultSC.SunMJ2000Ec.X DefaultSC.SunMJ2000Ec.Y DefaultSC.SunMJ2000Ec.Z
DefaultSC.SunMJ2000Ec.VMAG DefaultSC.SunMJ2000Ec.VX
DefaultSC.SunMJ2000Ec.VY DefaultSC.SunMJ2000Ec.VZ;
Propagate SolarSystemProp(DefaultSC) {DefaultSC.Saturn.RMAG = 54796292,
StopTolerance = 1e-005};
Report ReportFile1 DefaultSC.Saturn.RMAG DefaultSC.Saturn.Altitude
DefaultSC.SaturnMJ2000Ec.VMAG DefaultSC.SaturnMJ2000Ec.VX
DefaultSC.SaturnMJ2000Ec.VY DefaultSC.SaturnMJ2000Ec.VZ FuelMass
DefaultSC.UTCModJulian DefaultSC.UTCGregorian DefaultSC.SaturnEq.X
DefaultSC.SaturnEq.Y DefaultSC.SaturnEq.Z DefaultSC.SaturnMJ2000Ec.X
DefaultSC.SaturnMJ2000Ec.Y DefaultSC.SaturnMJ2000Ec.Z
DefaultSC.SunMJ2000Ec.VMAG DefaultSC.SunMJ2000Ec.VX
DefaultSC.SunMJ2000Ec.VY DefaultSC.SunMJ2000Ec.VZ DefaultSC.SaturnInertial.INC
DefaultSC.SaturnInertial.BdotR DefaultSC.SaturnInertial.BdotT DefaultSC.SunMJ2000Ec.X
DefaultSC.SunMJ2000Ec.Y DefaultSC.SunMJ2000Ec.Z;
Toggle SaturnView Saturnxyz On;
Propagate SaturnProp(DefaultSC) {DefaultSC.Saturn.Periapsis};
Report ReportFile2 DefaultSC.UTCModJulian DefaultSC.UTCGregorian
DefaultSC.Sun.RMAG DefaultSC.SunMJ2000Ec.X DefaultSC.SunMJ2000Ec.Y
DefaultSC.SunMJ2000Ec.Z DefaultSC.SunMJ2000Ec.VMAG DefaultSC.SunMJ2000Ec.VX
DefaultSC.SunMJ2000Ec.VY DefaultSC.SunMJ2000Ec.VZ
DefaultSC.SaturnMJ2000Ec.BdotR DefaultSC.SaturnMJ2000Ec.BdotT DefaultSC.Sun.ECC;
GMAT FuelMass = DefaultSC.FuelTank1.FuelMass;
Report ReportFile1 DefaultSC.Saturn.RMAG DefaultSC.Saturn.Altitude
DefaultSC.SaturnMJ2000Ec.VMAG DefaultSC.SaturnMJ2000Ec.VX
DefaultSC.SaturnMJ2000Ec.VY DefaultSC.SaturnMJ2000Ec.VZ FuelMass
DefaultSC.UTCModJulian DefaultSC.UTCGregorian DefaultSC.SaturnEq.X
DefaultSC.SaturnEq.Y DefaultSC.SaturnEq.Z DefaultSC.SaturnMJ2000Ec.X
DefaultSC.SaturnMJ2000Ec.Y DefaultSC.SaturnMJ2000Ec.Z
DefaultSC.SunMJ2000Ec.VMAG DefaultSC.SunMJ2000Ec.VX
DefaultSC.SunMJ2000Ec.VY DefaultSC.SunMJ2000Ec.VZ DefaultSC.SaturnInertial.INC
DefaultSC.SaturnInertial.BdotR DefaultSC.SaturnInertial.BdotT;
Stop;

```

```
Toggle Saturnxyz_plus On;  
Propagate SaturnProp(DefaultSC) {DefaultSC.Saturn.RMAG = 1064224};
```

B.1 Commands to Propagate Spacecraft to 1000 AU

```
Propagate SolarSystemProp(TitanExpress) {TitanExpress.Sun.RMAG = Kuiper_end};  
Toggle SolarSystemOuterView Off;  
Propagate SolarSystemProp(TitanExpress) {TitanExpress.Sun.RMAG = AU_1000};
```

APPENDIX C

GMAT EQUATIONS

C.1 Solar Radiation Pressure

Solar radiation pressure is a function of the solar flux (ϕ) and the speed of light (c). The value for solar flux decreases as the distance from the sun decreases. From Earth, solar flux has an average value of 1367 W/m^2 [56] and the speed of light in a vacuum is equal to $2.99792458e8 \text{ m/s}$ [26]. Thus,

$$P_{\odot} = \frac{1367 \frac{\text{W}}{\text{m}^2}}{2.99792458e8 \frac{\text{m}}{\text{s}}} = 4.5598e-6 \frac{\text{N}}{\text{m}^2} \quad (\text{C-1})$$

at the average orbit of the Earth, 1 AU or 149,597,870 km. Solar flux is proportional to the distance from the Sun squared [57]. Thus, the equation for solar radiation pressure at any distance from the Sun becomes

$$P_{\text{SR}} = P_{\odot} \left(\frac{1 \text{ AU}}{r_{s\odot}} \right)^2 = 4.5598e-6 \frac{\text{N}}{\text{m}^2} \left(\frac{1 \text{ AU}}{r_{s\odot}} \right)^2 \quad (\text{C-2})$$

where

$r_{s\odot}$ and 1 AU are in the same units

if $r_{s\odot}$ is in km or meters then 1 AU needs to be converted to appropriate units

C.2 Thrust and Specific Impulse Equations

$$F_T(T, P) = C_1 + C_2P + (C_3 + C_4P + C_5P^2 + C_6P^{C_7} + C_8P^{C_9} + C_{10}P^{C_{11}} + C_{12}C_{13}^{C_{14}P}) \left(\frac{T}{T_{\text{ref}}} \right)^{1+C_{15}+C_{16}P} \quad (\text{C-3})$$

$$I_{\text{sp}}(T, P) = K_1 + K_2P + (K_3 + K_4P + K_5P^2 + K_6P^{K_7} + K_8P^{K_9} + K_{10}P^{K_{11}} + K_{12}K_{13}^{K_{14}P}) \left(\frac{T}{T_{\text{ref}}} \right)^{1+K_{15}+k_{16}P} \quad (\text{C-4})$$

TableC-1: Thrust and Specific Impulse Coefficient Units [24]

Coeff.	Unit	Coeff.	Unit
C ₁	N	K ₁	s
C ₂	N/Pa	K ₂	s/Pa
C ₃	N	K ₃	s
C ₄	N/Pa	K ₄	s/Pa
C ₅	N/Pa ²	K ₅	s/Pa ²
C ₆	N/Pa ^{C₇}	K ₆	s/Pa ^{K₇}
C ₇	None	K ₇	None
C ₈	N/Pa ^{C₉}	K ₈	s/Pa ^{K₉}
C ₉	None	K ₉	None
C ₁₀	N/Pa ^{C₁₁}	K ₁₀	s/Pa ^{K₁₁}
C ₁₁	None	K ₁₁	None
C ₁₂	N	K ₁₂	s
C ₁₃	None	K ₁₃	None
C ₁₄	1/Pa	K ₁₄	1/Pa
C ₁₅	None	K ₁₅	None
C ₁₆	1/Pa	K ₁₆	1/Pa

C.3 Runge-Kutta 89 Table of Coefficients

i \ j	c _i	a _{ij}						
		1	2	3	4	5	6	7
1	0							
2	$\frac{1}{12}$	$\frac{1}{12}$						
3	$\frac{1}{9}$	$\frac{1}{27}$	$\frac{2}{27}$				$\frac{a, b}{c} \triangleq \frac{a + b\sqrt{6}}{c}$	
4	$\frac{1}{6}$	$\frac{1}{24}$	0	$\frac{1}{8}$				
5	$\frac{2,2}{15}$	$\frac{4,94}{375}$	0	$\frac{-94, -84}{375}$	$\frac{328,208}{375}$			
6	$\frac{6,1}{15}$	$\frac{9, -1}{150}$	0	0	$\frac{312,32}{1425}$	$\frac{69,29}{570}$		
7	$\frac{6, -1}{15}$	$\frac{927, -347}{1250}$	0	0	$\frac{-16248,7328}{9375}$	$\frac{-489,179}{3750}$	$\frac{14268, -5798}{9375}$	
8	$\frac{2}{3}$	$\frac{2}{27}$	0	0	0	0	$\frac{16, -1}{54}$	$\frac{16,1}{54}$
9	$\frac{1}{2}$	$\frac{19}{256}$	0	0	0	0	$\frac{118, -23}{512}$	$\frac{118,23}{512}$
10	$\frac{1}{3}$	$\frac{11}{144}$	0	0	0	0	$\frac{266, -1}{864}$	$\frac{266,1}{684}$
11	$\frac{1}{4}$	$\frac{5034, -271}{61440}$	0	0	0	0	0	$\frac{7859, -1626}{10240}$
12	$\frac{4}{3}$	$\frac{5996, -3794}{405}$	0	0	0	0	$\frac{-4342, -338}{9}$	$\frac{154922, -40458}{135}$
13	$\frac{5}{6}$	$\frac{3793,2168}{103680}$	0	0	0	0	$\frac{4042,2263}{13824}$	$\frac{231278,40717}{69120}$
14	1	$\frac{317}{1296}$	0	0	0	0	$\frac{5642, -337}{864}$	$\frac{5642,337}{864}$
15	$\frac{1}{6}$	$\frac{33617, -2168}{518400}$	0	0	0	0	$\frac{-3846,31}{13824}$	$\frac{155338, -520807}{345600}$
16	1	$\frac{-36487, -30352}{279600}$	0	0	0	0	$\frac{-29666, -4499}{7456}$	$\frac{2779182, -615973}{186400}$
\bar{b}_j		$\frac{103}{1680}$	0	0	0	0	0	0
b_j		$\frac{23}{525}$	0	0	0	0	0	0

$$EE = -\frac{7}{400}g_1 + \frac{63}{200}g_8 - \frac{14}{25}g_{10} - \frac{1024}{975}g_{11} - \frac{21}{36400}g_{12} - \frac{3}{25}g_{13} - \frac{9}{280}g_{14} + \frac{9}{25}g_{15} + \frac{233}{4200}g_{16}$$

Table continued:

i \ j		a_{ij}																		
		8	9	10	11	12	13	14	15	16										
1	0																			
2	$\frac{1}{12}$																			
3	$\frac{1}{9}$																			$\frac{a, b}{c} \triangleq \frac{a + b\sqrt{6}}{c}$
4	$\frac{1}{6}$																			
5	$\frac{2,2}{15}$																			
6	$\frac{6,1}{15}$																			
7	$\frac{6, -1}{15}$																			
8	$\frac{2}{3}$																			
9	$\frac{1}{2}$		$-\frac{9}{256}$																	
10	$\frac{1}{3}$		$-\frac{1}{16}$		$-\frac{8}{27}$															
11	$\frac{1}{4}$	$\frac{2232, -813}{20480}$	$\frac{-594 + 271\sqrt{6}}{960}$	$\frac{657, -813}{5120}$																
12	$\frac{4}{3}$	$-\frac{4176,3794}{45}$	$-\frac{340864,242816}{405}$	$\frac{26304, -15176}{45}$	$-\frac{26624}{81}$															
13	$\frac{5}{6}$	$\frac{7947, -2168}{11520}$	$-\frac{11048,542}{405}$	$-\frac{1383,542}{720}$	$\frac{2624}{1053}$	$\frac{3}{1664}$														
14	1	$-\frac{299}{48}$	$\frac{184}{81}$	$-\frac{44}{9}$	$-\frac{5120}{1053}$	$-\frac{11}{468}$	$\frac{16}{9}$													
15	$\frac{1}{6}$	$-\frac{12537,2168}{57600}$	$\frac{92,542}{2025}$	$-\frac{1797, -542}{3600}$	$\frac{320}{567}$	$-\frac{1}{1920}$	$\frac{4}{105}$	0												
16	1	$-\frac{94329,91056}{93200}$	$-\frac{23219,121408}{17475}$	$\frac{101226, -22764}{5825}$	$-\frac{169984}{9087}$	$-\frac{87}{30290}$	$\frac{492}{1165}$	0	$\frac{1260}{233}$											
\bar{b}_j		$-\frac{27}{140}$	$\frac{76}{105}$	$-\frac{201}{280}$	$\frac{1024}{1365}$	$\frac{3}{7280}$	$\frac{12}{35}$	$\frac{9}{280}$												
b_j		$\frac{171}{1400}$	$\frac{86}{525}$	$\frac{93}{280}$	$-\frac{2048}{6825}$	$-\frac{3}{18200}$	$\frac{39}{175}$	0	$\frac{9}{25}$	$\frac{233}{4200}$										
		$EE = -\frac{7}{400}g_1 + \frac{63}{200}g_8 - \frac{14}{25}g_{10} - \frac{1024}{975}g_{11} - \frac{21}{36400}g_{12} - \frac{3}{25}g_{13} - \frac{9}{280}g_{14} + \frac{9}{25}g_{15} + \frac{233}{4200}g_{16}$																		

APPENDIX D

SPHERE OF INFLUENCE CALCULATIONS

Laplace Equation for calculating radius of sphere of influence for a planet or moon [29]:

$$R_s = a_{ob} \left(\frac{M_{ob}}{M_{pb}} \right)^{\frac{2}{5}} \quad (D-1)$$

where

- R_s = radius of the sphere of influence of orbiting body
- a_{ob} = semimajor axis of orbiting body
- M_{ob} = mass of orbiting body
- M_{pb} = mass of primary body

Table D-1: Characteristics of Planets, Sun and Moon [27]

Symbol:	⊕	♄	☉	☾	
Body:	Earth	Saturn	Sun	Moon	
Mass ^a :	rel. to ☉	3.00e-6	2.858e-4	1.00	3.7e-8
	rel. to ⊕	1.00	95.16	3.329E+5	0.0123
Semimajor axis, a (km)		1.495979e8	1.4332643e9	-	3.84400e5

^aExcludes satellites; includes atmosphere

D.1 Earth's radius of sphere of influence:

$$R_s = 1.495979E + 8 \text{ km} \left(\frac{3.00e-6}{1} \right)^{\frac{2}{5}} = 924,217 \text{ km} \quad (D-2)$$

D.2 Saturn's radius of sphere of influence:

$$R_s = 1.4332643e9 \text{ km} \left(\frac{2.858e-4}{1} \right)^{\frac{2}{5}} = 54,796,292 \text{ km} \quad (\text{D-3})$$

D.3 Moon's radius of sphere of influence:

$$R_s = 3.84400e5 \text{ km} \left(\frac{0.0123}{1} \right)^{\frac{2}{5}} = 66183 \text{ km} \quad (\text{D-4})$$

APPENDIX E

CALCULATIONS OF SPACECRAFT DESIGN MODEL

E.1 Approximation of trip time:

Unit conversions for given values:

$$\alpha = 1 \frac{\text{kW}}{\text{kg}} \times \frac{1000 \text{ W}}{1 \text{ kW}} = 1000 \frac{\text{W}}{\text{kg}} = 1000 \frac{\text{J/s}}{\text{kg}} = 1000 \frac{\text{Nm/s}}{\text{kg}} = 1000 \frac{\text{kg} \frac{\text{m}}{\text{s}^2} \frac{\text{m}}{\text{s}}}{\text{kg}} = 1000 \frac{\text{m}^2}{\text{s}^3} \quad (\text{E-1})$$

$$R = 10.58 \text{ AU} \times \frac{149,597,870 \text{ km}}{\text{AU}} \times \frac{1000 \text{ m}}{1 \text{ km}} = 1.5827454646\text{e}12 \text{ m} \quad (\text{E-2})$$

Trip time calculation

$$t_{\text{trip}} = \frac{3}{2} \left[\frac{2R \sqrt{\frac{1}{2\alpha}}}{1 - \sqrt{\lambda}} \right]^{\frac{2}{3}} = \frac{3}{2} \left[\frac{2(1.5827454646\text{e}12 \text{ m}) \sqrt{\frac{1}{2(1000 \frac{\text{m}^2}{\text{s}^3})}}}{1 - \sqrt{0.2}} \right]^{\frac{2}{3}} = 38106910.5536 \text{ s} \quad (\text{E-3})$$

or

$$t_{\text{trip}} = 38106910.5536 \text{ s} \times \frac{1 \text{ day}}{86,400 \text{ s}} = 441 \text{ day} \quad (\text{E-4})$$

E.2 Specific Impulse:

$$I_{\text{sp}} = \frac{\sqrt{2\alpha t_b}}{g_0} = \frac{\sqrt{2 \left(1000 \frac{\text{m}^2}{\text{s}^3} \right) 225 \text{ day} \times \frac{86,400 \text{ s}}{\text{day}}}}{9.81 \frac{\text{m}}{\text{s}^2}} = 20,099.91 \text{ s} \cong 20,000 \text{ s} \quad (\text{E-5})$$

E.3 Exhaust Velocity

$$V_e = g_0 I_{sp} = 9.81 \frac{\text{m}}{\text{s}^2} 20,000 \text{ s} = 196,200 \frac{\text{m}}{\text{s}} \quad (\text{E-6})$$

E.4 Mass Flow Rate

$$\dot{m} = \frac{2\alpha m_{ps}}{V_e^2} = \frac{2 \left(1000 \frac{\text{m}^2}{\text{s}^3} \right) \left(10 \text{ mT} \times \frac{1000 \text{ kg}}{\text{mT}} \right)}{\left(196,200 \frac{\text{m}}{\text{s}} \right)^2} = 5.19556 \text{e-}4 \frac{\text{kg}}{\text{s}} \quad (\text{E-7})$$

E.5 Thrust and Recalculated Mass flow Rate

$$T = \dot{m} V_e = \left(5.19556 \text{E-}4 \frac{\text{kg}}{\text{s}} \right) 196,200 \frac{\text{m}}{\text{s}} = 101.937 \text{ N} \cong 102 \text{ N} \quad (\text{E-8})$$

$$\dot{m} = \frac{T}{V_e} = \frac{102 \text{ N}}{196,200 \frac{\text{m}}{\text{s}}} = 5.19878 \text{e-}4 \frac{\text{kg}}{\text{s}} \quad (\text{E-9})$$

E.6 Propellant Mass

$$m_p = \dot{m} t_b = 5.19878 \text{E-}4 \frac{\text{kg}}{\text{s}} \left(225 \text{ day} \times \frac{86,400 \text{ s}}{\text{day}} \right) = 10106 \text{ kg} \cong 10150 \text{ kg} \quad (\text{E-10})$$

E.7 Empty Mass of Spacecraft

$$m_e = \frac{1}{\lambda} m_{pl} - m_p = \frac{1}{0.2} 10 \text{ mT} - 10.15 \text{ mT} = 39.85 \text{ mT} \quad (\text{E-11})$$

E.8 Conformity Check

$$\lambda = \frac{m_{pl}}{m_i - m_{pl}} = \frac{10 \text{ mT}}{60 \text{ mT} - 10 \text{ mT}} = 0.2 \quad (\text{E-12})$$

APPENDIX F

MATLAB® SCRIPT FOR TIME STEP SIZE

```
clear all
close all
clc

%Constants
AU = 149597870; %units in km from Brown p 585
mu_sun = 132712439935.5; %units in km^3/s^2 from Brown p 592
g0 = 9.81; %units in m/s^2
mu_earth = 398600.4; %units in km^3/s^2 from Brown p 592

%conversions
kg = 1; %establishing base unit of mass in kilograms
mT = 1000*kg; %conversion from kg to metric tons (tonnes)
m = 1; %establishing base unit of distance in meters
km = 1000*m; %conversion from meters to kilometers
s = 1; %establishing base unit of time in seconds
day = 86400*s; %conversion from seconds to days
kmps = 1; %establishing base unit of kilometers per second
mps = kmps/km; %conversion from km per second to meters per second
N = 1; %establishing base unit of force in newtons (kg*m/s^2)

%Velocity of Earth (assume r = 1 AU and circular orbit)
V_E = sqrt(mu_sun/AU); %units in km/s

%Mean motion of Earth if e = 0 & r = 1 AU
mm_E = sqrt(mu_sun/AU^3);

%initial mass of spacecraft
mi = 60*mT;

%spacecraft exhaust velocity
Ve = 196200; %units in m/s

%straight-line distance from Earth to Saturn
%(planets on opposite side of Sun)
R_mag = 10.58*AU;

%spacecraft thrust
Ft = 102*N; %0.949;

%specific impulse;
%Isp = Ve/g0; %units in seconds

%mass flow rate
mdot = Ft/Ve;

%propulsion system operation time (burn time)
tb = 225*day;

%mass of propellant used in 225 days
mpu = mdot*tb*kg;
```



```

%final mass of spacecraft
mf_tot = mi - mpu; %units in kg

%Calculating gravity free total Delta-V
DV_tot = Ve*mps*log(mi/mf_tot); %units in km/s

%final velocity of spacecraft at tb ...
%also velocity of spacecfrt during coasting phase of trajectory
Vcoast = V_E + DV_tot;

%time increment step
dt = 3600*s;

%inital index value
i = 1;

%initalizing vector variables
i_max = tb/dt;
ms = zeros(i_max, 1);
DV = ms;
Vs = ms;
dr = ms;
r = ms;
t = ms;
mp(1) = mpu;
ms(1) = mi;
Vs(1) = V_E; %velocity of spacecraft initially equal to velocity of Earth
a_s = ms;

%determining distanced traveled from epoch to tb
while t(i) <= tb - dt
    a_s(i) = mdot/ms(i)*dr(i)/dt;
    i = i + 1;
    ms(i) = ms(i-1) - mdot*dt;
    DV(i) = Ve*mps*log(ms(i-1)/ms(i));
    Vs(i) = Vs(i-1) + DV(i);
    dr(i) = Vs(i)*dt;
    r(i) = r(i-1) + dr(i);
    t(i) = t(i-1) + dt;
end

Rcoast = R_mag - r(i);
t_coast = Rcoast/Vcoast;
t_tot = t(i) + t_coast;
t_tot_day = t_tot/day;

```

References

- [1] Adams, R. and Cassibry, J. T., "Future Directions for Fusion Propulsion Research at NASA," *41st AIAA/ASME/SAE/ASEE Joint Propulsion Conference & Exhibit*, AIAA-2005-4140, Tucson, AZ, July 2005.
- [2] Moeckel, W. E., "Comparison of Advanced Propulsion Concepts for Deep Space Exploration," *Journal of Spacecraft and Rockets*, vol. 9, no. 12, December 1972, pp. 863-868.
- [3] Hughes, S. P., "General Mission Analysis Tool (GMAT) Product Description", *Goddard Space Flight Center*, August, 2007, [Online], URL <http://gmat.gsfc.nasa.gov/> Retrieved 12 October 2010.
- [4] Tsiolkovsky, K., *The Study of Outer Space Rocket Devices*, vol. I of IV, Russia, 1903.
- [5] Betti, R. et al., "Thermonuclear Ignition in Inertial Confinement Fusion and Comparison," *Physics of Plasmas*, vol. 14, no. 5, April 2010.
- [6] Bussard, R. W. and Jameson, L. W., "Inertial-Electrostatic-Fusion Propulsion Spectrum: Air-Breathing to Interstellar Flight," *Journal of Propulsion and Power*, vol. II, no. 2, March-April 1995, pp. 365-372.
- [7] Thio, F. Y. C., "Status of the U. S. Program in Magneto-Inertial Fusion," *Journal of Physics: Conference Series*, vol. 112, no. 4, 2008, p. 042084.
- [8] Kammish, T. and Lee, M. J., "Gasdynamic Fusion Propulsion System for Space Exploration," *Journal of Propulsion and Power*, vol. 11, no. 3, May-June 1995, pp. 544-553.
- [9] Borowski, S. K., "A Physics/Engineering Assessment of a Tokamak-Based Magnetic Fusion Rocket," AIAA Paper 1986-1759, June 1986.
- [10] Orth, C. D., "VISTA – A Vehicle for Interplanetary Space Transport Application Powered by Inertial Confinement Fusion," Lawrence Livermore National Laboratory, Livermore, CA, Technical Report UCRL-TR-110500, May 2003.

- [11] Watanabe, Y., "Performance of Fusion-Fission Hybrid Nuclear Rocket Engine," *Fusion Energy in Space Propulsion*, edited by Kammash, T., Ed., Progress in Astronautics and Aeronautics, AIAA, Washington D.C., Vol. 197, 1995, pp. 195-206.
- [12] Moeses, E. I., "The National Ignition Facility and the Promise of Inertial Fusion Energy," *19th Topical Meeting on the Technology of Fusion Energy*, LLNL-CONF-464130, Las Vegas, NV, 2010.
- [13] Miley, G. H. et al., "Innovative Thecnology for an Inertial Electrostatic Confinement Fusion Propulsion Unit," *30th AIAA/ASME/SAE/ASEE Joint Propulsion Conference*, AIAA-1994-3321, Indianapolis, 1994.
- [14] Lindemuth, I. R. and Siemon, R. E., "The Fundamental Parameter Space of Controlled Thermonuclear Fusion," *American Journal of Physucs*, vol. 77, no. 5, May 2009, pp. 407-416.
- [15] Kirckpatrick, R. K., Linermuth, I. R., and Ward, M. S., "Magnetized target fusion - An overview," *Fusion Technology*, vol. 27, no. 3, May 1995, pp. 201-214.
- [16] Siemon, R. E., Lindermuth, I. R., and Schoenberg, K. F., "Why MTF is a Low Cost Path to Fusion," *Comments on Plasma Physics and Controlled Fusion*, vol. 18, no. 6, 1999, pp. 363-386.
- [17] Borowski, S. K., "Comparison of Fusion/Antiproton Propulsion System for Interplanetary Travel," *23rd AIAA/ASME/SAE/ASEE Joint Propulsion Conference & Exhibit*, AIAA-1987-1814, San Diego, July 1987.
- [18] Dugan, J. F. J., "Analysis if Trajectory Parameters for Probe and Round-Trip Missions to Mars," NASA, Cleveland, Technical Note D-281, 1960.
- [19] Adams, R. B. et al., "Conceptual Design of In-Space Vehicles for Human Exploration of the Outer Planets," NASA MSFC, Technical Paper 2003-212691, November 2003.
- [20] Polsgrove, T. et al., "Design of Z-pinch and Dense Plasma Focus Powered Vehicles," *49th AIAA Aerospace Sciences Meeting*, AIAA-2011-0962, Orlando, January 2011.
- [21] Hill, P. and Peterson, C., *Mechanics and Thermodynamics of Propulsion*, 2nd ed., Addison-Wesley, Reading, MA, 1992.
- [22] Kammash, T., Lee, M. J., and Galbraith, D. L., "High-Performance Fusion Rocket Manned Space Missions," *30th AIAA/ASME/SAE/ASEE Joint Propulsion Conference*, AIAA-1994-3266, Indianapolis, June 1994.

- [23] Goddard Space Flight Center, and Thinking Systems, Inc., "GMAT Architecture Specification," Goddard Space Flight Center, Greenbelt, MD, April 2011.
- [24] Goddard Space Flight Center, "GMAT Mathematical Specifications," Greenbelt, MD, April 2011.
- [25] Vallado, A., *Fundamentals of Astrodynamics and Applications*, McGraw-Hill, New York, 1997.
- [26] Serway, R. A. and Jewett, J. W. J., *Principle of Physics*, 3rd ed., Harcourt, Inc., Orlando, FL, 2002.
- [27] Brown, C. D., *Elements of Spacecraft Design*, AIAA, Reston, VA, 2002.
- [28] Kreyszig, E., *Advanced Engineering Mathematics*, 9th ed., John Wiley & Sons, Inc., Hoboken, 2006.
- [29] Bate, R. M., Mueller, D. D., and White, J. E., *Fundamentals of Astrodynamics*, Dover, New York, 1971.
- [30] Verner, J. H., "Explicit Runge-Kutta Methods with Estimates of the Local Truncation Error," *Journal on Numerical Analysis*, vol. 15, no. 4, August 1978, pp. 772-790.
- [31] Curtis, H. D., *Orbital Mechanics for Engineering Students*, Elsevier, Burlington, MA, 2005.
- [32] Ginsberg, J., *Engineering Dynamics*, Cambridge University Press, New York, 2008.
- [33] Doody, D., *Deep Space Craft*, Springer, New York, 2009.
- [34] Sutton, G. P. and Biblarz, O., *Rocket Propulsion elements*, 8th ed., John Wiley & Sons, Inc, Hoboken, NJ, 2010.
- [35] "Cassini Launch Press Kit," Jet Propulsion Laboratory, NASA, Pasadena, October 1997. [Online]. http://www.jpl.nasa.gov/news/press_kits/cassini.pdf
- [36] Space Launch Report, [Online Database] <http://www.spacelaunchreport.com> Retrieved 17 June 2012.
- [37] ATK, "ATK Space Propulsion Products Catalog," Tactical Propulsion and Controls, ATK, Elkton, MD, May 2008.

- [38] "Aerozine50 Specifications & DOT Shipping Information," Kennedy Space Center Propellants Division, NASA, Houston, October 2006. [Online].
<http://propellants.ksc.nasa.gov/commodities/Aerzone50.pdf>
- [39] "Cassini Mission Plan Revision N," Jet Propulsion Laboratory, NASA, Pasadena, JPL D-5564, May 2002.
- [40] Harland, D. M., *Missin to Saturn*, Springer, New York, 2002.
- [41] Buffington, B., "The Path to Scientific Discoveries: Designing the Cassini Solstice Mission Trajectory," *Ask Magazine*, no. 41, pp. 15-18, Winter 2011.
- [42] "New Horizons The first Mission to Pluto and the Kuiper Belt: Exploring Frontier Worlds," Applied Physics Laboratory, John Hopkins University, Laurel, MD, Mission Guide, January 2006.
- [43] Russell, C. T., Ed., *New Horizons: Reconnaissance of the Pluto-Charon System and the Kuiper Belt*, Springer, New York, 2009.
- [44] Andrews Space & Technology, "Space and Tech", 2001, [Online], URL
www.spaceandtech.com Retrieved 26 March 2012.
- [45] Choueiri, E. Y., "A Critical History of electric Propulsion: The First 50 Years (1906-1956)," *Jouneral of Propulsion and Power*, vol. 20, no. 2, March-April 2004, pp. 193-203.
- [46] Stuhlinger, E., "Possibilities of Electric Space Ship Propulsion," *5th International Astronautical Congress*, Innsbruck, Austria , 1954, pp. 100-119.
- [47] Humble, R. W., Henry, G. N., and Larson, W. J., *Space Propulsion Analysisi and Design*, McGraw-Hill, New York, 1995.
- [48] Jahn, R. G., *Physics of Electric Propulsion*, Dover, Mineola, NY, 2006.
- [49] "Launch Archives", *Dawn: Journey to the Asteroid Belt*, November, 2007, [Online], URL
http://www.nasa.gov/mission_pages/dawn/launch/index.html Retrieved 17 June 2012.
- [50] Jet Propulsion Laboratory, *Dawn: A Jouney to the Begining of the Solar System*, [Online Database] <http://dawn.jpl.nasa.gov/> Retrieved 5 April 2012.
- [51] Adams, R. B. and Richardson, G. A., "Using the Two-Burn Escape Maneuver for Fast Transfers in the Solar System and Beyond," *46th AIAA/ASME/SAE/ASEE Joint Propulsion Conference & Exhibit*, AIAA-2010-6595 , Nashville, TN, July 2010.

- [52] Committee on Data Management et.al., "Volume 1: Issues and Recommendations," *Data Management and Computation*, 1982.
- [53] Goddard Space Flight Center *Planetary Data Workshop*, edited by Kieffer, H. H., Ed., Scientific and Technical Information Branch, Washington, D.C., 1984.
- [54] "SPICE History", *Navigation and Ancillary Information Facility*, [Online], URL <http://naif.jpl.nasa.gov/naif/spicehistory.html> Retrieved 29 May 2012.
- [55] "The SPICE Concept", *Navigation and Ancillary Information Facility*, [Online], URL <http://naif.jpl.nasa.gov/naif/spiceconcept.html> Retrieved 29 May 2012.
- [56] IERS, "Radiation Pressure Reflectance Model," *IERS Technical Note 21*, edited by McCarthy, D. D., Ed., Paris, France, 1996, p. 81.
- [57] Montenbruck, O. and Gill, E., *Satellite Orbits: Models Methods Applications*, Springer, New York, 2000.